Oversampled Perfect Reconstruction Filter Bank Transceivers

Siavash Rahimi

Department of Electrical & Computer Engineering
McGill University
Montreal, Canada

March 2014

A thesis submitted to McGill University in partial fulfillment of the requirements for the degree of Doctor of Philosophy.

© 2014 Siavash Rahimi

2014/03/05

Contents

List of Figures

List of Tables

Abstract

Multicarrier modulation (MCM) is an efficient transmission technique for high data rate wired and wireless communications, where the channel bandwidth is divided into several subchannels with their own carriers. There are many different possible realizations for MCM systems, but with no doubt, orthogonal frequency division multiplexing (OFDM) has been the most prevalent solution in many current applications and standards. However, due to its use of a rectangular prototype filter, channel impairments such as narrowband interference (NBI) and carrier frequency offset (CFO) can greatly deteriorate the performance of OFDM. Moreover, future telecommunication networks call for higher data rate, increased bandwidth efficiency and flexibility in handling unsynchronized users. Filter bank multicarrier (FBMC) techniques have recently attracted considerable attention within the research community as a venue to fulfill these needs and potentially outperform the established OFDM in application areas such as dynamic spectrum access (DSA) and cognitive radio.

In this context, we first propose a novel method for the design of discrete Fourier transform (DFT) modulated oversampled perfect reconstruction filter bank (OPRFB), for transmultiplexing application in MCM systems. The perfect reconstruction (PR) property is enforced by employing a parametric class of paraunitary matrices to form the transmit/receive polyphase filters of the transceiver system. Specifically, the polyphase filters are obtained by cascading special types of paraunitary matrices characterized by a limited set of design parameters. To reduce the number of these parameters, three different factorization methods are employed and compared. Through the optimization of these design parameters, the stop-band energy of the subband filters can be minimized which leads to improved spectral containment. The performance of the proposed OPRFB design is investigated in a multicarrier transceiver application, where it is compared with OFDM and other FBMC structures. Numerical results show that the proposed scheme leads to a clear advantage not only in additive white Gaussian noise (AWGN) and frequency selective channels, but also in the presence of channel impairments such as NBI or CFO. In particular, it is found that a significant reduction in the bit error rate (BER) can be achieved by employing the proposed scheme.

Secondly, still in the context of single-user systems, we derive a data-aided joint maximum likelihood (ML) estimator of the CFO and the channel impulse response (CIR) for OPRFB transceiver systems operating over frequency selective fading channels. Then,

by exploiting the structural and spectral properties of these systems, we are able to considerably reduce the complexity of the proposed estimator through simplifications of the underlying likelihood function. The Cramer Rao bound (CRB) on the variance of unbiased CFO and CIR estimators is also derived. The performance of the proposed ML estimator is investigated by means of numerical simulations under realistic conditions with CFO and frequency selective fading channels. The effects of different pilot schemes on the estimation performance for applications over time-invariant and mobile time-varying channels are also examined. The results show that the proposed joint ML estimator exhibits an excellent performance, where it can accurately estimate the unknown CFO and CIR parameters for the various experimental setups under consideration.

Our third and final contribution deals with the extension of these newly proposed estimators to the multi-user case. More specifically, we consider the joint estimation of the CFO and channel equalizer coefficients based on the ML principle in the uplink of multi-user OPRFB (MU-OPRFB) systems. The performance of the proposed joint ML estimator is examined for various subband allocation schemes by means of numerical simulations. Also, different distributions of pilots over time are considered and their effects are investigated over mobile time-varying channels.

Sommaire

La modulation à porteuses multiples (MCM) est une technique de transmission efficace pour les communications filaires et sans fil à débit de données élevé, où la bande passante est divisée en plusieurs sous-canaux ayant chacun leur propre fréquence porteuse. Il existe de multiples réalisations possibles pour les systèmes MCM, mais sans aucun doute, le multiplexage orthogonal par répartition en fréquence (OFDM) est la solution la plus répandue dans les applications et normes présentement en vigueur. Toutefois, en raison de l'utilisation de filtres de synthèse et d'analyse rectangulaires, certaines imperfections causées par le canal de transmission, telles que les interférences à bande étroite (NBI) et le décalage de la fréquence porteuse (CFO), peuvent dégrader de manière significative les performances d'OFDM. Par ailleurs, les futurs réseaux de télécommunication nécessiteront des débits de transmission plus élevés, une plus grande efficacité de la bande passante et plus de flexibilité dans la gestion d'utilisateurs multiples non synchronisés. Les techniques de bancs de filtres à porteuses multiples (FBMC) ont récemment attiré l'attention de nombreux chercheurs, puis qu'elles offrent le potentiel de répondre à ces exigences et ainsi supplanter OFDM dans des domaines d'application tels que l'accès spectral dynamique (DSA) et la radio cognitive.

Dans ce contexte, nous proposons tout d'abord une nouvelle méthode pour la conception des bancs de filtres sur-échantillonnés à reconstruction parfaite (OPRFB) basés sur la modulation par transformation de Fourier discrète (DFT), pour les applications de transmultiplexage dans les systèmes MCM. La propriété de reconstruction parfaite (PR) est assurée par l'utilisation d'une famille paramétrique de matrices para-unitaires dans la réalisation des filtres polyphasés utilisés pour la transmission et la réception des données. Plus précisément, ces filtres sont donnés par le produit de sous-matrices para-unitaires particulières, chacune étant caractérisée par un nombre limité de paramètres de conception. Dans le but de réduire le nombre de ces paramètres, trois méthodes de factorisation matricielle différentes sont utilisées et comparées. L'optimisation des paramètres de conception pour la méthode choisie a pour but de minimiser l'énergie des filtres de synthèse et d'analyse dans la bande de coupure, ce qui conduit à une amélioration du confinement spectral. La performance des nouveaux bancs de filtres OPRFB ainsi obtenus est soumise à l'étude dans une application de transmission de données par MCM, où ils sont comparés avec OFDM et d'autres structures FBMC récemment proposées. Les résultats d'analyse

et de simulations montrent que les bancs de filtres OPRFB donnent lieu à un avantage marqué, non seulement pour les canaux à bruit gaussien blanc additif (AWGN) et sélectifs en fréquence, mais aussi en présence d'imperfections telles que les NBI et le CFO. En particulier, on constate une réduction significative du taux d'erreurs binaires (BER) lors de la transmission de données au moyen de la structure OPRFB proposée.

L'utilisation pratique des bancs de filtres OPRFB pour la transmission de données de type MCM sur les canaux à évanouissements sélectifs en fréquence requière la connaissance de certains paramètres, dont le CFO et la réponse impulsionnelle du canal (CIR). Notre deuxième contribution porte donc sur le développement et l'analyse d'un nouvel estimateur conjoint des paramètres CFO et CIR basé sur le principe de la vraisemblance maximale (ML) et utilisant une séquence d'entraînement (i.e. tonalités pilotes) connue, toujours dans un contexte à usager unique. Par la suite, nous exploitons les propriétés structurales et spectrales des systèmes OPRFB afin d'apporter des simplifications à la fonction de vraisemblance, ce qui permet de réduire considérablement la complexité de l'estimateur proposé. La borne de Cramer Rao (CRB) sur la variance des estimateurs non-biaisés des paramètres CFO et CIR est également dérivée. La performance du nouvel estimateur ML est soumise à l'étude par l'entremise de simulations numériques dans des conditions réalistes, soit en présence de CFO et de canaux à évanouissements en fréquence sélectifs. Les effets de différents motifs de tonalités pilotes sur la performance de l'estimation sont également examinés dans des applications sur des canaux invariants dans le temps, de même que sur des canaux radio mobiles variant dans le temps. Les résultats démontrent l'excellente performance du nouvel estimateur ML conjoint proposé, qui peut déterminer avec une grande précision les paramètres CFO et CIR inconnus dans les différentes configurations expérimentales soumises à l'étude.

Notre troisième et dernière contribution traite de l'extension de ce nouvel estimateur ML au cas d'usagers multiples. Nous considérons l'estimation conjointe du CFO et des coefficients CIR basée sur le principe ML dans la liaison montante des systèmes de transmission OPRFB multi-usagers (MU-OPRFB). Suite à son extension au cas multi-usagers, la performance de l'estimateur ML conjoint est examinée à l'aide de simulations numériques pour différents schémas d'allocation des sous-bandes entre les usagers. En outre, différentes distributions de tonalités pilotes dans le temps sont prises en compte et leurs effets sont étudiés sur des canaux radio mobiles variant dans le temps. Le potentiel d'application du nouvel estimateur ML aux systèmes multi-usagers est clairement démontré.

Acknowledgments

First and foremost, I would like to express my sincere gratitude to my supervisor, Prof. Benoit Champagne, for his continuous support. Without a doubt, this thesis would not have been possible without his inspiration, constructive advice and lots of helpful ideas. I would also thank him for my opportunities of giving tutorials, attending academic conferences and presenting my research to industrial partners. Furthermore, I would like to thank the other members of my Ph.D. committee, Prof. Fabrice Labeau and Prof. Hannah Michalska. Their invaluable advices helped to improve the technical quality of my research work. I also extend my thanks to the faculty and staff at Department of Electrical and Computer Engineering.

I am also grateful for the financial support provided by a scholarship from the Fonds quebcois de la recherche sur la nature et les technologies (FQRNT), by McGill University through the McGill Engineering Doctoral awards (MEDA), by the Loans and Bursaries Program of the Government of Quebec and by Prof. Champagne via research grants from the Natural Sciences and Engineering Research Council (NSERC) of Canada, the Government of Quebec through the PROMPT program and InterDigital Canada Ltee without which this thesis would not have been possible.

I am grateful to my fellow colleagues in the Telecommunications and Signal Processing Laboratory. It was a great honor to be your company. Particularly, Chao, Fang and Amir: you are so special to me because we started and almost graduated together. This journey would have been much more difficult without my best friends, Dara, Nima, Arash, Salar and Ali. I would also like to thank my beloved partner Golroo for her unconditional love and support and the many sacrifices she has made during my Ph.D. studies.

I am forever indebted to my family, first to my grandfather who taught me the value of education, and especially to my parents, Tala and Masoud, as they have given me everything they could, and they have been encouraging me to make my own decisions since I was a child.

List of Acronyms

4-QAM	4-point Quadrature Amplitude Modulation
3GPP	Third Generation Partnership Project
ADSL	Asymmetric Digital Subscriber Line
AFB	Analysis Filter Bank
AWGN	Additive White Gaussian Noise
bps	bit per second
BER	Bit Error Rate
BS	Base Station
CFO	Carrier Frequency Offset
CIR	Channel Impulse Response
CMT	Cosine Modulated Multitone
CP	Cyclic Prefix
CR	Cognitive Radio
CRB	Cramer Rao Bound
CS	Cosine-sine
CSD	Cosine-sine Decomposition
CSI	Channel State Information
DFT	Discrete Fourier Transform
DSL	Digital Subscriber Line
EMFB	Exponentially Modulated Filter Bank
FB	Filter Bank
FBMC	Filter Bank Multicarrier
FFT	Fast Fourier Transform
FIM	Fisher Information Matrix

FIR	Finite Impulse Response
FMT	Filtered Multitone
ICI	Intercarrier Interference
IDFT	Inverse Discrete Fourier Transform
ISI	Intersymbol Interference
ITU	International Telecommunication Union
LLF	Log-likelihood Function
LS	Least Squares
MAI	Multiple Access Interference
MCM	Multicarrier Modulation
MIMO	Multiple-Input and Multiple-Output
ML	Maximum Likelihood
MU-OPRFB	Multi-user Oversampled Perfect Reconstruction Filter Bank
MT	Mobile Terminal
NBI	Narrowband Interference
NPR	Nearly Perfect Reconstruction
OFDM	Orthogonal Frequency Division Multiplexing
OFDMA	Orthogonal Frequency Division Multiple Access
OPRFB	Oversampled Perfect Reconstruction Filter Bank
OQAM	Offset Quadrature Amplitude Modulation
PAM	Pulse Amplitude Modulation
PAPR	Peak-to-Average Power Ratio
PDF	Probability Density Function
PR	Perfect Reconstruction
QAM	Quadrature Amplitude Modulation
QMF	Quadrature Mirror Filter
QoS	Quality of Service
RF	Radio Frequency
RMSE	Root Mean Squared Error
SC	Single Carrier
SFB	Synthesis Filter Bank
SNR	Signal-to-Noise Ratio
SIR	Signal-to-Interference Ratio

SVD	Singular Value Decomposition

Chapter 1

Introduction

This chapter provides a general introduction to the thesis, which aims at developing new multicarrier modulation (MCM) techniques based on oversampled perfect reconstruction filter bank (OPRFB) transceivers. A high level overview of MCM and its applications in broadband communications is given in Section 1.1, while a literature review of various MCM systems and related parameter estimation methods is presented in Section 1.2. The research objectives and contributions of the thesis are discussed in Section 1.3. Finally, an outline of the upcoming chapters and the notations are presented in Section 1.4.

1.1 Multicarrier Modulation

Multicarrier modulation (MCM) is a method of transmitting a digital information sequence by splitting it into several components and sending each of these over separate carrier signals [1]. An MCM transmitter should efficiently combine several low-rate input signals into a single high-rate signal, which is then transmitted over a channel, and the corresponding receiver should be able to reconstruct good approximations of the low-rate signals, as depicted in Figure 1.1. To this end, the transmitter employs a so-called synthesis filter bank (SFB), while the receiver employs an analysis filter bank (AFB), which comprises a set of parallel matching receive filters [2–4]. Therefore, the combined SFB and AFB structure, also called transmultiplexer, can be considered to be the core of an MCM system.

In recent years, orthogonal frequency division multiplexing (OFDM) [5], a form of MCM, has become the physical layer of choice for many wireless communication systems, e.g., IEEE 802.11, IEEE 802.16 and E-UTRA LTE [5–8]. From the filter bank point of

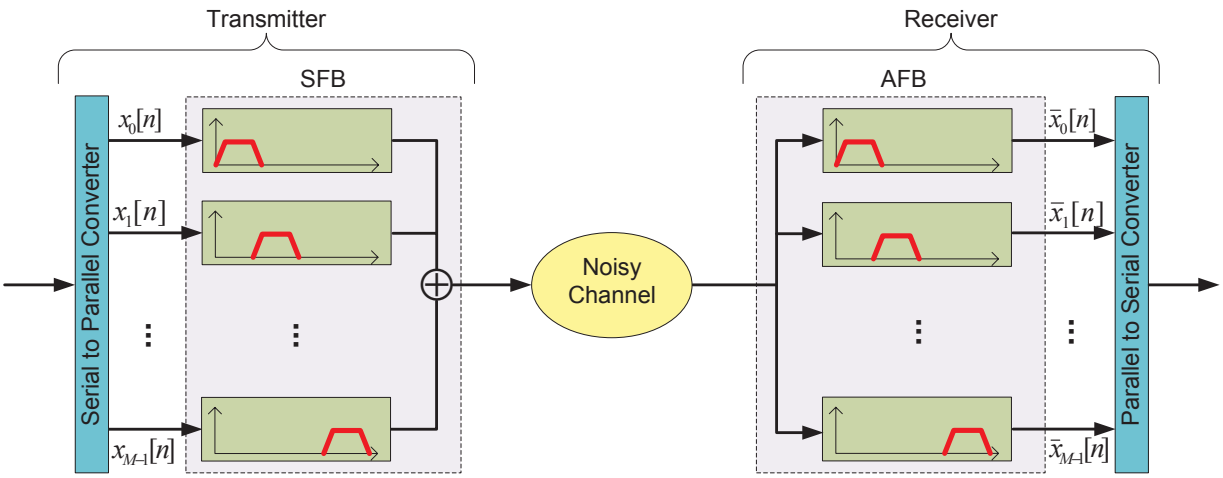

Fig. 1.1 Generic multicarrier modulation system

view, OFDM is based on the use of the inverse and forward discrete Fourier transform (DFT) for modulation and demodulation, respectively. Consequently, the prototype filter is a rectangular window whose length is equal to the number of subchannels. In the case of an ideal transmission channel, perfect signal recovery is possible because subchannel filters are orthogonal. For practical channels, OFDM uses a cyclic prefix (CP), which is longer than the channel impulse response (CIR) or the maximum multipath delay, to eliminate intersymbol interference (ISI) caused by channel spreading. Nevertheless, the DFT-based subchannel filters are not spectrally well isolated. They consist of a mainlobe along with high sidelobes that extend over a wide frequency band and therefore overlap with adjacent subchannels. In particular, the first sidelobe of a subchannel is only 13 dB below the mainlobe. These sidelobes overlap with adjacent subchannels and interfere with the mainlobes across the entire band. This can lead to an extensive intercarrier interference (ICI) problem in case of highly frequency selective channels or system imperfections such as carrier frequency offset (CFO). Also, the system performance may degrade significantly in the presence of narrowband interference (NBI). Indeed, the energy of a NBI will spread into many adjacent subchannels and this cannot be avoided by simply switching-off the subchannel in which the interference lies. Therefore, despite its popularity, OFDM suffers from some important drawbacks including poor spectral containment due to low side-lobe attenuation, sensitivity to narrow-band noise [9], large peak-to-average power ratio (PAPR) [10], sensitivity to Doppler shift and frequency synchronization [11,12], and loss of efficiency

caused by cyclic prefix.

To avoid such drawbacks, filter bank multi-carrier (FBMC) systems have been proposed which benefit from improved frequency selectivity through the use of longer, and thus better shaped prototype filters in the frequency-domain [2, 13]. The main elements of an FBMC system consist of a SFB (transmitter) and a AFB (receiver), which in practice are interconnected by a transmission channel. In these systems, the data on the transmitter side is split into M parallel data channels, up-sampled by integer K and passed through a bank of subband filters; the filter outputs are then summed and transmitted over the channel. At the receiver, the noisy data are passed through a bank of M subband filters, whose outputs are downsampled by K and equalized as needed to remove undesirable channel effects; finally, the original information sequence is reconstructed from the individually decoded data sub-streams. In the following section, we review the current research trends in the area of FBMC systems and as well as selected works related to the problem area of interest in this thesis.

1.2 Literature Review

In the context of FBMC systems, depending on the oversampling ratio, K/M, the system can be categorized as oversampled ($K/M > 1$) or maximally decimated ($K/M = 1$); whereas the perfect reconstruction (PR) property refers to a situation where the output of the transmultiplexer under the assumption of ideal channel, is a delayed version of the input. In practice, even in the presence of a non-ideal channel, the PR property can be exploited to simplify equalization. For instance, it is shown in [14] that in the case of a large number of subcarriers in PR filter bank (FB) systems, the channel induced ISI can be easily removed by means of a one-tap equalizer per subcarrier.

Alternatively, considering that non-ideal channels will introduce distortion and prevent the PR of the transmitted signal, some researchers have investigated the design of nearly-perfect reconstruction (NPR) FBs for MCM applications [15–19], where small amounts of ISI and ICI are present even in the ideal channel case. In practice, the level of these interferences can be controlled through optimization of the analysis/synthesis filters (see, e.g., [17, 18]) and kept sufficiently small compared to the distortion inflicted by the channel on the demodulated signals. In [17], a windowing method for the design of NPR systems is proposed that can reduce the number of design parameters considerably. This method

employs a class of prototype filters closely related to the so-called Nyquist filters [20]. Compared to the simple one-tap per subband equalizers for PR systems, NPR design entails the use of more complex equalizers at the receiver to combat both the ISI introduced by the channel and the distortion due to the non-PR nature of the FBs, which adds to the system's complexity [21].

The main advantage for oversampled FBs (i.e. $K > M$) over critically sampled ones ($K = M$) is that in the former case, additional design freedom is available that can be used to obtain PR and additional spectral containment and hence, better noise immunity within each subband. However, the use of oversampling leads to increased redundancy, and loss of spectral efficiency. Therefore, to remain competitive with existing OFDM systems, these redundancies in oversampled FBs should not exceed that introduced by the cyclic prefix in OFDM. As reducing redundancy leads to better bandwidth efficiency, the design of oversampled FB with smaller redundancy has been of great research interest [22–26]. In [22], it has been shown that OPRFB exists for redundancy $K - M < L$ under very general conditions, where L is the length of the CIR.

To reduce design and implementation complexity, modulated FBs are commonly used as a computationally efficient solution in the practical application of FBMC systems. In this approach, the M transmit and M receive subband filters are all derived from a single prototype filter, typically a finite impulse response (FIR) filter of length D, so that the total number of design parameters is significantly reduced. In this regard, both cosine modulation [16, 17, 19, 27–31] and complex exponential modulation, namely DFT modulation [15, 18, 25, 32–38], can be employed. With cosine modulation, however, the digital transmission is restricted to real symbol constellations which pose certain difficulties. Firstly, the process of equalization is more complicated since channel non-linearities, which cause phase rotations in the transmitted signals, necessitate the use of complex post combiners in the receiver [39,40]. Secondly, the extension of cosine modulation to multiple-input and multiple-output (MIMO) systems is nontrivial because most of the MIMO coding schemes require a complex orthogonality property, whereas cosine modulation only provides real orthogonality [13].

The use of DFT modulated filter banks in FBMC systems is investigated in [32,33]. The proposed system is referred to as filtered multitone (FMT), where oversampling is allowed to increase the spectral containment. Since complex constellation symbols, whose phase can easily be corrected, are employed in FMT, the cancellation of the ISI can be performed without post combiners. In particular, with a sufficiently large number of subbands such

that the width of each subband is small enough, a simple one-tap equalizer per subband can combat ICI in mildly frequency selective channels [41]. While the prototype filter in FMT system is not designed such that PR is enforced [32, 33, 41, 42], the goal of achieving PR property is desirable. For instance, PR greatly simplifies the equalization process, since one does not need to worry about any distortion generated by the FB itself.

Another popular realization of DFT modulated FBMC systems is OFDM/OQAM, which uses offset-quadrature amplitude modulation (OQAM), instead of common quadrature amplitude modulation (QAM) signaling to maintain orthogonality between adjacent subbands [15,18,34,43]. This requires the use of OQAM pre-processing and post-processing blocks in the transmitter and receiver of such systems, so that only pure real or imaginary signals are fed to the subband filters. These modifications add to the system complexity and makes the channel estimation more challenging. Although it is possible to maintain the PR property in OFDM/OQAM systems, most of the literature focuses on the NPR design of such systems [18, 43], which also makes the equalization process more complicated. The implementation of OFDM/OQAM in MIMO scenarios also poses a practical difficulty, in that the Alamouti space-time coding scheme cannot be directly applied to it [44, 45].

Motivated by the above considerations, the focus of our work in this thesis is on the investigation of DFT modulated OPRFBs and their application to MCM systems for efficient broadband communications. In the rest of this section, we present selected recent works from the literature specific to the problems of prototype filter design, synchronization and equalization for single-user and multi-user applications, all under the common OPRFB framework.

1.2.1 Oversampled perfect reconstruction filter bank

From an engineering perspective, the design of a DFT modulated OPRFB faces a number of challenges. In particular, when the number of subbands is large (which is typically the case in broadband communication applications), the number of parameters to be optimized increase dramatically. In turn, this may prevent the application of conventional design approaches due to the extremely high computational complexity of the numerical optimization. Also, with higher spectral efficiencies (i.e., K/M close to 1), the design process becomes even more stringent; yet this case is of particular practical interest.

In this regard, to reduce realization complexity and simplify design, it is of great im-

portance to provide an efficient structure based on a minimum number of parameters or elementary building blocks, i.e. delay and rotation matrices. In [46–51], it is established that the PR property of the OPRFB is equivalent to the paraunitaryness of the polyphase matrices associated to transmit and receive FBs. The first attempts to find an efficient factorization for paraunitary matrices in this field were focused on critically sampled PR FBs as reported in [2, 52–54]; unfortunately these techniques cannot be applied to oversampled PR FBMC systems. Alternatively, a parameterization of the polyphase matrix of OPRFBs can be found in [47, 55]; nevertheless, these works do not provide an explicit factorization in terms of elementary building blocks. In [35], it has been demonstrated that the parameterization of the polyphase matrix in the oversampled case can be achieved with different degrees of freedom, i.e. with different numbers of independent rotation parameters, but this approach does not provide a formal construction algorithm and the solution sets are redundant. As a result, in [56], it is shown that by employing a sequence of transformations, being either rotations or shifts, on these results, the non-redundant solutions can be extracted. Similarly, using the dyadic-based factorization [57], another design method for OPRFBs in the context of MCM is presented in [36]. However, the size of the associated parameter vector is relatively large, suggesting that this method can be further improved. Besides these structural aspects, the methods presented in the literature for the design of OPRFB only obtained limited success in improving the spectral efficiency, or equivalently, reducing the oversampling ratio K/M. These efforts start with an oversampling ratio of 2 in [47] and continue with values of 3/2 [55] and 5/4 [25, 35]. It is only recently that authors in [36, 56] succeeded in presenting a 9/8 and 17/16 oversampling ratio in the design of OPRFB, respectively.

1.2.2 Synchronization and equalization

The performance of FBMC systems in data transmission over frequency selective channels is studied in [41,58,59] for different prototype filters. It is generally shown that FBMC systems can outperform OFDM by a sizeable margin under non-ideal conditions of operation due to the better spectral containment of their subband filters. Nevertheless, they remain sensitive to the time and frequency selectivity of the channel and require accurate estimation of the CIR to combat these impairments through equalization. Moreover, similar to other types of MCM, FBMC systems are more sensitive to CFO than single carrier (SC) systems, since

the CFO induced by the mismatch between the transmitter and receiver oscillators may result in ISI or ICI [12,38,60–64]. As a result, it is of particular interest to develop efficient CFO and CIR estimation techniques in order to compensate these channel impairments in FBMC systems and in particular, for the subset of OPRFB systems.

In the past, a vast body of literature has been devoted to the study of CFO and CIR estimation algorithms for OFDM systems by relying on training sequence [11], cyclic prefix [65,66], iterative maximum likelihood (ML) [67,68] and expectation-maximization [69,70]. However, the consideration of these problems in the more general context of FBMC is fairly recent. CFO estimation for OFDM/OQAM systems is addressed in [59,71,72] and the CIR estimation for these systems is reviewed in [73]. In particular, joint synchronization methods based on scattered pilots and the conjugate symmetry property of OFDM/OQAM are presented in [59] and [72], respectively. One of the main efforts to jointly estimate the CFO and CIR for critically sampled FMT systems is developed in [74], where the CIR is estimated in the frequency-domain after CFO estimation in the time-domain. Several methods have also been proposed to mitigate the sensitivity of FBMC systems to synchronization errors assuming known or simplified CIR. A time-domain data-aided symbol timing and CFO synchronization method based on the least squares (LS) approach is developed in [71] for FMT and OFDM/OQAM systems operating over frequency-flat additive white Gaussian noise (AWGN) channel. Alternatively, in [75,76], the authors propose a frequency-domain ML-based data-aided CFO estimation algorithm for FMT systems. The results in these works show that the data-aided methods outperform the blind ones (i.e., non-data-aided) proposed in [77,78] in terms of estimation accuracy and complexity.

Unfortunately, while the above mentioned contributions to the estimation of CFO and CIR in the context of FBMC systems are valuable, they cannot be directly applied to OPRFB systems due to intrinsic structural differences in signal and filter formats. For instance, the essential assumption in the method proposed in [75,76], i.e., the constant CFO effect over the duration of the receive filters, is not valid for OPRFB systems as they employ relatively longer prototype filters. In addition, a majority of these works are based on an oversimplified broadband flat fading channel model, where the CIR reduces to a single coefficient [71,77–79].

1.2.3 Extension to multi-user applications

In recent years, orthogonal frequency division multiple access (OFDMA), which is an extension of OFDM to multi-user scenarios, has become part of the new standards for broadband wireless access [80]. Despite its appealing features, OFDMA imposes strict requirements on the frequency and timing synchronization, where inaccurate compensation of CFO results in ICI and multiple access interference (MAI), while timing error leads to interblock interference (IBI) and severe error rates [81]. However, it has been shown that FBMC methods in the multi-user context can effectively cancel MAI due to their low sidelobe filters [82]. They also exhibit a superior performance and lower computational complexity compared to OFDMA [63, 82]. Finally, most of the FBMC methods allow unsynchronised users to transmit simultaneously which significantly increases the system flexibility.

In this thesis, we also focus on multi-user implementation of OPRFB systems referred to as multi-user OPRFB (MU-OPRFB). In contrast to OFDM and some other FBMC methods that require at least one frequency guard interval between users, MU-OPRFB systems can still separate the users without employing any frequency guard interval due to the selectivity of their filters, so that higher bandwidth efficiency can be achieved. However, similar to other MCM systems, OPRFB transceivers are sensitive to CFO, which will lead to performance degradation unless it is properly compensated. Also, the effects of frequency selectivity of the channel in these transceivers should be removed through equalization at the receiver side.

The estimation procedure of the CFO and channel equalizer coefficients in the downlink of MU-OPRFB systems is similar to the single-user OPRFB situation. That is, each mobile terminal (MT) exploits a dedicated subset of received pilot signals to find the unknown parameter for his/her particular connection. However, this process in the uplink transmission is more challenging, since the base station (BS) receives a waveform that consists of the superposition of the users' transmitted signals affected by different CFOs and CIRs. Once the uplink CFO and equalizer coefficients (based on the estimated CIR) of each user have been estimated, they must be employed to compensate the effects of CFO and frequency selective fading channel to recover the data from each user.

Once the uplink CFO and CIR coefficients of each user have been estimated, they must be employed to compensate their effects through appropriate frequency synchronization and channel equalization mechanisms. There have been several methods proposed for CFO

compensation for FBMC systems, however, they are not suitable for OPRFB transceivers due to inherent structural differences. Recently, a maximum likelihood (ML) based CFO recovery method for single-user OPRFB transceivers has been reported in [79], where the channel is modeled as a simple flat fading additive white Gaussian noise (AWGN) channel. However, this method is not flexible enough to address the multi-user synchronization requirements and cannot provide the required equalizer coefficients.

There have been several methods proposed for CFO compensation in multi-user FBMC systems, however, they are not suitable for OPRFB transceivers due to the structural differences as briefly explained in Section 1.2.2. In [81], it is shown that the choice of CFO estimation method in multi-user context depends on the adopted subband allocation scheme. Moreover, channel estimation can only be performed within the allocated subbands of each individual user separately, as each user is only assigned a subset of the whole frequency band. Recently, the block allocation schemes, in which a block of contiguous bands is allocated to each user, has drawn more attention in the industry, as e.g., in LTE [80]. Therefore, it is of special interest to develop synchronization and equalization methods and algorithms that perform well with various allocation schemes, and especially with the blocked one.

1.3 Thesis Objectives and Contributions

The aim of the proposed research in this thesis is to develop an efficient FB based transmission technique for MCM applications. To be more specific, the main goal of this thesis can be stated as follows:

1. To develop computationally tractable methods for the design of OPRFB transceiver system with good spectral containment

2. To propose and investigate new techniques of CFO and CIR estimation, and especially the joint estimation of the required CFO and CIR parameters, for the purpose of synchronization and channel equalization in the application of OPRFB over frequency selective channel and in the presence of CFO.

3. To extend the above parameter estimation techniques to the uplink transmission in the multi-user applications of OPRFB

Regarding the first objective, we propose an efficient design method for OPRFB transceiver system. The PR property is enforced by employing a parametric class of elementary paraunitary transformations to form the polyphase filtering matrices of the transmit and receive sub-systems. In turn, the prototype filter coefficients of the analysis and synthesis FBs can be naturally expressed in terms of the entries of these paraunitary polyphase matrices, allowing for a complete yet efficient parameterization of the desired OPRFB. The design is formulated as a minimization problem over the new parameter space, where the objective function is the stop-band attenuation of the subband filters. By employing the Hermitian unitary and post-filtering factorization methods of paraunitary matrices [53, 54], we are able to reduce the number of representation parameters compared to the approach in [36, 37]; hence, the optimization process is faster and less complex than with other available approaches. The resulting prototype filters benefit from excellent spectral containment, i.e. high stop-band attenuation and sharp transition band. Unlike some other recently proposed methods, there is no restriction on the choice of the upsampling factor K versus the number of subbands M. In particular, we can further reduce the oversampling ratio of the FBMC system to 33/32, as will be presented. Such flexibility is essential to achieve different spectral efficiencies in a variety of application scenarios. The bit error rate (BER) performance of the proposed FBs in MCM transceiver applications is evaluated via extensive computer experiments in frequency selective and AWGN channels. The result show increased immunity of the new system against NBI and colored noise, as compared to OFDM. Furthermore, because it employs sharp PR filters with much lower sidelobes, the proposed transceiver structure outperforms ODFM and other recently proposed methods when used in the presence of CFO.

For the second objective, we begin by developing a data-aided joint ML estimator of the CFO and CIR that is specifically designed for OPRFB systems operating over frequency selective fading channels. Then, by exploiting the structural and spectral properties of these systems, we are able to considerably reduce the complexity of the proposed estimator through simplifications of the underlying likelihood function. The Cramer Rao bound (CRB) on the variance of the joint unbiased CFO and CIR estimators is also derived as a by-product of the ML analysis. The performance of the proposed joint ML estimator is investigated by means of simulations under realistic conditions of transmission with CFO and frequency selective fading channels. The effects of using different pilot schemes for applications in wireless scenarios over time-invariant and (mobile) time-varying channels are

also examined. The results show that the proposed joint ML estimator exhibits an excellent performance, where it can accurately estimate the unknown CFO and CIR parameters for the various experimental setups under consideration. Using these estimates, it is possible to compensate the effects of CFO and frequency selective fading channel on the transmission performance of OPRFB-based MCM systems under realistic wireless conditions. Finally, by employing different pilot patterns, we show that in mobile scenarios with fast time-varying channels, the proposed joint estimator and compensation methods still exhibit a reliable performance.

Finally, in connection with the third objective, we develop a data-aided joint ML estimator of the CFO and CIR that is specifically designed for application of OPRFB in the uplink of multi-user MCM systems operating over frequency selective fading channels. Using the estimated CFO and CIR respectively, we are able to compute the frequency offset and find the one-tap per subband equalizer coefficients for the allocated subbands of each individual user. This method is tested via simulations over realistically modeled frequency selective channels with different subband allocation schemes. Moreover, different pilot patterns have been considered for the proposed estimation method over the time varying channel. The simulation results, for different experimental setups, demonstrate that the proposed estimation scheme can provide a reliable performance in the application of MU-OPRFB.

Parts of the research presented in this thesis have been published or submitted for publication in peer-reviewed journals and refereed conferences, as listed below:

Journal papers:

[J-1] S. Rahimi and B. Champagne, "Oversampled perfect reconstruction DFT modulated filter banks for multi-carrier transceiver systems," Signal Processing, vol. 93, no. 11, Nov. 2013, pp. 2942-2955.

[J-2] S. Rahimi and B. Champagne, "Joint channel and frequency offset estimation for oversampled perfect reconstruction filter bank transceivers," submitted to IEEE Transactions on Communications, Sept. 2013, currently under revision.

[J-3] S. Rahimi and B. Champagne, "Joint synchronization and equalization in uplink transmission of multi-user OPRFB transceivers," to be submitted to IEEE Wireless Communications Letters, Dec. 2013.

Conference papers:

[C-1] S. Rahimi and B. Champagne, "Perfect reconstruction DFT modulated oversampled filter bank transceivers," in *Proc. European Signal Processing Conference (EUSIPCO)*, Barcelona, Spain, Aug. 2011, pp. 1588-1592.

[C-2] S. Rahimi and B. Champagne, "On the robustness of oversampled filter bank multicarrier systems against frequency offset," in *Proc. IEEE International Symposium Wireless Communication Systems (ISWCS)*, Paris, France, Aug. 2012, pp. 944-948.

[C-3] S. Rahimi and B. Champagne, "Carrier frequency recovery for oversampled perfect reconstruction filter bank transceivers," in *Proc. International Conference on Wireless and Mobile Communications (ICWMC)*, Nice, France, July 2013, pp. 140-145.

Note that the author of this thesis is the main contributor of all the aforementioned, coauthored publications.

1.4 Thesis Organization and Notations

Chapter 2 presents an up-to-date review of the MCM techniques including OFDM and other notable FBMC methods. The basics of multirate signal processing along with different types of FBs are also discussed in this chapter. The newly proposed efficient design method for OPRFB transceivers is presented in Chapter 3, where its performance over AWGN and frequency selective channels is compared with OFDM and other FBMC methods. In Chapter 4, a data-aided joint ML estimator of the CFO and CIR that is specifically designed for the purpose of synchronization and equalization of OPRFB systems is developed and evaluated under various conditions of operation. In Chapter 5, extension of the joint estimation/compensation method for application to the uplink of a OPRFB system in multi-user scenario is presented. Finally, Chapter 6 briefly summarizes the main contribution of the thesis, presents some concluding remarks and provides suggestions for future work.

Bold-faced letters indicate vectors and matrices, e.g. $\mathbf{A}$. The (i,j)th entry of a matrix is represented by $[\mathbf{A}]_{i,j}$. The superscripts T and H stand for the transpose and Hermitian transpose of a vector or matrix, respectively, while the superscript $*$ denotes complex conjugation. $\mathbf{I}_K$ and $\mathbf{0}_{K\times M}$ respectively denote the $K \times K$ identity matrix and $K \times M$

zero matrix. The paraconjugate operation on a matrix function $\mathbf{E}(z)$ is defined by $\tilde{\mathbf{E}}(z) = \mathbf{E}(1/z^*)^H$. A $M \times K$ matrix function $\mathbf{E}(z)$ is said to be paraunitary if $\tilde{\mathbf{E}}(z)\mathbf{E}(z) = c\mathbf{I}_K$, where $c > 0$ is a constant. $\lfloor x \rfloor$ and $\lceil x \rceil$ denote the integer floor and ceiling of x. Finally, a is congruent to b modulo m, $[a]_m = b$ or $a \equiv b (\mathrm{mod}\ m)$, whenever $a - b$ is divisible by m. $E\{.\}$, $\mathsf{Re}[.]$ and $\mathsf{Im}[.]$ stand for the expected value, real part and imaginary part of their arguments, respectively.

Chapter 2

Background on Filter Bank Multicarrier Modulation

The basic idea behind MCM can be simply explained as follows. Consider a communication system with data rate R bits per second (bps) and bandwidth B. The coherence bandwidth of the channel is assumed to be $B_c < B$, so that the transmitted signal experiences frequency selective fading. MCM seeks to divide the transmitted bit stream into several substreams and send these over different subbands[1], where M denotes the number of subbands. The data rate in each of these subbands, denoted R_M, is much less than the total data rate, typically $R_M \simeq R/M$, and the bandwidth of each subband B_M is much less than the total system bandwidth, $B_M \simeq B/M$. The number of subbands M (or substreams) is chosen to ensure that the bandwidth of each subchannel B_M is less than the coherence bandwidth of the broadband channel B_c, i.e., $B_M \ll B_c$, so that each subchannel experiences relatively flat fading. Alternatively, in the time-domain, the symbol time T of the modulated signal in each subband is inversely proportional to the subchannel bandwidth, that is $T \simeq 1/B_M \gg 1/B_c \simeq T_c$, where T_c denotes the delay spread of the channel. Thus if the number of subbands is large enough, the symbol time is much larger than the delay spread, so each subband experiences little ISI degradation.

In this chapter, a comprehensive description of common MCM methods and their applications is presented. In Section 2.1, OFDM is reviewed in detail as it is one of the most popular forms of MCM. The basic properties of multirate FBs are then presented in Section

[1]The terms *subchannel*, *subband* and *subcarrier* are used interchangeably in this thesis.

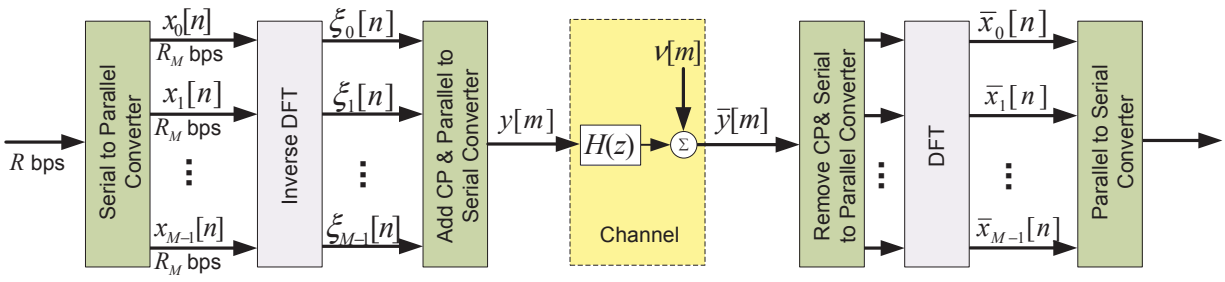

Fig. 2.1 OFDM with IDFT/DFT implementation

2.2. Some notable FBMC techniques are finally discussed in Section 2.3.

2.1 OFDM

The OFDM realization of MCM is shown in block diagram form in Figure 2.1. The input data stream, which consists of complex modulated symbols (such as, e.g., QAM), with data rate R bps, is passed through a serial-to-parallel converter, whose output is a set of M parallel data streams $x_0[n], \cdots, x_{M-1}[n]$, which correspond to the symbols transmitted over each subcarrier at sampled time $n \in \mathbb{Z}$. The resulting substreams, with data rate $R_M = R/M$, are then passed through an inverse DFT (IDFT) operation block. At each time n, the IDFT yields the OFDM time-domain samples consisting of the sequence $\xi_i[n]$ of length M, defined as

$$\xi_i[n] = \frac{1}{\sqrt{M}} \sum_{j=0}^{M-1} x_j[n] w^{-ij}, \quad 0 \le i \le M-1, \tag{2.1}$$

where $w = e^{-\jmath 2\pi/M}$. To avoid ISI, a CP of length L_{cp} is then added to the OFDM symbol as depicted in Figure 2.2. Further details about the purpose of the CP function will be explained in the next section. The resulting samples are assembled by the parallel-to-serial converter into a time-domain sequence $y[m]$ of length $M + L_{cp}$ and passed through the radio frequency (RF) chain (not shown) for transmission over the channel. Specifically, the final digital stream $y[m]$ is passed through a digital-to-analog converter, resulting in the baseband OFDM signal which in then upconverted to carrier frequency f_c.

The transmitted signal is filtered by the CIR, which is modeled as an FIR filter of length

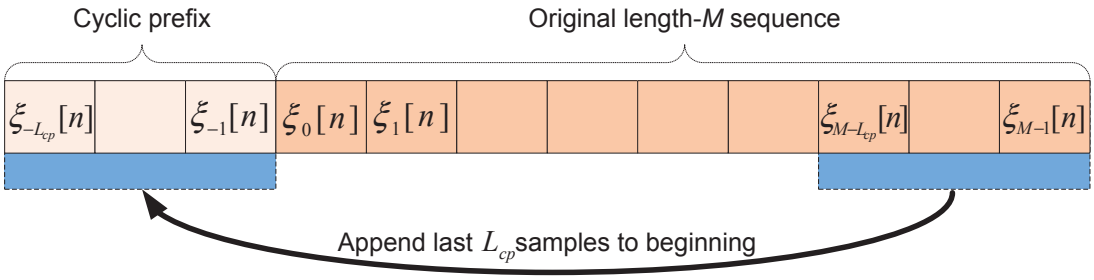

Fig. 2.2 Addition of CP with length L_{cp} to the OFDM samples

Q with discrete-time baseband equivalent system function

$$H(z) = \sum_{l=0}^{Q-1} h[l] z^{-l}, \tag{2.2}$$

where $h[l]$ is the impulse response of the channel. In practice, the channel output is corrupted by an additive noise sequence $v[m]$, which also includes additional noise generated within the RF front-end of the receiver. The received signal is downconverted to baseband where it is sampled by an analog-to-digital converter to obtain the received baseband discrete-time signal $\bar{y}[m]$. The input-output relationship of the noisy channel can therefore be expressed as

$$\begin{aligned} \bar{y}[m] &= y[m] * h[m] + v[m] \\ &= \sum_{l=0}^{Q-1} h[l] y[m-l] + v[m], \quad L_{cp} - 1 \leq m \leq M - 1, \end{aligned} \tag{2.3}$$

where $*$ denotes discrete-time convolution.

At the receiver side, assuming perfect symbol synchronization, the prefix of $\bar{y}[m]$ consisting of the first L_{cp} samples is removed and the remaining time samples are serial-to-parallel converted. In the absence of noise, the DFT of the resulting signal can be expressed as

$$\bar{x}_i[n] = x_i[n] H_i[n], \tag{2.4}$$

where $H_i[n]$ is the flat fading channel gain associated with the ith subchannel during the transmission time of the nth symbol. It can be seen from (2.4) that the ith subband output

is a scaled version of the input. The demodulator can use the channel gains to recover the original symbols by dividing out these gains, as in

$$\hat{x}_i[n] = \bar{x}_i[n]/H_i[n], \tag{2.5}$$

where $\hat{x}_i[n]$ denotes the equalized output of the ith subband. As a result, the OFDM system can effectively decompose the wideband frequency selective channel into a set of narrowband orthogonal subchannels with different QAM symbols being sent over each subchannel. However, this simple frequency equalization technique can lead to noise enhancement, as the noise in the ith subchannel is also scaled by $1/H_i[n]$ during the equalization process.

In practice, there exist some other preferred approaches such as precoding, adaptive loading and coding across subchannels to mitigate the effects of flat fading subchannels [83]. Also, when M is large, the IDFT and DFT blocks can be efficiently implemented using the fast Fourier transform (FFT) algorithm [84].

2.1.1 The Cyclic Prefix

Consider the application of an input sequence $\xi_0[n],\ \cdots, \xi_{M-1}[n]$ of length M to a discrete-time channel with FIR $h[m]$ of integer length[2] $Q = T_c/T_s$, where T_c is the channel delay spread and T_s is the sampling time of the discrete-time signal. To avoid the effect if ISI between adjacent symbols, a CP is appended to the sequence $\xi_i[n]$. Specifically, the CP for $\xi_i[n]$ is defined as the sub-sequence $\xi_{M-Q+1}[n],\ \cdots, \xi_{M-1}[n]$ and consists of the last $Q-1$ values of the channel input sequence, where $Q \leq M-1$ is assumed. For each consecutive input sequences of length M, also called block, the last $Q-1$ samples of each block are appended at its beginning as shown in Figure 2.2, which produces a new sequence $y[m],\ -Q+1 \leq m \leq M-1$ of length $M+Q-1$, where $y[-Q+1],\ \cdots, y[M-1] \equiv \xi_{M-Q+1}[n],\ \cdots, \xi_{M-1}[n],\ \xi_0[n],\ \cdots, \xi_{M-1}[n]$. This relation can also be written completely as

$$y[m] = \xi_{[m]_M}[n], \quad -Q+1 \leq m \leq M-1 \tag{2.6}$$

where $[m]_M$ denotes m modulo M. Hence for $0 \leq m \leq M-1$ and $0 \leq l \leq Q-1$, (2.6) implies that $y[m-l] = \xi_{[m-l]_M}[n]$. When $y[m]$ is passed through a channel with impulse

[2]That is $h[m]$=0 for $m < 0$ and $m \geq Q$.

response $h[m]$, the channel output $\bar{y}[m]$ for $0 \leq m \leq M-1$, can be expressed as

$$\begin{aligned} \bar{y}[m] &= y[m] * h[m] \\ &= \sum_{l=0}^{Q-1} h[l] y[m-l] \\ &= \sum_{l=0}^{Q-1} h[l] \xi_{[m-l]_M}[n] \\ &= \xi_m[n] \circledast h[m] \end{aligned} \tag{2.7}$$

where $\circledast$ denotes the M-point *circular convolution* and is defined as

$$a[m] \circledast b[m] = \sum_{l=0}^{M-1} a[l] b[m-l]_M. \tag{2.8}$$

Therefore, by adding a CP to the channel input, the linear convolution of $y[m]$ with the CIR $h[m]$ is effectively transformed into a circular convolution.

On the receiver side, the CP is removed and a DFT of the remaining time samples is computed. Let $\bar{x}_i[n]$ denote the output of the ith subband, which is obtained through the DFT operation, applied on $\bar{y}[m]$:

$$\bar{x}_i[n] = \mathrm{DFT}\{\bar{y}[m]\} = \frac{1}{\sqrt{M}} \sum_{m=0}^{M-1} \bar{y}[m] w^{im} \tag{2.9}$$

where $0 \leq i \leq M-1$. Based on the DFT properties, we can therefore write

$$\begin{aligned} \bar{x}_i[n] &= \mathrm{DFT}\{\bar{y}[m]\} \\ &= \mathrm{DFT}\{\xi_m[n] \circledast h[m]\} = x_i[n] H_i[n]. \end{aligned} \tag{2.10}$$

As a result, in the absence of noise (i.e., assuming $v[m] = 0$ in (2.3)), the input signal can be recovered as

$$x_i[n] = \frac{\bar{x}_i[n]}{H_i[n]} \tag{2.11}$$

Here, the transmitted block $y[m]$ for $-Q+1 \leq m \leq M-1$ has length $M+Q-1$, out

of which $Q-1$ samples associated to CP are redundant. However, during transmission, the first $Q-1$ samples of $\bar{y}[m] = y[m] * h[m]$ in a given block, i.e., those with index $-Q+1 \leq m \leq -1$, are corrupted by ISI associated with the last $Q-1$ samples of a prior block. Because of the CP , these corrupted samples can be discarded without any loss relative to the original input sequence. Therefore, this process can also be interpreted in the time-domain as using a guard band of duration T_c (the channel delay spread) before every block of M time-domain samples of duration MT_s to remove the ISI between these data blocks.

However, this simplicity in the data recovery process with OFDM is achieved at a cost of underutilizing two resources. First, the $Q-1$ samples that are added to the input block, result in a relative overhead of $(Q-1)/(M+Q-1)$, and consequently an effective data rate of only $M/(M+Q-1)$. The second loss is the transmit power required to send the CP that is also wasted as the corresponding received samples are discarded at the receiver. In practice, the length of the CP should exceed the channel delay spread T_c to remain effective in eliminating ISI, that is $L_{cp}T_s \geq T_c \simeq (Q-1)T_s$, hence the minimum CP length $L_{cp} \geq Q-1$. Therefore, to minimize the overhead (in both cases) due to the CP, it is preferred to have M as large as possible. OFDM schemes that insert zero signal samples instead of the CP have been proposed to reduce the loss in the transmit power; these are known as OFDM with zero padding. However, these schemes have their own shortcomings as well, such as increasing receiver complexity [85], and in general, OFDM with CP is the preferred choice in practice.

2.1.2 OFDM Challenges

Although the signals transmitted on the subbands of an OFDM system are mutually orthogonal in the time-domain, they have significant overlap in the frequency-domain. This is illustrated in Figure 2.3, which shows the magnitude response of various modulated DFT subband filters derived from a common prototype filter with rectangular impulse response. Specifically, let

$$w_l[n] = \begin{cases} e^{\frac{j2\pi ln}{M}}, & 0 \leq n \leq M-1 \\ 0, & \text{otherwise} \end{cases} \tag{2.12}$$

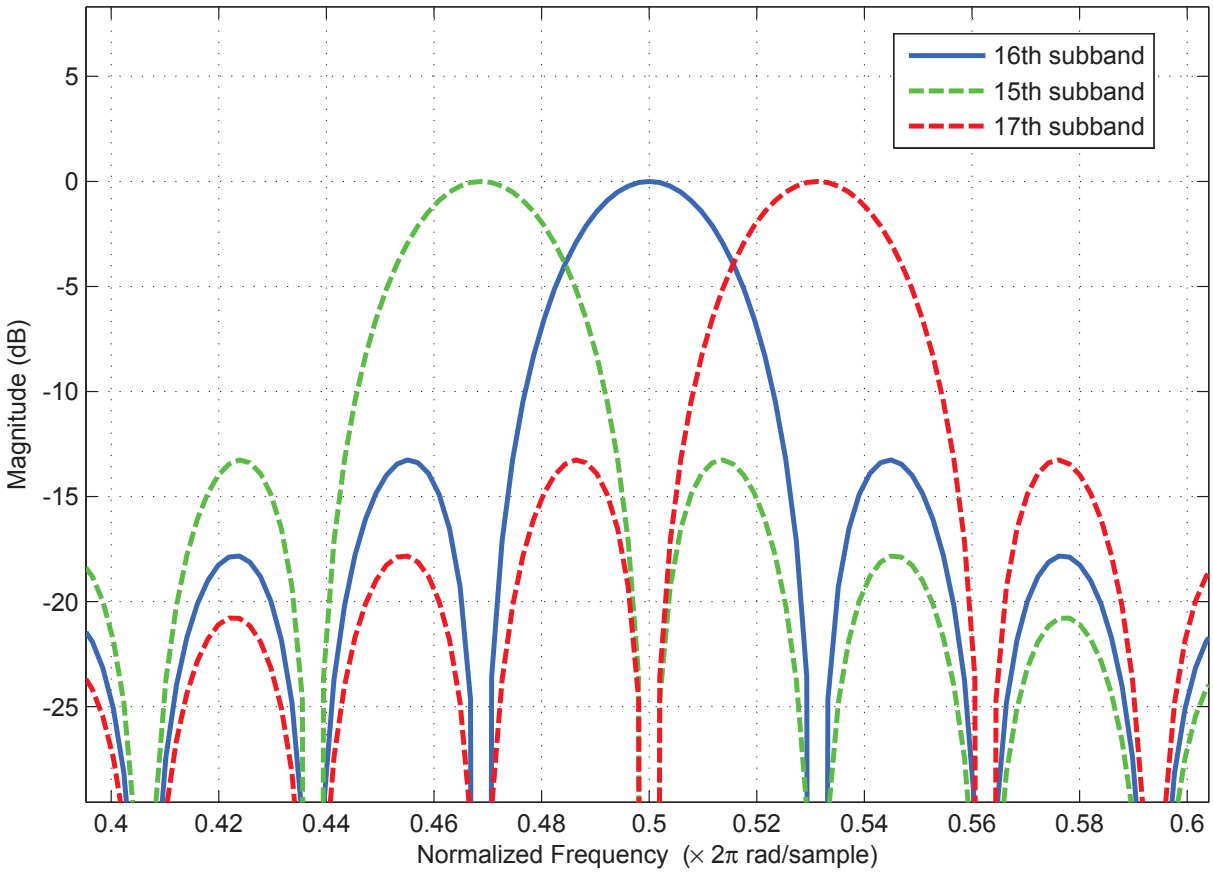

Fig. 2.3 Magnitude of the frequency response of three adjacent subband filters of OFDM ($M = 64$, $l \in \{15, 16, 17\}$)

with corresponding discrete-time Fourier transform (DTFT)

$$W_l(\omega) = \sum_{n=0}^{M-1} w_l[n] e^{-\jmath\omega n} \tag{2.13}$$

where $0 \leq l \leq M-1$. Figure 2.3 shows the magnitude response $|W_l(\omega)|$ of selected subband filters from this set for $l \in \{15, 16, 17\}$ We note in particular, the large spectral overlap of adjacent mainlobes and the high sidelobe level, where the first sidelobe in only 13 dB lower than the mainlobe. Nevertheless, under ideal conditions, these prototype signals $w_l[n]$ are orthogonal when transmitted synchronously in time and the frequency separation of the subcarriers is then perfect.

In practice, the subcarrier separation is imperfect and this is generally caused by vari-

ous effects, such as mismatched oscillators between the transmitter and receiver, Doppler frequency shifts and timing synchronization errors. For instance, mobility of the receiving terminal results in ICI, as the orthogonality among the subcarriers is destroyed due to the Doppler frequency shift or Doppler spreading [11]. In the past, a vast body of literature has been devoted to studying the effects of frequency and timing offset in OFDM systems and developing means to overcome their impact, by considering the use of CP and other training sequences [11, 65, 66], and applying various estimation methods such as iterative maximum likelihood (ML) [67, 68] and expectation-maximization [69, 70].

Another important drawback of OFDM is its sensitivity to NBI, which can degrade performance not only by corrupting the data on the subband where it is present, but also the data of neighbouring subbands due to the low attenuation of the sidelobes. As a result, the BER performance of an OFDM system degrades rapidly in the presence of NBI. In wireline ADSL systems, where NBI is common, adaptive data loading is employed to combat NBI [86]. However, this method requires accurate channel state information (CSI) feedback from receiver to transmitter, which is not always possible in wireless systems. Various methods intended for interference mitigation in wireless OFDM, including coded OFDM [87, 88], spread spectrum OFDM [89], as well as post-detection techniques involving equalizers [90], frequency-domain subtractive cancellation using singular value decomposition [91] and excision-based techniques [92] have been reported in the literature and compared in [9]. These methods either require modifications to the transmitted OFDM signal which are not supported by current OFDM standards, or substantial signal processing to estimate and remove the interference from all OFDM frequency bins.

Yet, another issue with OFDM, that is also relevant to other MCM methods, is the relatively high PAPR that is inherent in the transmitted signal. When the signals in many of the various subbands add constructively in phase, large signal peaks in the transmitted signal power occur. Such large peaks may result in clipping in a digital-to-analog converter or can saturate the power amplifier. Therefore, to reduce the PAPR in complex MCM systems, different methods have been reported in the literature, as summarized in [93].

The application of OFDM to the multiuser context, in the form of OFDMA, has been recently proposed in a number of standards such as IEEE 802.16 [7]. In OFDMA, each user is allocated a subset of the subcarriers for its data transmission. To prevent ICI, the user signals must be precisely time-synchronized at the receiver input. As a result, OFDMA only works well in the downlink transmission, where all the subcarriers are transmitted form the

BS. The synchronization in the uplink of OFDMA is challenging because of the physical separation between the users and may not be feasible in some scenarios. Therefore, some additional countermeasure steps based on signal processing techniques have to be taken to minimize the interference between the signals originating from different users. These extra synchronization measures are strict and add significant complexity to the implementation of such systems.

Currently, wireless networks are characterized by static spectrum allocation policies. Due to the increase in spectrum demand, these policies have resulted in spectrum scarcity in particular spectrum bands. Moreover, spectrum utilization data reveal that a large portion of the assigned frequency bands is used sporadically [94], leading to underutilization of a significant amount of spectrum. In order to solve this spectrum inefficiency problem, dynamic spectrum access techniques were recently proposed, where cognitive radio (CR) is the key underlying technology behind these techniques. CR aims to address the spectrum scarcity problem by opportunistically identifying the vacant or underutilized portions of the spectrum and transmitting within these bands, while ensuring that any licensed users of the same bands are not affected. Recently, some forms of OFDM have also been proposed for CR systems in channel sensing for coexistence of licensed and unlicensed users [95]. However, the receiver and transmitter filters of OFDM have large sidelobes that can lead to leakage of signal powers between the subbands of different users. Also, OFDM suffers from spectral inefficiency as it requires 5/24/92 subbands as guard-bands to achieve -20/-30/-40 dB interference level, respectively, in reference to the subchannel power level.

Despite these shortcomings and challenges facing OFDM, it has to be emphasized that OFDM also benefits from many important and desirable features as stated before. However, although widely adopted in the current standards, OFDM is not necessarily the best solution for many future wireless applications. In the following sections, some other MCM methods, and specifically FBMC techniques, along with their advantages and shortcoming are presented as an alternative to OFDM.

2.2 Multirate Filter Banks

In general, a FB consists of an array of M filters, indexed by $i \in \{0, \cdots, M-1\}$, where each filter processes a discrete-time input signal $x_i[n]$ and produces a corresponding output $y_i[n]$. When the inputs of all the M filters are equal (i.e., the input branches of the M

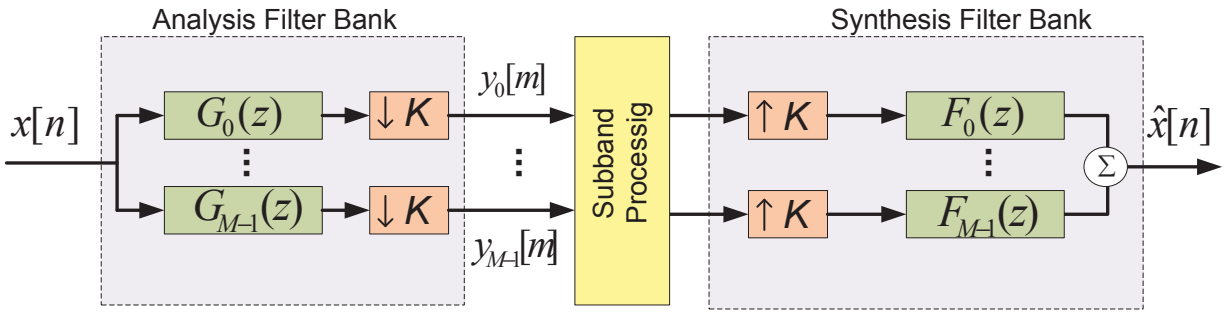

Fig. 2.4 Use of AFB followed by SFB for subband processing application

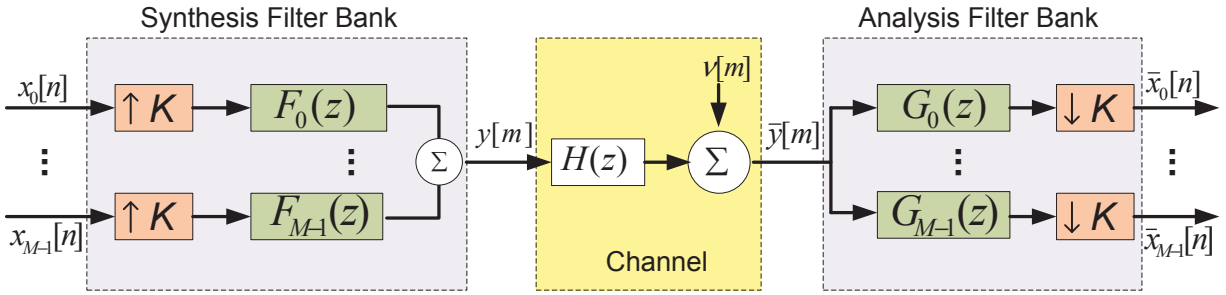

Fig. 2.5 Use of SFB followed by AFB for MCM application

filters are connected to a single pick-off node where the input is applied), or $x_i[n] = x[n]$ for $0 \leq i \leq M-1$, the filters analyze this input $x[n]$ based on their frequency characteristics. This particular configuration of the FB is called a AFB, and is illustrated at the left-hand side of Figure 2.4. Alternatively, when the individual inputs $x_i[n]$ are processed by the FB and their associated outputs $y_i[n]$ are added together (i.e., the output branches of the M filters are connected to a common adder), a new signal is synthesized as $y[n] = \sum_{i=0}^{M-1} y_i[n]$. The resulting configuration is called a SFB, as shown in the right-hand side of Figure 2.4.

FBs that work at different sampling rates are called multirate FBs and are the main structural elements in the application of multirate signal processing [2–4]. For instance, in many applications, the output of each filter $y_i[n]$ in the analysis FB only occupies a small portion of the available bandwidth at the given sampling rate. The resulting signals can therefore be downsampled to lower the number of operations without losing the information in the original signals, as long as the conditions of the Nyquist sampling theorem hold [2]. Conversely, the inputs of the system which are narrowband in nature can be upsampled

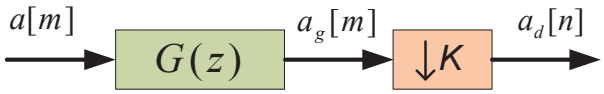

Fig. 2.6 K-fold decimation with anti-aliasing filter

and band-pass filtered so that each occupy a desired portion of the spectrum. In this way, by adding the resulting outputs, each occupying a different portion of the spectrum, a new signal with broader bandwidth can be obtained.

The real power of FBs can be exploited when these two building blocks, namely the AFB and SFB, are used in pairs as illustrated in Figure 2.4. Important applications of such systems can be found in speech coding [96], video coding [97] and adaptive filtering, e.g., acoustic echo cancellation [98]. In an analogous manner, the reverse combination of these two blocks as depicted in Figure 2.5, forms a transceiver, sometimes called transmultiplexer, that is the basis for multicarrier communications. In this application, the input signals $x_i[n]$ for $i \in \{0, \cdots, M-1\}$ can be interpreted as a collection of narrowband signals which are aggregated by the SFB for transmission over a broadband channel. The AFB then perform the reverse operation to obtain the recovered signals $\bar{x}_i[n]$ corresponding to the original input $x_i[n]$. In this thesis, we focus on the latter configuration, i.e., SFB followed by AFB, which is reviewed in much further details below.

2.2.1 Basic Multirate Operations

The above described operations of downsampling (decimation) or upsampling (interpolation), form the basic building blocks of multirate processing systems. These operations are reviewed briefly in the following paragraphs.

Decimation

Decimation by an integer factor K, or simply K-fold decimation, is denoted by $\downarrow K$. It is defined as the process of reducing the signal sampling rate by only selecting one of every Kth symbol of the filtered sequence. The filtering of the input signal to prevent aliasing is usually performed before the downsampling as depicted in the block diagram form in Figure 2.6. Consider a discrete-time signal $a[m]$ and an antialiasing filter with a FIR $g[m]$

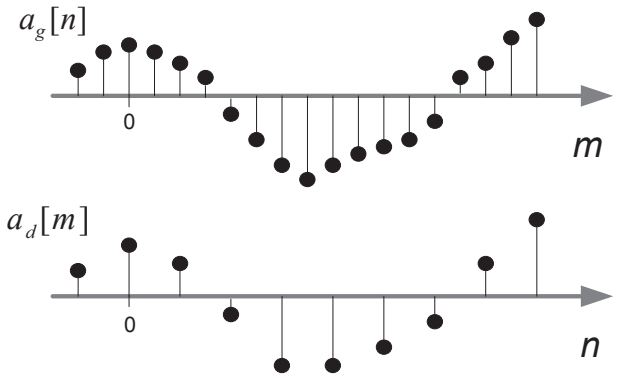

Fig. 2.7 Downsampling by a factor of 2 in the time-domain

of length D. The discrete-time filter output $a_g[m]$ is given as

$$\begin{aligned} a_g[m] &= a[m] * g[m] \\ &= \sum_{l=0}^{D-1} a[m-l]g[l] \\ &= \sum_{l} a[l]g[m-l], \end{aligned} \tag{2.14}$$

where the summation over l on the right-hand-side of (2.14), is delimited by the finite support of this FIR filter $g[l]$. The output of the decimator block, $a_d[n]$, can be expressed in the time-domain as

$$a_d[n] = a_g[Kn]. \tag{2.15}$$

This operation is illustrated for $K = 2$ in Figure 2.7. Thus, $a_d[n]$ can be expanded in terms of the input signal $a[n]$ and the analysis filter coefficients $g[n]$ as follows

$$a_d[n] = \sum_{l=0}^{D-1} a[Kn-l]g[l] = \sum_{l} a[l]g[Kn-l]. \tag{2.16}$$

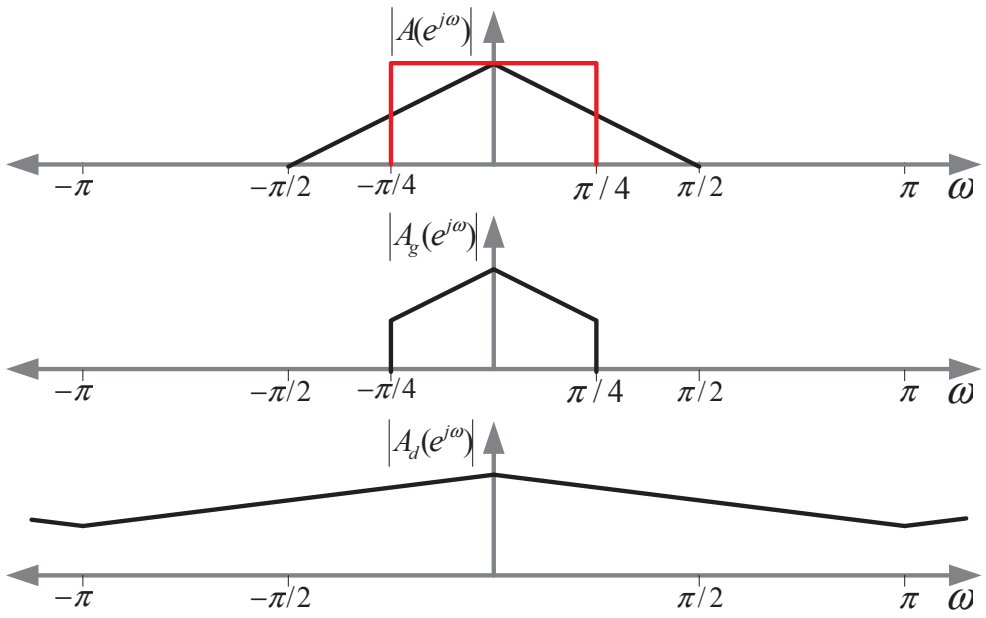

Fig. 2.8 Downsampling by a factor of 4 with ideal anti-aliasing complex filter in three steps (top) input signal (middle) filtered signal (bottom) downsampled signal

let $A(z)$, $A_d(z)$, $A_g(z)$ and $G(z)$ denote the z-transform[3] of signals $a[n]$, $a_d[n]$, $a_g[n]$ and the FIR filter $g[n]$, respectively. The above time-domain formulation corresponds the following equations in the z-domain.

$$A_g(z) = A(z)G(z) \tag{2.17}$$

$$\begin{aligned} A_d(z) &= \frac{1}{K}\sum_{l=0}^{K-1} A_g(z^{1/K}e^{-\jmath 2\pi l/K}) \\ &= \frac{1}{K}\sum_{l=0}^{K-1} A(z^{1/K}e^{-\jmath 2\pi l/K})G(z^{1/K}e^{-\jmath 2\pi l/K}) \end{aligned} \tag{2.18}$$

In turn, frequency-domain representation of these operations are obtained by setting $z = e^{-\jmath\omega}$ in the above expressions. In particular, the output spectrum of the downsampled

[3]The z-transform of discrete-time signal $a[n]$ is defined as $A(z) = \sum_{n=-\infty}^{\infty} a[n]z_{-n}$, where z is the complex variable.

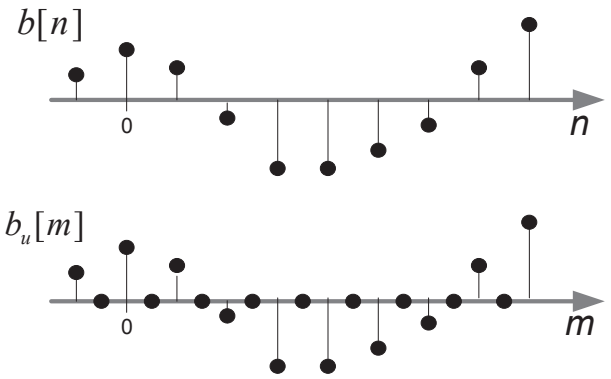

Fig. 2.9 Upsampling by a factor of 2 in the time-domain

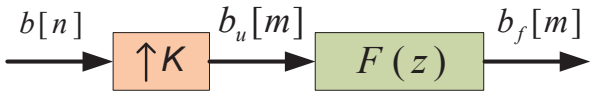

Fig. 2.10 K-fold interpolation with anti-imaging filter

signal $a_d[n]$ in Figure 2.6 consists of the repetitions of its input spectrum, i.e., $A_g(e^{-\jmath\omega})$, but expanded by a factor K, shifted by multiples of 2π. Figure 2.8 illustrates the representation spectra of the various signals $a[n]$, $a_d[n]$ and $a_g[n]$ in the K-fold decimation process, for the special case $K = 4$.

Interpolation

Sampling rate expansion by an integer factor K, or simply K-fold upsampling, is denoted by $\uparrow K$. It is defined as the insertion of $K - 1$ zeros between adjacent samples of the low rate input signal, that is

$$b_u[m] = \begin{cases} b[m/K], & \text{if } m/K \in \mathbb{Z} \\ 0, & \text{otherwise} \end{cases} \tag{2.19}$$

where $b[n]$ and $b_u[m]$ are the input and output of the upsampling block. This operation is illustrated for $K = 2$ in Figure 2.9.

To prevent imaging, the filtering of the output $b_u[m]$ is usually performed after the

downsampling as depicted in the block diagram form in Figure 2.10. Consider an anti-imaging (interpolation) filter with a FIR $f[m]$ of length D. The discrete-time filter output $b_f[m]$ is given as

$$\begin{aligned} b_f[m] &= b_u[m] * f[m] \\ &= \sum_{l=0}^{D-1} f[l] b_u[m-l] \\ &= \sum_{l} b_u[l] f[m-l], \end{aligned} \tag{2.20}$$

where the summation over l in the right-hand-side of (2.20), is delimited by the finite support of the FIR filter $f[m]$. Since $K-1$ out of every K consecutive values of $b_u[l]$ are zero, the interpolation output can be expressed as

$$b_f[m] = \sum_{l} b[l] f[m - lK]. \tag{2.21}$$

The corresponding equations in the z-domain are

$$B_u(z) = B(z^K), \tag{2.22}$$

$$B_f(z) = B_u(z)F(z) = B(z^K)F(z), \tag{2.23}$$

where $B(z)$, $B_u(z)$, $B_f(z)$ and $F(z)$ respectively, denote the z-transform of signals $b[m]$, $b_u[m]$, $b_f[m]$ and the FIR filter $f[m]$. Figure 2.11 illustrate representation spectra of the various signals $b[m]$, $b_u[m]$ and $b_f[m]$ in the K-fold interpolation process, for the special case $K = 4$. It can be seen that the input signal spectrum is compressed and, as a result, the fundamental frequency range $-\pi \leq \omega \leq \pi$ now contains repeated images of this basic spectral shape. The interpolation filter then can be used to remove the undesired images of the original spectrum.

Noble Identities

The Noble identities provide the means for interchanging the operations of filtering and up/downsampling. The first identity, illustrated in block diagram form in Figure 2.12,

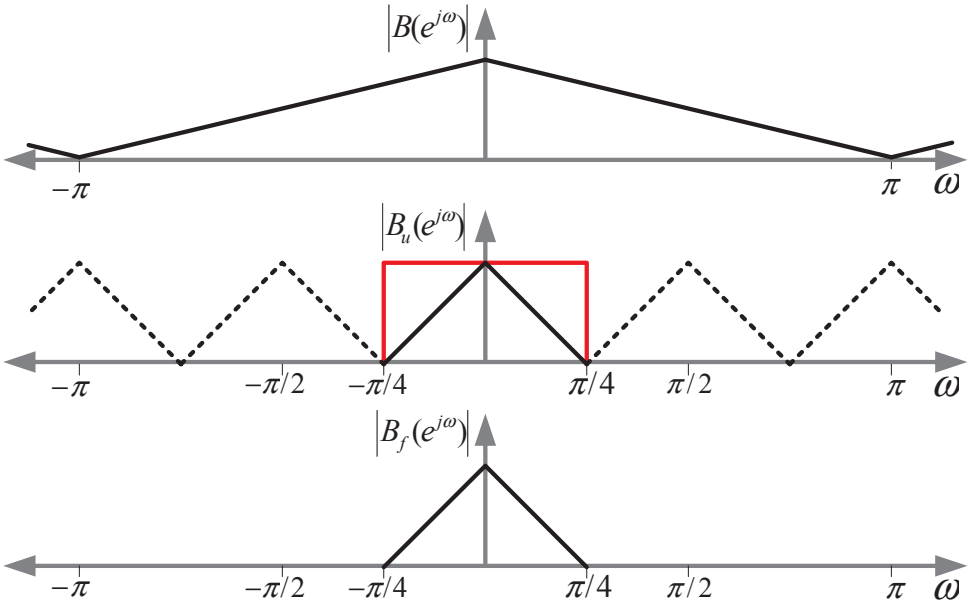

Fig. 2.11 Upsampling by a factor of 4 with interpolation filter in three steps (top) input signal (middle) upsampled signal (bottom) filtered signal

indicates that linear filtering of the low-rate output of a decimator by K with $G(z)$ is equivalent to filtering of the high-rate input with $G(z^K)$ followed by a K-fold decimator. Similarly, the second identity, illustrated in block diagram form in Figure 2.13, indicates that K-fold interpolation of the low-rate output of a linear filter with $F(z)$ is equivalent to filtering with $F(z^K)$ of the high-rate output of a K-fold interpolator.

In practice, the interchange of the up/downsampling blocks with the linear filter through Noble identities is quite useful. Indeed, it makes it possible to implement the filtering operation at a lower sampling rate, and can lead to a more efficient implementation of multi-rate system through the use of the polyphase decomposition, as will be exemplified in Chapter 3.

2.2.2 Transceiver Transfer Relations and Reconstruction Conditions

Based on the multirate equations provided in the previous section, the input-output relations for the transceiver structure depicted in Figure 2.5 can be derived. First, using (2.21), the output of each filter in SFB, denoted as $y_i[m]$ for $0 \leq i \leq M-1$, can be expressed in

Fig. 2.12 First Noble identity

Fig. 2.13 Second Noble identity

terms of the input signal $x_i[n]$ as

$$y_i[m] = \sum_p x_i[p] f_i[m - pK]. \tag{2.24}$$

As a result, the output of the SFB , i.e., $y[m]$, which is the summation of subbands' outputs is written as

$$\begin{aligned} y[q] &= \sum_{j=0}^{M-1} y_j[q] \\ &= \sum_{j=0}^{M-1} \sum_p x_j[p] f_j[q - pK]. \end{aligned} \tag{2.25}$$

In the absence of noise and assuming an ideal channel transmission[4], that is as $\bar{y}[m] = y[m]$. Also, similar to (2.16), the outputs of the AFB, i.e., $\bar{x}_i[n]$ for $0 \leq i \leq M-1$, can be expressed as

$$\bar{x}_i[n] = \sum_q \bar{y}[q] g_i[nK - q]. \tag{2.26}$$

[4]In practice, the transmitted signal $y[m]$ is filtered by the CIR and corrupted by an additive noise.

Substituting (2.25) in (2.26), the we obtain

$$\begin{aligned}\bar{x}_i[n] &= \sum_q \sum_{j=0}^{M-1} \sum_p x_j[p] f_j[q-pK] g_i[nK-q] \\ &= \sum_{j=0}^{M-1} \sum_p x_j[p] \left(\sum_q f_j[q-pK] g_i[nK-q] \right). \end{aligned} \tag{2.27}$$

It is desirable that the input and the output signals, i.e., $x_i[n]$ and $\bar{x}_i[n]$ for $0 \leq i \leq M-1$, be similar as possible to simplify the recovery process of the transmitted signals. As noted in Section 1.2, if the FB is designed so that the inputs $x_i[n]$ and the outputs $\bar{x}_i[n]$ of the transceiver are exactly the same, i.e., $x_i[n] = \bar{x}_i[n]$, the FB is called a PR FB. Using (2.27), the PR condition on subband filters can be derived as

$$\sum_q f_j[q-pK] g_i[nK-q] = \delta_{ij}\delta_{np}, \tag{2.28}$$

where the summation is over the finite support of the subband filters and δ_{ij} denotes the Kronecker delta function, i.e., $\delta_{ij} = 1$ if $i = j$ and $\delta_{ij} = 0$, otherwise. the input-output relationship (2.27) can be equivalently expressed in the z-domain as follows

$$\begin{aligned}\bar{X}_i(z) &= \frac{1}{K} \sum_{l=0}^{K-1} Y(z^{1/K} e^{-\jmath 2\pi l/K}) G_i(z^{1/K} e^{-\jmath 2\pi l/K}) \\ &= \frac{1}{K} \sum_{l=0}^{K-1} \sum_{j=0}^{M-1} X_j(z) F_j(z^{1/K} e^{-\jmath 2\pi l/K}) G_i(z^{1/K} e^{-\jmath 2\pi l/K}) \\ &= T_{i,i}(z) X_i(z) + \sum_{\substack{j=0 \\ j\neq i}}^{M-1} T_{i,j}(z) X_j(z), \end{aligned} \tag{2.29}$$

where

$$T_{i,j}(z) = \frac{1}{K} \sum_{l=0}^{K-1} F_j(z^{1/K} e^{-\jmath 2\pi l/K}) G_i(z^{1/K} e^{-\jmath 2\pi l/K}). \tag{2.30}$$

$T_{i,j}(z)$ represents the transfer function between the input of the jth subband, $x_j[n]$, and the output of the ith subband, $\bar{x}_i[n]$. In practice, for $i \neq j$, $T_{i,j}(z)$ represents the leakage.

The PR condition (2.28), therefore, can be expressed in the z-domain as

$$T_{i,j}(z) = \begin{cases} 1, & i = j \\ 0, & i \neq j \end{cases} \tag{2.31}$$

2.2.3 Modulated Filter Banks

Although it is possible to divide the available spectrum into unequal subbands, as in wavelet multitone techniques [40, 99], it is common to divide the spectrum into subbands of the same size. In this case, the subchannels use the same up and downsampling rates, and the resulting FB is called a uniform FB [2]. In the mid-seventies, a two channel system referred to as the quadrature mirror filter (QMF) was proposed as one of the first uniform FBs [100]. The idea behind QMF was generalized to the case of M channels FBs in the following decade. Early works employed the original two channel QMF block in a nested tree fashion to divide the subchannels recursively into smaller subbands, while keeping the same properties as the two channel QMF blocks [101]. The parallel M-channel FB structure, as opposed to the tree configuration, was later introduced in [102, 103] where it was shown that PR with overlapping subband filters is possible. To devise an arbitrary M-channel FB transceiver, it is necessary to design and implement M transmit and M receive filters which makes the design process quite complex. To overcome this limitation, modulated filter banks have been proposed [2] and are now widely used as a computationally efficient solution whenever FBs are needed. In this approach, the transmit and receive subband filters are all derived from a single prototype filter, which can be more efficiently designed due to the reduced number of free parameters. In this regard, cosine modulated FBs and DFT modulated FBs can be employed, where the basic idea is to shift the lowpass prototype filter in frequency to the desired center frequency of each subband. These approaches are reviewed below.

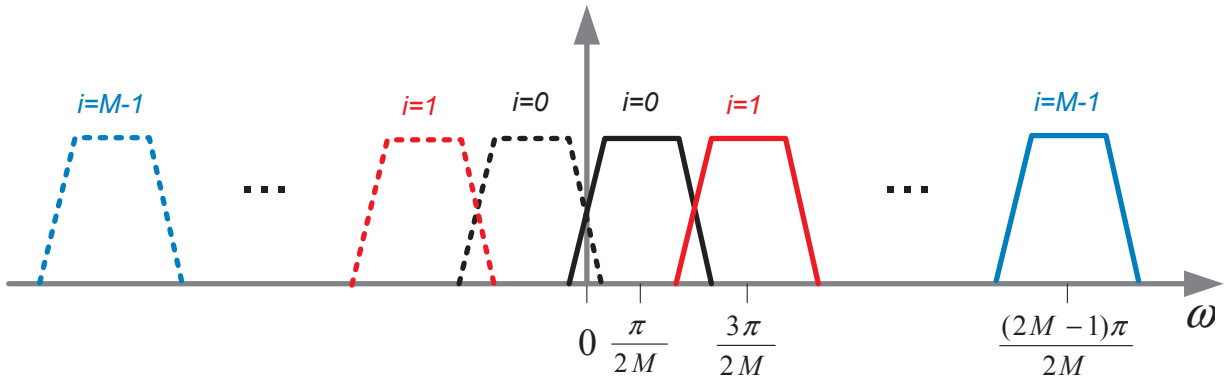

Fig. 2.14 Cosine modulated filter bank with odd stacked subbands

Cosine Modulated Filter Banks

The analysis and synthesis filters for cosine modulated FBs are formed from a single FIR prototype filter of length D with system function

$$F_p(z) = \sum_{n=0}^{D-1} f_p[n] z^{-n}, \tag{2.32}$$

where $f_p[n]$ for $0 \leq n \leq D-1$ is the corresponding impulse response. In effect, cosine modulation amounts to a positive frequency shift in range $[0, \pi]$, in which the passband of the prototype filter is moved around a new center frequency within that range. In the special form of cosine modulation proposed in [17], the ith synthesis subband filter, $f_i[n]$ for $0 \leq n \leq D-1$ and $0 \leq i \leq M-1$, is derived from the prototype filter $f_p[n]$ through

$$f_i[n] = 2 f_p[n] \cos\left((i + \frac{1}{2}) \frac{\pi}{M} (n - \frac{D}{2}) - (-1)^i \frac{\pi}{4} \right). \tag{2.33}$$

Similarly, the analysis subband filters can be constructed as

$$g_i[n] = 2 f_p[n] \cos\left((i + \frac{1}{2}) \frac{\pi}{M} (n - \frac{D}{2}) + (-1)^i \frac{\pi}{4} \right). \tag{2.34}$$

This particular choice of cosine modulated FB is designed for critical sampling of real-valued signals. Here, the FB is denoted as *odd stacked*, where the lowpass prototype filter

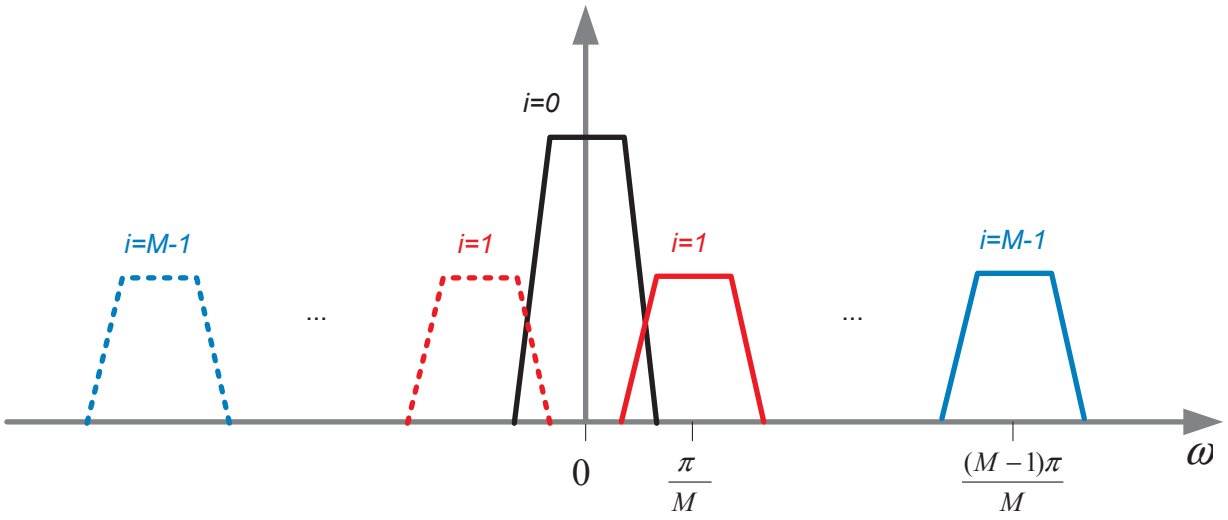

Fig. 2.15 Cosine modulated filter bank with even stacked subbands

is frequency shifted around new center frequencies at $\omega_i = (i + \frac{1}{2})\frac{\pi}{M}$ for $0 \leq i \leq M-1$ by multiplying $f_p[n]$ with cosine sequences. It can be seen that if the prototype filter is real valued[5], then the synthesis and analysis subband filters are real-valued as well. In other words, the cosine modulation of $f_p[n]$ generates two passbands in the frequency range $[-\pi, \pi]$ with center frequencies at $\pm\omega_i$ and frequency response that are complex conjugate of each other, i.e., $F_i^*(e^{-\jmath\omega}) = F_i(e^{\jmath\omega})$. As a result, if a real-valued signal is applied at the input of a cosine modulated (analysis) FB, the corresponding subband signals are also real-valued. Employing well-known properties of the DTFT [84], the frequency response of the synthesis subband filter $f_i[n]$ as

$$\begin{aligned} F_i(e^{\jmath\omega}) &= \sum_{n=0}^{D-1} f_i[n] e^{-\jmath\omega n} \\ &= \sum_{n=0}^{D-1} 2 f_p[n] \cos\left((i+\frac{1}{2})\frac{\pi}{M}(n-\frac{D}{2}) - (-1)^i\frac{\pi}{4}\right) e^{-\jmath\omega n} \\ &= e^{\jmath\phi_i} F_p(e^{\jmath(\omega-\omega_i)}) + e^{-\jmath\phi_i} F_p(e^{\jmath(\omega+\omega_i)}) \end{aligned} \tag{2.35}$$

[5]Equivalently, a real-valued filter $f_p[n]$ results in a conjugate symmetry frequency response with respect to zero frequency , that is $F_p^*(e^{-\jmath\omega}) = F_p(e^{\jmath\omega})$

where $F_p(e^{\jmath\omega}) = \sum_{n=0}^{D-1} f_p[n]e^{-\jmath\omega n}$ is the frequency response of the prototype filter and $\phi_i = -(i+\frac{1}{2})\frac{\pi}{M}\frac{D}{2} + (-1)^i\frac{\pi}{4}$ is the phase of the modulated filters. Alternatively, in the so-called *even stacking* form of cosine modulation, the subband filters can be shifted around center frequencies at $\bar{\omega}_i = \frac{i\pi}{M}$. The odd and even stacking options are depicted in Figures 2.14 and 2.15. We note that there exist other similar types of cosine modulated FBs with minor differences in the location of subband center frequencies and the phase of the modulation sequences. However, they all share many characteristics with the above particular choices of cosine modulation, as described by (2.33) and (2.34).

The cosine modulated FBs can be implemented efficiently using the discrete cosine transform and designed to have PR or NPR property [3]. However, some of the odd-stacked cosine modulated FBs with symmetric[6] prototype filter are inherently PR systems, and this allows the use of unconstrained non-linear optimization methods to design the prototype filter [2]. Note that by using two different prototype filters for the synthesis and analysis FBs, other beneficial properties such as better stopband attenuation can be achieved. However, the design process is more complicated as the number of design parameters is doubled and the PR property is not guaranteed.

Due to the real-valued nature of the cosine modulated FBs, it is more common to apply them only on input signals derived from real symbol constellation. Indeed, using complex symbols makes the process of equalization more complicated, since any non-linear channel will cause a phase rotation in the transmitted signals. In turn, this requires the use of computationally expensive post combiners on the receiver side that need to perform various linear combinations of the present and past received symbols from different subchannels [39, 40]. In [16, 29], the authors propose a method to simplify the post combiner structure by employing a modified receiver structure. Although the computational complexity of the receiver is increased,it is reported in these works that a two-tap per subcarrier equalizer is sufficient to mitigate the ISI, which is considerably less than the number of taps normally required for the proper operation of post-combiners. Another timely issue with cosine modulated FBs is their extension to MIMO systems. In particular, the application of Alamouti space-time coding scheme [104] is nontrivial because most of the MIMO coding schemes require a complex orthogonality property, whereas cosine modulation only provides real orthogonality [13].

[6] $f_p[n]$ of length D is symmetric when $f_p[n] = f_p[D-1-n]$, where $0 \leq n \leq D-1$.

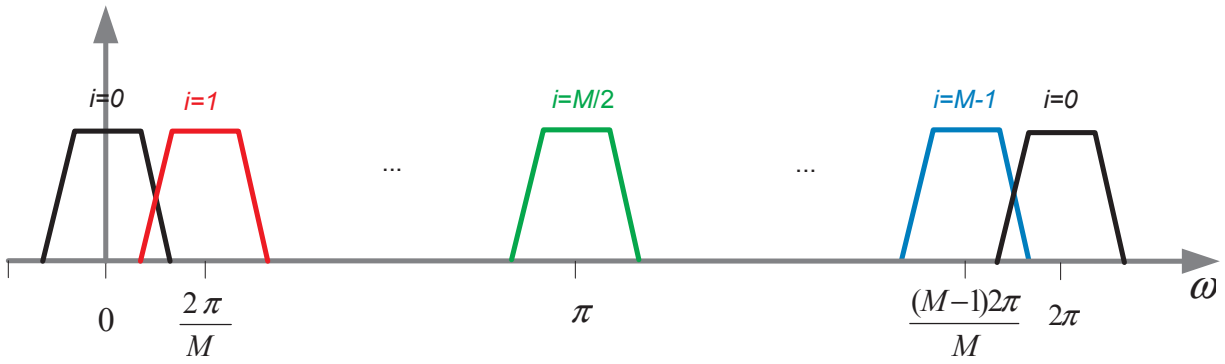

Fig. 2.16 DFT modulated filter bank

DFT Modulated Filter Banks

The DFT modulated FBs can be viewed as a complex extension of the cosine modulated ones. A common prototype filter is used to generate the subband filters but now the modulating sequence is complex-valued and the whole frequency range is divided into uniform subbands. In the literature, there exist many variations of complex modulated FBs, such as the modified DFT modulated FB [105] and the exponentially modulated FB [106, 107]. However, all these further developments of the modulated FB theory show similar characteristics to the basic DFT modulated FBs and can be fitted in the same category. In this approach, subband filters are shifted across the whole frequency range $[0, 2\pi]$, where it provides even-stacked subbands with complex conjugate property, as depicted in Figure 2.16. Considering the general transceiver structure in Figure 2.5, the time-domain coefficients of the synthesis and analysis subband filters in DFT modulated FBs, denoted as $f_i[n]$ and $g_i[n]$ respectively, can be obtained from those of the corresponding prototype filters coefficients, $f_p[n]$ and $g_p[n]$ respectively, through the following modulation operations:

$$f_i[n] = f_p[n]w^{-in} = f_p[n]e^{\jmath 2\pi in/M} \tag{2.36}$$

$$g_i[n] = g_p[n]w^{-in} = g_p[n]e^{\jmath 2\pi in/M} \tag{2.37}$$

for $0 \leq i \leq M-1$, $0 \leq n \leq D-1$ and $w = e^{-\jmath 2\pi/M}$. Thus, the system functions of the synthesis and analysis subband filters can be expressed as

$$F_i(z) = F_p(zw^i) = \sum_{n=0}^{D-1} f_p[n] w^{-in} z^{-n} \tag{2.38}$$

$$G_i(z) = G_p(zw^i) = \sum_{n=0}^{D-1} g_p[n] w^{-in} z^{-n} \tag{2.39}$$

where $F_p(z) = \sum_{n=0}^{D-1} f_p[n] z^{-n}$ and $G_p(z) = \sum_{n=0}^{D-1} g_p[n] z^{-n}$ represent the system functions of the synthesis and analysis prototype filters, respectively.

A key advantage of DFT modulated FBs over basic OFDM is that by employing longer prototype filters, much more selective subband filters can be designed. We point out however that having the PR property is not guaranteed by default and requires the use of special techniques in the design of the prototype filters. DFT modulated FB can be viewed as a generalized form of OFDM. In fact, if $K = M$, where K denotes the interpolation/decimation factor in Figure 2.5, and both $F_p(z)$ and $G_p(z)$ are M-tap rectangular filters, i.e., $f_p[n] = g_p[n] = 1$ for $0 \leq n \leq M-1$, the resulting synthesis/analysis DFT modulated FB reduces to the use of a simple IDFT/DFT operation, like the one being used for OFDM as in Figure 2.1 [36]. It can be shown that DFT modulated FB can be more efficiently implemented by employing the FFT algorithm and the polyphase decomposition of the prototype filters.

2.2.4 Oversampled Filter Banks

A FB used in either the subband processing or the transceiver configurations is called critically sampled if the interpolation/decimation factor is equal to the number of subbands, that is if $K = M$. As a result, in a critically sampled system, the transmission rate at the input and output of both the AFB and SFB is identical. In the transceiver configuration, when the interpolation/decimation factor is greater than the number of subbands, i.e., $K > M$, the FB is said to be oversampled[7]. In this case, on average, every K output

[7]In subband processing configuration (Figure 2.4), the condition $K < M$ represents the oversampled case.

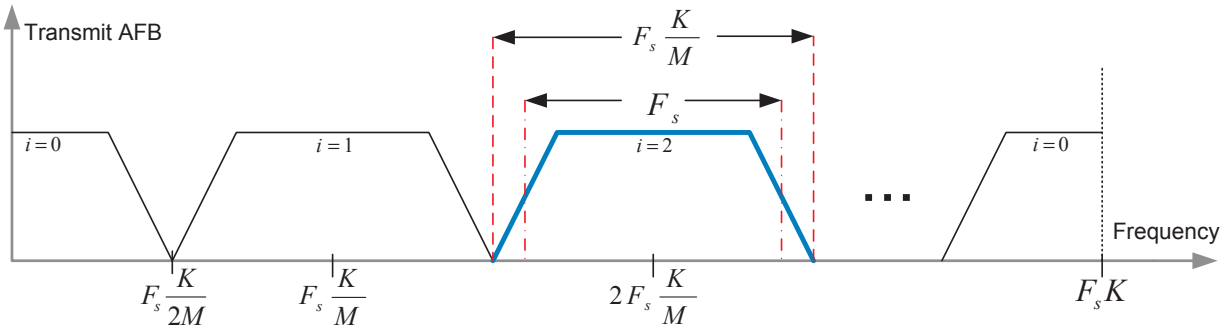

Fig. 2.17 Spectral characteristics of an oversampled FBMC system

samples of the transmitter contain $K - M$ redundant samples. Figure 2.17 illustrates the spectral characteristics of the transmit AFB, where the ith spectral shape corresponds to the frequency response of the ith subband filter. In this figure, $F_s K/M$ is the frequency spacing between adjacent subbands, where the sampling rate of the input signal in each band is $F_s = 1/T_s$. In effect, the transmission bandwidth $B = KF_s$ is divided to M equally spaced subchannels, where the signals on each channel occupy an effective bandwidth of F_s, which in total have a bandwidth of MF_s. Therefore, the spectral efficiency η of the system can be derived as

$$\eta = \frac{MF_s}{KF_s} = M/K \tag{2.40}$$

It is evident that larger oversampling ratio increases the frequency spacing and decreases the spectral efficiency. However, to achieve PR and good spectral containment in DFT modulated FBs, some redundancy should be added to the system and in this respect, oversampling is an ideal candidate to fulfill these requirements. The main advantage of oversampled FBs (i.e. $K > M$) over critically sampled ones ($K = M$) is that in the former case, additional design freedom is available that can be used to obtain PR property and additional spectral containment, hence, better interference and noise immunity within each subband. This additional design freedom is a consequence of the non-uniqueness of the receiving filters satisfying PR property, for a given set of oversampled transmitting filters [46].

The CP in OFDM systems and zero padding in vector coding transceiver systems [108] are examples of other common forms of redundancy. Consider a typical model of a broadband transmission system where the residual channel (following the time-domain equal-

ization) is represented by an FIR filter $H(z)$ of length L , i.e., $H(z) = \sum_{m=0}^{L-1} h[m]z^{-m}$. As mentioned in Section 2.1, in OFDM or the vector coding system, PR is achieved using redundancy in the form of CP or zero padding, where the amount of redundancy is $K - M \geq L$. Therefore, to remain competitive, these redundancies in oversampled FBs should not exceed that introduced by the CP or zero padding in these existing systems.

Over the past few decades, oversampled FBs have drawn a considerable amount of attention within the research community. Initially, most of the research was focused on the subband processing structure, as shown in Figure 2.4 with decimation and interpolation factors less than the number of subband filters, i.e., $K < M$ [46–48, 109, 110]. The connection between subband processing and MCM transceivers (i.e., transmultiplexing) system was first acknowledged by Vetterli in [102]. It can be shown that in the general oversampled case [103], a duality relationship between subband processing and transmultiplexer systems, such as the one established in [102, 111] for critically decimated systems, does not exist. However, for DFT modulated FBs, there exists such a duality relation between these two processing configurations [112]. As a result, any oversampled DFT modulated FB design, i.e. its prototype filter, can be used in both configurations, provided the number of subbands and oversampling factor are exchanged. In [46–51], it is established that the PR property of these oversampled systems is equivalent to the paraunitaryness of the polyphase matrices of transmit and receive FBs.

2.3 A Basic Survey of Different FBMC Types

In this section, some of the most popular FBMC techniques will be presented and their characteristics will be summarized.

2.3.1 Cosine Modulated Multitone

Cosine modulated multitone (CMT) is a common FBMC technique that employs cosine modulated FBs [16, 29]. The transceiver structure is similar to that in Figure 2.5, where the FB is critically sampled ($K = M$) and a delay block is added before the AFB at the receiver to adjust the total delay introduced by the system so that it is equal to an integral multiple of M. The subband filters of this system are derived through cosine modulation of the prototype filter as in (2.33) and (2.34). Although it is possible to design the prototype filter to achieve PR property in CMT systems [113], the authors prefer to design NPR FBs

and hence benefit from superior spectral containment of the subband filters as compared to the PR case [16, 17, 29]. In these works, the prototype filter is designed with the aim of minimizing ISI and/or ICI and maximizing the stopband attenuation.

For instance, a generalized windowing approach is used in [17] to design the prototype filter with a cost function $J(\mathbf{x})$ that sums ISI and ICI power, where $\mathbf{x}$ contains the design parameters. This method has the advantage of involving only four unknown adjustable parameters in the design process, independently of the number of subbands and the order of the prototype filter. The latter, denoted as $f_p[n]$, is obtained from the application of the window method [84] in the form

$$f_p[n] = w[n]h_c[n], \tag{2.41}$$

where $w[n]$ is a symmetric window function of length D[8] and $h_c[n]$ is the impusle response of an ideal lowpass filter given as

$$h_c[n] = \frac{\sin(\omega_c(n - \frac{D-1}{2}))}{\pi(n - \frac{D-1}{2})} \tag{2.42}$$

with ω_c being the cut-off frequency of the causal ideal lowpass filter. We note that in (2.42), the sinc function is shifted by $(D-1)/2$ to make $f_p[n]$ symmetrical and hence preserves the linear phase property. The particular window function under consideration in [17] is the generalized cosine window function with four terms, i.e.,

$$w[n] = \sum_{i=0}^{3} (-1)^i A_i \cos(\frac{2\pi i n}{D-1}) \tag{2.43}$$

where the weighting coefficients A_i, for $0 \leq i \leq 3$, are normalized such that $\sum_{i=0}^{3} A_i = 1$. Consequently, the complete CMT system under design is characterized by only four unknown parameters as represented by vector $\mathbf{x} = [A_0, A_1, A_2, \omega_c]$; these parameters are adjusted by minimizing the underlying cost function $J(\mathbf{x})$ referred to above.

In particular, as pointed out in Section 2.2.3, in the case of complex-valued input signals, channel non-linearities can cause phase rotations in the received signal, which in turn requires the use of more computationally expensive equalization or receiver structures.

[8] i.e., satisfying $w[n] = 0$ for $n < 0$ or $n \geq D$ and $w[n] = w[D-1-n]$

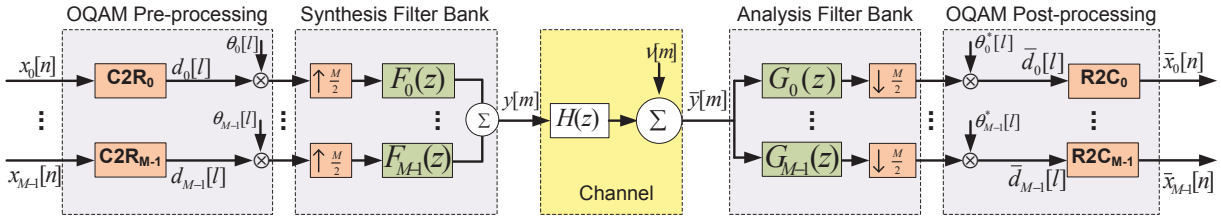

Fig. 2.18 OFDM/OQAM transceiver chain with OQAM pre-processing and post-processing blocks

Also, the extension of CMT to MIMO systems becomes challenging, and there has been only few reported studies for very specific applications [114].

2.3.2 OFDM/OQAM

OFDM with OQAM based modulation, denoted as OFDM/OQAM[9], is one of the most common FBMC techniques studied in the literature [15,18,34,43]. The core of OFDM/OQAM is a critically sampled transceiver structure as shown in Figure 2.18. Its main processing blocks consist of OQAM pre-processing, SFB, AFB and OQAM post-processing, in that order. The two OQAM processing blocks are used for the transformation between QAM and OQAM symbols so that only pure real or imaginary signals can be fed to the subband filters. The OQAM pre-processing block performs a simple complex-to-real conversion, where the real and imaginary parts of a complex-valued symbol $x_i[n]$ at time n are separated to form two new symbols, interlaced in time and denoted as $d_i[l]$, where $l = 2n$ and $l = 2n+1$. The order of these new symbols depends on the parity of the subband index as given by

$$d_i[2n] = \begin{cases} \mathsf{Re}[x_i[n]], & i \text{ even} \\ \mathsf{Im}[x_i[n]], & i \text{ odd} \end{cases} \tag{2.44}$$

$$d_i[2n+1] = \begin{cases} \mathsf{Im}[x_i[n]], & i \text{ even} \\ \mathsf{Re}[x_i[n]], & i \text{ odd} \end{cases} \tag{2.45}$$

[9]It is also referred to as staggered multitone or pulse-shaped OFDM.

This complex-to-real operation (denoted as C2R in the Figure 2.18) increases the sample rate by a factor of 2. The second operation is the multiplication by a complex exponential sequence

$$\theta_i[n] = e^{\jmath\frac{\pi}{2}(i+n)} = \jmath^{(i+n)} \tag{2.46}$$

It should be noted that the sign of $\theta_i[n]$ sequence can be chosen arbitrarily, but the pattern of real and imaginary samples has to follow the same definition as (2.46).

The operations in the SFB and AFB are similar to what has already been covered in Section 2.2, where the upsampling/downsampling factor is now $K = M/2$. This value of upsampling factor, combined with the doubling of the sampling rate in OQAM pre-processing block, makes the system critically sampled. In OFDM/OQAM systems, DFT modulated FBs or a similar types of complex modulation FBs, are often used to generate the subband filters from a single real-valued linear-phase prototype filter $f_p[m]$. Specifically, the impulse response of the subband synthesis and analysis filter, say $f_i[m]$ and $g_i[m]$ respectively, are obtained as

$$f_i[m] = f_p[m]e^{\jmath\frac{2\pi i}{M}(m-\frac{D-1}{2})} \tag{2.47}$$

$$g_i[m] = f_i^*[D-1-m] = f_p[m]e^{\jmath\frac{2\pi i}{M}(m-\frac{D-1}{2})} \tag{2.48}$$

where $0 \leq i \leq M-1$ and $0 \leq m \leq D-1$. When the prototype filter is linear phase, it can be seen from these expressions that the resulting subband filters are also linear phase. To guarantee downsampling at the correct phase, an extra delay has to be included at the input of the AFB [34].

Finally, the OQAM post-processing block converts back the outputs of the AFB to QAM symbols. To this end, the output of the ith AFB subchannel is multiplied by the complex conjugate sequence $\theta_i^*[n]$. Then, the real-to-complex conversion (denoted as R2C in the figure) is carried out in which two successive real-valued symbols, say $\bar{d}_i[2n]$ and $\bar{d}_i[2n+1]$, are combined to form a complex-valued symbol $\bar{x}_i[n]$ and these decrease the sample rate by a factor 2. The precise realization of this conversion depends on the parity

of the subband index, as given by

$$\bar{x}_i[n] = \begin{cases} \bar{d}_i[2n] + \jmath \bar{d}_i[2n+1], & i \text{ even} \\ \bar{d}_i[2n+1] + \jmath \bar{d}_i[2n], & i \text{ odd} \end{cases} \tag{2.49}$$

Regarding the design of OFDM/OQAM FBMC systems, the main focus is on the prototype filter. Although PR OFDM/OQAM designs are feasible, the high spectral containment of the prototype filter with NPR property is often favoured to the PR design. In particular, a frequency-domain technique, called as frequency sampling [115], is considered in [18, 43], where only a few adjustable parameters are required to derive the scalable closed-form formula for the prototype filter. The latter has length $D = LM - 1$, where L is a positive integer called overlapping factor. In this method, the IDFT of the desired frequency response at uniformly spaced frequency points is used to derive the prototype filter impulse response coefficients. The impulse response of the resulting real-valued symmetric FIR prototype filter can be formulated as [18]

$$f_p[m] = A[0] + 2\sum_{l=1}^{U} (-1)^l A[l] \cos\left(\frac{2\pi l}{LM}(m+1)\right) \tag{2.50}$$

the coefficient $A[l]$ are the desired values of the frequency response, the parameter $U = (LM-2)/2$ and $0 \leq m \leq D-1$. In [105] , it is shown that the proper lowpass filter characteristics, e.g., DC gain of unity, are guaranteed as long as the following holds.

$$\begin{aligned} &A[0] = 1 \\ &A[l]^2 + A[L-l]^2 = 1, \text{ for } 1 \leq l \leq \lfloor L/2 \rfloor \\ &A[l] = 0, \text{ for } L \leq l \leq U \end{aligned} \tag{2.51}$$

These relations reduce the number of free design parameters as for the common choice of $L = 4$, there is only one free parameter, in terms of which $A[0] = 1$, $A[1] = x$, $A[2] = 1/\sqrt{2}$ and $A[3] = \sqrt{1-x^2}$. Thus, based on the optimization criterion the coefficient $A[1]$ is adjusted.

Different frequency-domain design criteria have been investigated for such systems, where mostly the stopband region of the filter is taken into account in the objective function.

The stopband attenuation criterion (also called least squares) attempts to minimize the stopband energy of the prototype filter with the objective function defined as

$$J(x) = \int_{\omega_s}^{\pi} |F_p(e^{\jmath\omega})|^2 d\omega, \tag{2.52}$$

where ω_s is the stopband frequency. Alternatively, a minimax criterion can be employed where the objective function is defined as

$$J(x) = \max_{\omega\in[\omega_s,\pi]} |F_p(e^{\jmath\omega})| \tag{2.53}$$

and the goal is to minimize the maximum stopband ripple. Similar to the design criterion used in the CMT system described in Section 2.3.1, the total interference power that originates from the FB structure, including ICI and ISI, can also be considered as an objective function to be minimized.

The configuration shown in Figure 2.18 is not very efficient for practical applications because the filtering operations are performed at the higher sampling rate, leading to a huge amount of unnecessary calculations. Fortunately, various efficient structures have been proposed to reduce this complexity, including lapped transforms, lattice structures and polyphase structures [2,3]. However, the polyphase structures are the only one suitable for the NPR FBs [43]. In these structures, the filtering operations are done at the lower sampling rate and unnecessary calculations are avoided using the Noble identities provided in Section 2.2. Also, since DFT modulation is used to derive the subband filters, the polyphase matrix can be decomposed into the cascade of a DFT operation followed by multiplication with a simplified polyphase matrix.

Except for the type of modulation, OFDM/OQAM and CMT systems are developed based on similar principles and as such, a formal mathematical derivation of the relationship between these two types of systems is given in [19]. In terms of bandwidth efficiency, FBMC transceivers based on OFDM/OQAM, similar to their CMT counterpart in Section 2.3.1, are superior to OFDM, as they are critically sampled and do not employ a CP. If the number of subchannels is sufficiently large so that the channel frequency response over each subband can be approximated by a flat gain, a single-tap equalizer per subcarrier will suffice [29]. However, the use of OQAM pre-processing and post-processing blocks results in the increased complexity of OFDM/OQAM systems, as compared to OFDM

systems. Finally, the implementation of OFDM/OQAM systems in MIMO scenarios poses a practical difficulty, for the same reason as pointed out earlier for CMT [44, 45].

2.3.3 FMT

FMT is another FBMC approach based on multirate FBs that has been specifically developed for digital subscriber line (DSL) applications [32, 33] and has been subsequently investigated for application over wireless channels [21]. In this method, the subband filters are derived by DFT modulation of a common prototype filter and the transceiver structure is similar to the general FB structure depicted in Figure 2.5. A computationally efficient DFT-based polyphase FB architecture is proposed for these systems in [32,33]. As opposed to CMT and OFDM/OQAM methods which employ critically sampled FBs, FMT allows the use of oversampling and, as a result, the added redundancy can be used to gain desirable properties, such as frequency guard bands as in Figure 2.17. However, the critically sampled implementation of the FMT is also possible.

In FMT, the DFT modulated transmit and receive subband filters are obtained by frequency shift of two prototype filters, respectively $f_p[n]$ and $g_p[n]$ as in (2.36) and (2.37), where the receive prototype filter is matched to the transmit one, i.e., $g_p[n] = f_p^*[D - 1 - n]$. The design of the prototype filter is one of the main research problems related to FMT, where ICI and ISI can be minimized or even completely removed. However, most of this research is focused on NPR design where a tradeoff between the minimization of ICI and/or ISI and the spectral containment, e.g., higher stopband attenuation, is pursued [32, 33, 41, 42]. Moreover, some conventional filters including sinc, Gaussian, and truncated square-root raised cosine filters, are employed as prototypes for FMT systems and their performance is compared with OFDM [41, 58, 116].

Communication systems that employ multi-antenna MIMO configurations to increase the system throughput and the reliability of the link have become very popular in the past decade. Unlike some popular FBMC methods, e.g., CMT and OFDM/OQAM, the application of FMT to MIMO channels is straightforward [117–119]. Moreover, it is shown that FMT can have better performance than OFDM due to the better sub-channel spectral containment. In particular, compared to OFDM, a simple one-tap equalizer per subchannel is sufficient to yield superior signal-to-interference ratio (SIR) and BER performance for FMT in fast fading environments [41, 58, 116]. Although MCM systems are robust to

channel frequency selectivity, they are sensitive to CFO [12, 61–64], but FMT appears to be more robust to this this kind of channel impairment [120].

2.3.4 DFT modulated OPRFB

As previously mentioned, the prototype filter of FMT systems is not designed such that PR is enforced [32, 33, 41, 42], however, the goal of achieving PR property is desirable. In practice, even in the presence of a non-ideal channel, the PR property can be exploited to simplify equalization. While the PR requirement makes the FB design more challenging, oversampling provides the extra design freedom to fulfill this property [46]. Recently, a new type of FBMC systems, denoted here as OPRFB systems has been proposed, where DFT modulated oversampled FBs are employed to achieve the PR property as well as other beneficial spectral containment features [35, 36]. In terms of configuration and structure, these systems are similar to FMT, however, the PR property is enforced and as a result the FB is restricted to oversampled FBs.

In [35], it has been demonstrated that the parameterization of the polyphase matrix in the oversampled case can be achieved with different degrees of freedom, i.e. with different numbers of independent rotation parameters, but this approach does not provide a formal construction algorithm and the solution sets are redundant. Also, it is recognized that the design becomes significantly complex as the number of subbands increases. Therefore, it has been proposed to perform polynomial fitting of the design parameters to reduce the degree of freedom, but this however yields a quasi-orthogonal FB. Similarly, the design approach proposed in [36] suffers from its use of a large number of design parameters. In general, in the case of a large number of subbands, the number of design parameters to be optimized increases drastically and the conventional design processes rapidly becomes computationally prohibitive. In the same way, increasing the spectral efficiency (i.e., K/M close to 1) can make the design process overwhelming. However, high spectral efficiency is of particular interest.

Yet considering the performance of current third generation (3G) broadband wireless communication systems and the anticipated requirement for fourth generation (4G) and beyond [8], this limiting cases are currently of great practical interest. In the next chapter the OPRFB will be investigated in detail, where an efficient design method is presented.

Chapter 3

OPRFB Transceivers

In this chapter[1], we present an efficient design method for OPRFB transceivers. The system model under study and the associated design problem are exposed in Section 3.1. A convenient decomposition of the polyphase filtering matrices of the transmit and receive sub-systems into main paraunitary factors is developed in Section 3.2. In Section 3.3, the final parameterization of the polyphase matrices is achieved through a further decomposition of one of these factors into elementary paraunitary building blocks. The design of the resulting OPRFB through optimization of their parameters is presented in Section 3.4, along with design examples of prototype filters. Experimental results of the proposed OPRFB transceivers are investigated through numerical simulations under different channel and interference conditions in Section 3.5. Finally, Section 3.6 concludes the chapter.

3.1 Background and Problem Formulation

The OPRFB transceiver system under consideration is depicted in Figure 3.1, where integer parameters M and K represent the number of subbands and the upsampling factor, respectively; as explained before, we consider oversampled FBs, where $K > M$. Let $x_i[n]$ denote the complex-valued data sequence transmitted on the ith subband, $i \in \{0, \ldots, M-1\}$, where $n \in \mathbb{Z}$ is the discrete-time index at the low sampling rate F_s. Sequence $x_i[n]$ is expanded by a factor of K and then passed through its corresponding subband filter with system function $F_i(z) = \sum_{m \geq 0} f_i[m] z^{-m}$, where $f_i[m]$ denotes the filter impulse response

[1]Parts of Chapter 3 have been presented at the 2011 European Signal Processing Conference [37].

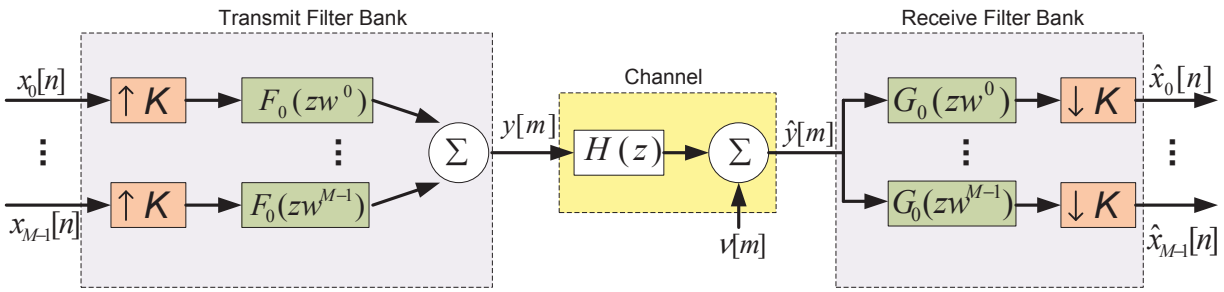

Fig. 3.1 Oversampled FB transceiver

and $z \in \mathbb{C}$. The filtered signals are then added together to form the transmitter output $y[m]$, where $m \in \mathbb{Z}$ is the discrete-time index at the high sampling rate KF_s:

$$y[m] = \sum_{i=0}^{M-1} \sum_{n=-\infty}^{\infty} f_i[m - nK] x_i[n]. \tag{3.1}$$

In an actual implementation, $y[m]$ would be D/A converted and modulated for transmission over a desired frequency band, followed by demodulation and A/D conversion on the receiver side; here, we focus on a baseband representation of these operations which is equivalent from a signal processing viewpoint. The physical transmission channel (including transmitter back-end and receiver front-end) is modeled as a linear time-invariant discrete-time filter with finite impulse response (FIR) $h[l]$ and corresponding system function $H(z) = \sum_{l=0}^{Q-1} h[l] z^{-l}$, where positive integer Q denotes the filter length. During its transmission, signal $y[m]$ is corrupted by various additive perturbation sources (radio interference, crosstalk, thermal noise, etc.). Accordingly, the channel output is expressed as

$$\hat{y}[m] = \sum_{l=0}^{Q-1} h[l] y[m - l] + \eta[m] + \beta[m] \tag{3.2}$$

where $\eta[m]$ is modeled as a (zero-mean) additive white Gaussian noise (AWGN) process and $\beta[m]$ denotes other possible interferences.

In the receiver, the ith subband signal $\hat{x}_i[n]$ is recovered by passing the channel output $\hat{y}[m]$ through a corresponding subband filter with system function $G_i(z) = \sum_{m \geq 0} g_i[m] z^m$, where $g_i[m]$ denotes the (time-reversed) impulse response (for convenience in analysis, $G_i(z)$ is assumed to be non-causal; in practice, causality can be restored simply by introducing

an appropriate delay in the receiver), and decimating the result by a factor of K:

$$\hat{x}_i[n] = \sum_{m=-\infty}^{\infty} g_i[m - nK]\hat{y}[m]. \tag{3.3}$$

As discussed in Section 2.2.3, the transmit and receive subband filters of a DFT modulated FB are derived from common prototype filters, typically of the FIR type with system functions $F_0(z) = \sum_{n=0}^{D-1} f_0[n]z^{-n}$ and $G_0(z) = \sum_{n=0}^{D-1} g_0[n]z^n$, respectively, where D is the common filter length. In this work, D is restricted to be a multiple of M and K, i.e. $D = d_M M = d_K K$, where d_M and d_K are positive integers. Denoting by P the least common multiple of M and K, we can also write $D = d_P P$ and $P = p_M M = p_K K$, with d_P, p_M and p_K integers. Defining $w = e^{-\jmath 2\pi/M}$, the system functions of the transmit and receive filters for the ith subband are respectively obtained as

$$F_i(z) = F_0(zw^i) = \sum_{n=0}^{D-1} f_0[n]w^{-in}z^{-n}, \tag{3.4}$$

$$G_i(z) = G_0(zw^i) = \sum_{n=0}^{D-1} g_0[n]w^{in}z^{n}. \tag{3.5}$$

Let us consider the K-fold polyphase representation of the ith transmit filter $F_i(z)$:

$$F_i(z) = \sum_{r=0}^{K-1} z^{-r} P_{i,r}(z^K), \tag{3.6}$$

$$P_{i,r}(z) = \sum_{n=0}^{d_K-1} f_0[Kn + r]w^{-i(Kn+r)}z^{-n}. \tag{3.7}$$

We define the $K \times M$ transmit polyphase matrix $\mathbf{P}(z)$, with entries $[\mathbf{P}(z)]_{r,i} = P_{i,r}(z)$ for $r \in \{0, \ldots, K-1\}$ and $i \in \{0, \ldots, M-1\}$. Similarly, the ith receive filter $G_i(z)$ admits the polyphase representation

$$G_i(z) = \sum_{r=0}^{K-1} z^{r} R_{i,r}(z^K), \tag{3.8}$$

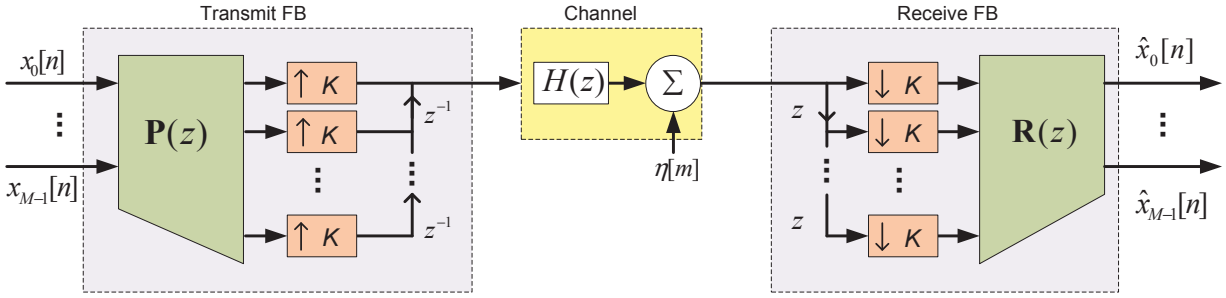

Fig. 3.2 Oversampled DFTM FB transceiver in polyphase representation

$$R_{i,r}(z) = \sum_{n=0}^{d_K-1} g_0[Kn+r] w^{i(Kn+r)} z^n. \tag{3.9}$$

We also define the $M \times K$ receive polyphase matrix $\mathbf{R}(z)$, with entries $[\mathbf{R}(z)]_{i,r} = R_{i,r}(z)$. Using the above polyphase matrix representations in combination with Noble identities [2], the FB transceiver structure in Figure 3.1 can be represented as shown in Figure 3.2.

To ensure that transmission is free from ISI and ICI, the prototype filter characteristics are often chosen to satisfy a PR constraint [33,35,36], where in the case of an ideal channel (i.e. $H(z) = 1$, $\eta[m] = 0$ and $\beta[m] = 0$), the PR conditions is stated as $\hat{x}_i[n] = cx_i[n]$ for all $i \in \{0, \ldots, M-1\}$ and $n \in \mathbb{Z}$, where c is a constant. Alternatively, this can be expressed in terms of the transmit and receive polyphase matrices as [35]

$$\mathbf{R}(z)\mathbf{P}(z) = c\mathbf{I}_M. \tag{3.10}$$

In this work, we consider that the transmit and receive prototype filters are paraconjugate of each other, i.e. $G_0(z) = \tilde{F}_0(z)$ or equivalently, $g_0[n] = f_0^*[n]$. Selecting the receive prototype filter in this way implies that the polyphase matrices of the transmit and receive FBs are also paraconjugate, i.e., $\mathbf{R}(z) = \tilde{\mathbf{P}}(z)$ [2]. Consequently, if $\mathbf{P}(z)$ can be made paraunitary, then the PR property of the transceiver system will be achieved since $\mathbf{R}(z)\mathbf{P}(z) = \tilde{\mathbf{P}}(z)\mathbf{P}(z) = c\mathbf{I}_M$. In this case, and assuming an ideal channel, the output of each subband on the receiver side will be a scaled replica of the corresponding subband input on the transmitter side, or $\hat{x}_i[n] = cx_i[n]$.

In addition to guaranteeing the PR property of the system, there are numerous advantages for choosing paraunitary FBs as above [2]: no matrix inversion is required in the

design; the transmit and receive filters are FIR with the same length, and can be obtained by time-reversal and conjugation of each other (paraconjugate operator); the passband region of the prototype filter's magnitude response is constant and the objective function does not have to explicitly include passband error. Within this framework, the main problems addressed in this section can be stated as follows:

(1) To find an efficient parameterization of the prototype filter coefficients $f_0[n]$, in terms of a parameter vector $\boldsymbol{\theta}$ with reduced dimensionality, such that the transmit and receive polyphase matrices are paraunitary and the resulting FBs benefits from the PR property (3.10);

(2) Through the choice of a suitable objective function and its optimization over the parameter space, to design improved OPRFBs for applications to broadband multicarrier transmissions under practical impairments.

3.2 A Factorization of Polyphase Matrix $\mathbf{P}(z)$

In this section, the polyphase matrix of the OPRFB, $\mathbf{P}(z)$, is decomposed into paraunitary factors to establish the PR property. First, we factor the DFT matrix out of $\mathbf{P}(z)$ and highlight that the remaining matrix term, denoted $\mathbf{U}(z)$, should be paraunitary as well. Next, we investigate the structure of $\mathbf{U}(z)$, especially the relationship between its entries and to the desired prototype filter coefficients.

Finally, we explain how to generate a matrix $\mathbf{U}(z)$ with the desired structure in terms of paraunitary building blocks.

3.2.1 Preliminary Factorization of $\mathbf{P}(z)$

We consider the factorization of the polyphase matrices $\mathbf{P}(z)$ (and consequently $\mathbf{R}(z)$) using an approach similar to that in [36,121]. We begin by defining the $M \times M$ DFT matrix $\mathbf{W}$, with entries $[\mathbf{W}]_{i,j} = w^{ij}$, for all $i, j \in \{0, \ldots, M-1\}$. We also define the block matrices $\mathbf{L}_0$ and $\mathbf{L}_1(z)$, of respective sizes $D \times M$ and $K \times D$, as follows

$$\mathbf{L}_0 = [I_M, I_M, \ldots, I_M]^T, \tag{3.11}$$

$$\mathbf{L}_1(z) = [I_K, z^{-1}I_K, \ldots, z^{-(d_K-1)}I_K]. \tag{3.12}$$

Considering first the transmit FB, we represent the D coefficients of the prototype filter $F_0(z)$ by means of diagonal matrix

$$\mathbf{\Gamma}_f = \text{diag}(f_0[0], \ldots, f_0[D-1]). \tag{3.13}$$

Then, using the fact that $w^{M+c} = w^c$, we can write $\mathbf{P}(z)$ in a factored form as follows (see Appendix A):

$$\mathbf{P}(z) = \mathbf{L}_1(z)\mathbf{\Gamma}_f\mathbf{L}_0\mathbf{W}^* = \mathbf{U}(z)\mathbf{W}^*, \tag{3.14}$$

where we define

$$\mathbf{U}(z) = \mathbf{L}_1(z)\mathbf{\Gamma}_f\mathbf{L}_0. \tag{3.15}$$

Proceeding as above, the following factorization can be developed for the receive FB:

$$\mathbf{R}(z) = \mathbf{W}\mathbf{L}_0^T\mathbf{\Gamma}_h\tilde{\mathbf{L}}_1(z), \tag{3.16}$$

where $\mathbf{\Gamma}_h = \text{diag}(h_0[0], \ldots, h_0[D-1]) = \mathbf{\Gamma}_f^*$. Therefore, we can write

$$\mathbf{R}(z) = \mathbf{W}\tilde{\mathbf{U}}(z) = \tilde{\mathbf{P}}(z). \tag{3.17}$$

Finally, since $\mathbf{W}\mathbf{W}^* = M\mathbf{I}_M$, we note from (3.14) that the paraunitaryness of $\mathbf{P}(z)$ will follow automatically from that of $\mathbf{U}(z)$. That is:

$$\mathbf{R}(z)\mathbf{P}(z) = \mathbf{W}\tilde{\mathbf{U}}(z)\mathbf{U}(z)\mathbf{W}^* = M\mathbf{I}_M \tag{3.18}$$

if $\tilde{\mathbf{U}}(z)\mathbf{U}(z) = \mathbf{I}_M$.

3.2.2 Structure of $\mathbf{U}(z)$

In order to fulfil the PR property, the paraunitaryness of $\mathbf{U}(z)$ should be guaranteed in the design process. Thus, the structure of $\mathbf{U}(z)$ will be further examined in this section. We begin by partitioning the $D \times M$ matrix $\mathbf{\Gamma}_f\mathbf{L}_0$ into the following format,

$$\mathbf{\Gamma}_f\mathbf{L}_0 = [\mathbf{F}_0^T|\mathbf{F}_1^T|\ldots|\mathbf{F}_{d_K-1}^T]^T, \tag{3.19}$$

where matrices $\mathbf{F}_n$, $n \in \{0, \ldots, d_K - 1\}$, are of size $K \times M$ with entries

$$[\mathbf{F}_n]_{i,r} = \begin{cases} f_0[nK + i], & \text{if } nK + i \equiv r \pmod{M} \\ 0, & \text{otherwise} \end{cases} \tag{3.20}$$

Matrix $\mathbf{U}(z)$ (3.15) can then be expressed as

$$\mathbf{U}(z) = \mathbf{L}_1(z)[\mathbf{F}_0^T|\mathbf{F}_1^T|\ldots|\mathbf{F}_{d_K-1}^T]^T = \sum_{n=0}^{d_K-1} \mathbf{F}_n z^{-n}. \tag{3.21}$$

Introducing the change of variables $n = qp_K + \alpha$, where $q \in \{0, \ldots, d_P - 1\}$ and $\alpha \in \{0, \ldots, p_K - 1\}$, we can rewrite $\mathbf{U}(z)$ as

$$\mathbf{U}(z) = \sum_{q=0}^{d_P-1} \sum_{\alpha=0}^{p_K-1} \mathbf{F}_{qp_K+\alpha}\, z^{-qp_K-\alpha}. \tag{3.22}$$

Noting that $p_K K = P$ and $P \equiv 0 \pmod{M}$, we obtain from (3.20) that

$$[\mathbf{F}_{qp_K+\alpha}]_{i,r} = \begin{cases} f_0[qP + \alpha K + i], & \alpha K + i \equiv r \pmod{M} \\ 0, & \text{otherwise} \end{cases} \tag{3.23}$$

We note that given a pair of indices (i, r), $[\mathbf{F}_{qp_K+\alpha}]_{i,r}$ is identically zero except possibly for one specific value of $\alpha \in \{0, \ldots, p_K - 1\}$ which, if it exists, is denoted as $\alpha_{i,r}$ and satisfies

$$\alpha_{i,r} K + i \equiv r \pmod{M}. \tag{3.24}$$

If this is the case, then it follows from (3.23) and (3.24) that

$$[\mathbf{U}(z)]_{i,r} = z^{-\alpha_{i,r}} \sum_{q=0}^{d_P-1} f_0[qP + \alpha_{i,r}K + i] z^{-qp_K}; \tag{3.25}$$

otherwise $[\mathbf{U}(z)]_{i,r} = 0$. Finally, by introducing the polynomials

$$G_{i,r}(z) = \sum_{q=0}^{d_P-1} f_0[qP + \alpha_{i,r}K + i] z^{-q}, \tag{3.26}$$

we can simplify equation (3.25) as

$$[\mathbf{U}(z)]_{i,r} = z^{-\alpha_{i,r}} G_{i,r}(z^{p_K}). \tag{3.27}$$

3.2.3 Expressing $\mathbf{U}(z)$ in terms of Paraunitary Building Blocks

Several efficient parameterizations of paraunitary matrices have been developed and studied in the literature. Here, we would like to employ some of these parameterizations to construct matrix $\mathbf{U}(z)$. Unfortunately, the elements of an arbitrarily generated paraunitary matrix, say $\mathbf{B}(z)$, will not in general match the structure of $\mathbf{U}(z)$ in (3.15). That is, $\mathbf{B}(z)$ must be further restricted such that its components are compatible with $\mathbf{U}(z)$. The exact way of realizing this depends on whether or not M and K are coprime. The details are provided below.

M and K coprime

When M and K are coprime, i.e. when the least common multiple of M and K is their product $P = MK$ [122], we have $p_K = M$ and $p_M = K$ and, consequently, a unique $\alpha_{i,r}$ in (3.24) exists for all the entries of $\mathbf{U}(z)$. We define two paraunitary matrices $\mathbf{D}_0(z)$ and $\mathbf{D}_1(z)$ as

$$\mathbf{D}_0(z) = \mathrm{diag}(z^{\alpha_{0,0}}, z^{\alpha_{1,0}}, \ldots, z^{\alpha_{p_M-1,0}}), \tag{3.28}$$

$$\mathbf{D}_1(z) = \mathrm{diag}(z^{\alpha_{0,0}}, z^{\alpha_{0,1}}, \ldots, z^{\alpha_{0,p_K-1}}). \tag{3.29}$$

The entries of the product $\mathbf{D}_0(z)\mathbf{U}(z)\mathbf{D}_1(z)$ can be written as

$$[\mathbf{D}_0(z)\mathbf{U}(z)\mathbf{D}_1(z)]_{i,r} = z^{\alpha_{i,0}+\alpha_{0,r}} [\mathbf{U}(z)]_{i,r}. \tag{3.30}$$

Using the index pairs $(i,0)$, $(0,r)$, and (i,r) in (3.24), we can show that $(\alpha_{i,0} + \alpha_{0,r} - \alpha_{i,r})K \equiv 0 \pmod{M}$. Equivalently, introducing

$$\hat{\alpha}_{i,r} = \alpha_{i,0} + \alpha_{0,r} - \alpha_{i,r}, \tag{3.31}$$

we have

$$\hat{\alpha}_{i,r} K \equiv 0 \pmod{M}. \tag{3.32}$$

Then, by using (3.27), we can rewrite (3.30) as

$$[\mathbf{D}_0(z)\mathbf{U}(z)\mathbf{D}_1(z)]_{i,r} = z^{\hat{\alpha}_{i,r}} G_{i,r}(z^{p_K}). \tag{3.33}$$

Since $0 \leq \alpha_{i,r} < p_K$, $\hat{\alpha}_{i,r}$ can take only two values, i.e. 0 or p_K. Accordingly, the entries of $\mathbf{D}_0(z)\mathbf{U}(z)\mathbf{D}_1(z)$ are polynomials in z^{p_K}. Let $\mathbf{B}(z)$ be an arbitrary paraunitary matrix $\mathbf{B}(z)$ of order $L-1$ with entries

$$[\mathbf{B}(z)]_{i,r} = \sum_{q=0}^{L-1} b_{i,r}[q] z^{-q}. \tag{3.34}$$

Then, it follows from (3.29)-(3.30) that

$$\mathbf{U}(z) = \tilde{\mathbf{D}}_0(z)\mathbf{B}(z^{p_K})\tilde{\mathbf{D}}_1(z), \tag{3.35}$$

$\mathbf{U}(z)$ will be paraunitary as well and the PR condition will be satisfied.

Hence, each entry of $\mathbf{U}(z)$ can be represented in terms of the corresponding entry of $\mathbf{B}(z)$ as

$$[\mathbf{U}(z)]_{i,r} = z^{-(\alpha_{i,0}+\alpha_{0,r})} [\mathbf{B}(z^{p_K})]_{i,r} \tag{3.36}$$

Clearly, this will be consistent with (3.28) if the following identity is satisfied:

$$[\mathbf{B}(z^{p_K})]_{i,r} = z^{\hat{\alpha}_{i,r}} G_{i,r}(z^{p_K}) = z^{\hat{\alpha}_{i,r}} \sum_{q=0}^{d_P-1} f_0[qP + \alpha_{i,r}K + i] z^{-qp_K} \tag{3.37}$$

which is the desired equation linking the prototype filter coefficients to the entries of an arbitrary paraunitary matrix. Depending on the value of $\hat{\alpha}_{i,r}$, the coefficients of the prototype filter for $i \in \{0, \ldots, K-1\}$, $r \in \{0, \ldots, M-1\}$, and $q \in \{0, \ldots, d_P - 2\}$, can be retrieved as

$$\hat{\alpha}_{i,r} = 0 \implies \begin{cases} f_0[qP + \alpha_{i,r}K + i] = b_{i,r}[q] \\ f_0[D - P + \alpha_{i,r}K + i] = 0 \end{cases} \tag{3.38}$$

$$\hat{\alpha}_{i,r} = p_K \implies \begin{cases} f_0[(q+1)P + \alpha_{i,r}K + i] = b_{i,r}[q] \\ f_0[\alpha_{i,r}K + i] = 0 \end{cases} \tag{3.39}$$

where some of the prototype filter coefficients are pre-assigned to zero based on (3.37)[2]. Moreover, the proper value of L, corresponding to the matrix $\mathbf{B}(z)$, can be determined to be $L = d_P - 1$ such that there is enough entries to derive all the remaining prototype filter coefficients and preserve the PR property of the system.

M and K non-coprime

In this case, we can not find the proper $\alpha_{i,r}$ that satisfy (3.24) for some pairs (i, r). Thus, the resulting $\mathbf{U}(z)$ consists of zero and non-zero entries. Let τ denote the greatest common divisor of K and M, i.e. $\tau = KM/P$. For $l \in \{0, \ldots, \tau - 1\}$, we define the $p_M \times p_K$ submatrices $\mathbf{U}_l(z)$ in terms of entries of $\mathbf{U}(z)$ as

$$[\mathbf{U}_l(z)]_{a,b} = [\mathbf{U}(z)]_{l+a\tau,l+b\tau}, \tag{3.40}$$

where $a \in \{0, \ldots, p_M - 1\}$, $b \in \{0, \ldots, p_K - 1\}$ and the entries of $\mathbf{U}(z)$ are provided by (3.25). According to [48], the paraunitaryness of $\mathbf{U}_l(z)$ for $l \in \{0, \ldots, \tau - 1\}$ guarantees the paraunitaryness of $\mathbf{U}(z)$. It is straightforward to show that for $i = l + a\tau$ and $r = l + b\tau$, the congruence relation (3.24) can be simplified to

$$\alpha_{l+a\tau,l+b\tau} p_M + a \equiv b \pmod{p_K}. \tag{3.41}$$

Because p_K and p_M are coprime, the $p_M \times p_K$ submatrices $\mathbf{U}_l(z)$ can now be expressed in a similar fashion as in the previous subsection, i.e. (3.36). Specifically, let $\mathbf{B}_l(z)$ for $l \in \{0, \ldots, \tau - 1\}$ be arbitrary paraunitary matrices of size $p_M \times p_K$. Each one of these matrices can be mapped to its corresponding FB polyphase submatrix $\mathbf{U}_l(z)$ through the following transformation

$$\mathbf{U}_l(z) = \tilde{\mathbf{D}}_0(z)\mathbf{B}_l(z^{p_K})\tilde{\mathbf{D}}_1(z). \tag{3.42}$$

Note that when M and K are non-coprime, τ different matrices $\mathbf{B}_l(z)$ should be generated.

[2]The assignments of these coefficients to zero explains the different ranges of variation for q in (3.37) and (3.38)-(3.39)

3.3 Choice of a Parameterization for Paraunitary Matrix $\mathbf{B}(z)$

In this section, different approaches to parameterize a paraunitary matrix are investigated and compared to find the most efficient way to build matrix $\mathbf{B}(z)$ in the coprime case (3.34) or matrices $\mathbf{B}_l(z)$ for $l \in \{0, \ldots, \tau - 1\}$ in the non-coprime case (3.42)[3]. To this end, a constructive procedure for factoring a paraunitary polynomial matrix $\mathbf{B}(z)$ with order $L-1$ as a product of elementary paraunitary matrices is required.

A basic approach for the factorization of paraunitary matrix with constrained filter length is proposed in [52]. By employing this *order-based* method, any paraunitary matrix of order $L-1$ can be factorized into a product of $L-1$ order-one building blocks. This method is implemented in [37] to parameterize the polyphase matrix for design of real prototype filters of OPRFB. The completeness[4] of this order-based method is proved in [53], where it is developed into a more efficient structure based on the cosine-sine (CS) decomposition of Hermitian unitary matrices. As a result, compared to the order-based method in [52], the authors of [53] are able to reduce the number of free parameters by half in their method, denoted as cosine-sine decomposition *(CSD)-based* method here. However, as noted in [54], even though being complete and minimal[5], the CSD-based method involves redundant parameterized subsets. Thus, by consecutive removal of extra degrees of freedom in adjacent stages, another factorization method, denoted as *post-filtering based* method, is developed in [54], which can further reduce the number of parameters. Here, we develop these three parametrization methods, namely order-based, CSD-based and post-filtering based, and then compare them in terms of number of parameters required to represent a arbitrary paraunitary matrix.

3.3.1 Order-based method

We first generate a square $p_M \times p_M$ paraunitary matrix $\mathbf{\Delta}(z)$, then apply the transformation

$$\mathbf{B}(z) = \mathbf{\Delta}(z)\mathbf{\Upsilon}, \tag{3.43}$$

[3] To simplify the presentation, we use the same notation, $\mathbf{B}(z)$, for both cases

[4] A paraunitary factorization is said to be complete if any paraunitary matrix can be factorized in that form.

[5] A structure (or implementation or realization) is said to be minimal if the number of delay elements is the smallest possible.

where $\mathbf{\Upsilon}^T = [\mathbf{I}_{p_K}, \mathbf{0}_{p_K \times (p_M - p_K)}]$. With regard to $\mathbf{\Delta}(z)$, the decomposition for an $p_M \times p_M$ paraunitary matrix in terms of order-one paraunitary matrices as in [2, 52] is used. For a paraunitary matrix of order $L-1$, this decomposition can be written in terms of delay matrices and unitary matrices as follows

$$\mathbf{\Delta}(z) = \mathbf{R}_{L-1}\mathbf{\Lambda}(z)\mathbf{R}_{L-2}\mathbf{\Lambda}(z)\dots\mathbf{R}_0, \tag{3.44}$$

where $\mathbf{\Lambda}(z)$ is a delay matrix

$$\mathbf{\Lambda}(z) = \mathrm{diag}(\mathbf{I}_{p_M - r_c}, z^{-1}\mathbf{I}_{r_c}), \tag{3.45}$$

with $r_c = \lfloor p_M/2 \rfloor$ and $\mathbf{R}_j$ is a unitary product of $p_M(p_M-1)/2$ Givens rotation matrices [123]:

$$\mathbf{R}_j = \prod_{p=0}^{p_M-1} \prod_{q=p+1}^{p_M-1} \mathbf{G}_{p,q}(\theta_{p,q}^j) \tag{3.46}$$

For each real Givens rotation matrix $\mathbf{G}_{p,q}(.)$, one parameter $\theta_{p,q}^j$ is required [124]. Due to the fact that there are $p_M(p_M-1)/2$ different off-diagonal positions above the diagonal, the number of parameters $\mu_r^{(1)}$ required to construct a $p_M \times p_M$ real paraunitary matrix as in (3.44) is

$$\mu_r^{(1)} = Lp_M(p_M-1)/2. \tag{3.47}$$

Recall that the factorization of $\mathbf{B}(z)$ is performed to obtain the parameterized prototype filter coefficients. By using the real Givens rotation matrices, all the coefficients of the resulting prototype filter will be real. Since DFT modulated FBs are being utilized, there is no advantage in employing real prototype filters in terms of implementation cost, while prototype filters with complex coefficients may benefit from better spectral containments. Therefore, by using complex Givens rotation matrices, we can remove this constraint and assess the characteristics of the resulting complex prototype filters compared to the real ones. Note that for each complex Givens rotation matrix two arbitrary rotation angles are needed, say θ_1 and θ_2, where a 2×2 complex Givens rotation matrix is given by

$$\begin{bmatrix} \cos\theta_1 & e^{\jmath\theta_2}\sin\theta_1 \\ -e^{-\jmath\theta_2}\sin\theta_1 & \cos\theta_1 \end{bmatrix} \tag{3.48}$$

Note that the real Givens rotation matrix is obtained by setting $\theta_2 = 0$ in (3.48). Similar to the real case, $\mu_c^{(1)}$ denotes the number of parameters to construct a $p_M \times p_M$ complex paraunitary matrix as:

$$\mu_c^{(1)} = Lp_M(p_M - 1). \tag{3.49}$$

3.3.2 CSD-based method

In [53], based on the singular value decomposition (SVD) of coefficient matrices of $\mathbf{\Delta}(z)$, it was proved that (3.44) is complete and any paraunitary matrix $\mathbf{\Delta}(z)$ can be represented via (3.44). However, due to the highly nonlinear relation between the rotation angles in (3.44)-(3.46) and the resulting coefficients of matrix $\mathbf{B}(z)$, it is reasonable to characterize it with fewer parameters and reduce the optimization complexity. In [53], it has been shown that there are some redundancies in the representation (3.44)-(3.46) of $\mathbf{\Delta}(z)$ and that the number of required parameters can indeed be reduced. Specifically, (3.44) can be factored as

$$\mathbf{\Delta}(z) = \bar{\mathbf{R}}_{L-1}(z)\bar{\mathbf{R}}_{L-2}(z)\dots\mathbf{R}_0, \tag{3.50}$$

where $\bar{\mathbf{R}}_l(z)$, which stands for the product $\mathbf{R}_l\mathbf{\Lambda}(z)$, takes the form

$$\bar{\mathbf{R}}_l(z) = \frac{1}{2}(\mathbf{I} + \mathbf{A}_l) + \frac{1}{2}(\mathbf{I} - \mathbf{A}_l)z^{-1}. \tag{3.51}$$

In this representation, $\mathbf{A}_l$ is a Hermitian unitary matrix with the special structure

$$\mathbf{A}_l = \mathrm{diag}(\mathbf{V}_l, \mathbf{W}_l)\mathbf{Q}_l\mathbf{\Gamma}_l\mathbf{Q}_l\mathrm{diag}(\mathbf{V}_l^H, \mathbf{W}_l^H), \tag{3.52}$$

where, $\mathbf{V}_l$ and $\mathbf{W}_l$ are $\lfloor p_M/2 \rfloor \times \lfloor p_M/2 \rfloor$ and $\lceil p_M/2 \rceil \times \lceil p_M/2 \rceil$ unitary matrices, respectively, $\mathbf{\Gamma}_l$ is a diagonal matrix with diagonal entries ± 1 (i.e., exactly r_c of these entries are equal

to -1 with $\binom{p_M}{r_c}$ combinations), and $\mathbf{Q}_l$ is a real orthogonal matrix of the form

$$\mathbf{Q}_l = \begin{cases} \begin{bmatrix} \hat{\mathbf{C}}_l & \hat{\mathbf{S}}_l \\ \hat{\mathbf{S}}_l & -\hat{\mathbf{C}}_l \end{bmatrix}, & \text{for even } p_M \\ \\ \begin{bmatrix} \hat{\mathbf{C}}_l & 0 & \hat{\mathbf{S}}_l \\ 0 & \pm 1 & 0 \\ \hat{\mathbf{S}}_l & 0 & -\hat{\mathbf{C}}_l \end{bmatrix}, & \text{for odd } p_M \end{cases} \tag{3.53}$$

In (3.53), $\hat{\mathbf{C}}_l$ and $\hat{\mathbf{S}}_l$ are $\lfloor p_M/2 \rfloor \times \lfloor p_M/2 \rfloor$ real diagonal matrices with entries $[\hat{\mathbf{C}}_l]_{n,n} = \cos(\alpha_{l,n})$ and $[\hat{\mathbf{S}}_l]_{n,n} = \sin(\alpha_{l,n})$.

We note that with CSD-based method as explained above and using real Givens rotations to obtain $\mathbf{V}_l$ and $\mathbf{W}_l$, the coefficients or the entries of $\mathbf{B}(z)$ and the resulting prototype filter's coefficients will be real. Alternatively, by using complex Givens rotation matrices for $\mathbf{V}_l$ and $\mathbf{W}_l$, complex prototype filters can be derived. The numbers of required parameters to generate $\mathbf{\Delta}(z)$ by this approach (3.50)-(3.53) are $\mu_r^{(2)}$ and $\mu_c^{(2)}$ for the real and complex cases, respectively.

$$\mu_r^{(2)} = (L-1)\left(\frac{\lfloor \frac{p_M}{2} \rfloor (\lfloor \frac{p_M}{2} \rfloor - 1)}{2} + \frac{\lceil \frac{p_M}{2} \rceil (\lceil \frac{p_M}{2} \rceil - 1)}{2} + \lfloor \frac{p_M}{2} \rfloor\right) + \frac{p_M(p_M-1)}{2} \tag{3.54}$$

$$\mu_c^{(2)} = (L-1)\left(\lfloor \frac{p_M}{2} \rfloor (\lfloor \frac{p_M}{2} \rfloor - 1) + \lceil \frac{p_M}{2} \rceil (\lceil \frac{p_M}{2} \rceil - 1) + \lfloor \frac{p_M}{2} \rfloor)\right) + p_M(p_M-1) \tag{3.55}$$

Note that these values are almost half of the number of parameters used in the order-based method (3.44).

3.3.3 Post-filtering based method

In [54], the authors developed an algorithm called post-filtering based method and further reduced the number of required parameters. By consecutive removal of extra degrees of freedom in adjacent stages, which is accomplished through a new CS decomposition and implementing a post-filtering based structure, they succeeded in eliminating redundant parameters. This structure is derived by forward simplification of (3.44) as follows

$$\mathbf{\Delta}(z) = \hat{\mathbf{R}}_{L-1}\mathbf{\Lambda}(z)\hat{\mathbf{R}}_{L-2}\mathbf{\Lambda}(z)\ldots\mathbf{R}_0, \tag{3.56}$$

where

$$\hat{\mathbf{R}}_l = \mathrm{diag}(\mathbf{V}_{l,0}, \mathbf{V}_{l,1})\mathbf{\Sigma}_l, \tag{3.57}$$

in which, $\mathbf{V}_{l,0}$ and $\mathbf{V}_{l,1}$ are special $(p_M - r_c) \times (p_M - r_c)$ and $r_c \times r_c$ unitary matrices, respectively. In particular, by absorbing extra parameters into $\hat{\mathbf{R}}_{l-1}$,$\mathbf{V}_{l,0}$ requires $(p_M - 2r_c)(p_M - 2r_c - 1)/2$ fewer parameters than a unitary matrix of a same size in the real case [54]. Likewise, in the complex case, there is a reduction of $(p_M - 2r_c)(p_M - 2r_c - 1)$ in the number of design parameters. Moreover, when $2r_c < p_M$, $\mathbf{\Sigma}_l$ is a $p_M \times p_M$ matrix that can be expressed as

$$\mathbf{\Sigma}_l = \begin{bmatrix} \mathbf{I} & 0 & 0 \\ 0 & \mathbf{C}_l & -\bar{\mathbf{S}}_l \\ 0 & \bar{\mathbf{S}}_l^H & \mathbf{C}_l \end{bmatrix}, \tag{3.58}$$

where, $\mathbf{C}_l$ and $\bar{\mathbf{S}}_l$ are $r_c \times r_c$ diagonal matrices with entries $[\mathbf{C}_l]_{n,n} = \cos(\alpha_{l,n})$ and $[\bar{\mathbf{S}}_l]_{n,n} = e^{\jmath\beta_{l,n}}\sin(\alpha_{l,n})$, where $\alpha_{l,n}$ is a rotation angle and $\beta_{l,n}$ is a phase. Similarly, when $2r_c > p_M$, another CS decomposition is derived for $\mathbf{\Sigma}_l$ in [54]. But as r_c corresponds to the number of delay elements z^{-1} in $\mathbf{\Lambda}(z)$, it is preferable to choose $r_c \leq p_M/2$, while it does not violate the completeness of (3.56). In this case $2r_c < p_M$, the numbers of parameters $\mu_r^{(3)}$ and $\mu_c^{(3)}$ required to construct a $p_M \times p_M$ real and complex paraunitary matrix are, respectively

$$\begin{aligned} \mu_r^{(3)} &= (L-1)\left(\frac{(p_M - r_c)(p_M - r_c - 1)}{2} - \frac{(p_M - 2r_c)(p_M - 2r_c - 1)}{2} + \frac{r_c(r_c-1)}{2} + r_c\right) \\ &\quad + \frac{p_M(p_M-1)}{2}, \end{aligned} \tag{3.59}$$

$$\begin{aligned} \mu_c^{(3)} &= (L-1)\Big((p_M - r_c)(p_M - r_c - 1) - (p_M - 2r_c)(p_M - 2r_c - 1) + r_c(r_c-1) + 2r_c\Big) \\ &\quad + p_M(p_M-1). \end{aligned} \tag{3.60}$$

By considering the extra parameters required to form $\mathbf{\Gamma}_l$ in (3.50), it can be shown that the number of design parameters in the post-filtering method to generate a paraunitary matrix of size p_M is less than or equal to the one in the CSD-based method. Furthermore, the number of parameters μ in the post-filtering based approach (3.56) is a quadratic function

of r_c which reaches its maximum at $\lfloor p_M/2 \rfloor$.

Table 3.1 lists representative sizes of the parameter vectors of different design methods, including: the dyadic based method [36,57], the order-based method (3.44), the CSD-based method (3.50), and the post-filtering based method (3.56).

These sizes are for real and complex prototype filters of length $D = 1728$ in FBMC system with $M = 64$ subbands and $K = 72$ as upsampling/downsampling factor. These values are derived for $r_c = 1$ using (3.47), (3.49), (3.54), (3.55), (3.59) and (3.60) and considering the fact that $\tau = 8$ different matrix $\mathbf{B}(z)$ (or $\mathbf{\Delta}(z)$) should be constructed. Unfortunately, due to its limitation, the dyadic based method [36, 57] cannot be used to design complex prototype filters. Moreover, we note that one of the advantages of the other three methods over the dyadic based method is that the range of the parameters is limited to the interval $[0, 2\pi]$. Finally, compared to the CSD-based method, the post-filtering based method does not use the extra sign parameters. While as in (3.52), p_M sign parameters are needed for each $\mathbf{\Gamma}_l$ in the CSD-based method. Based on the results of Section 3.2 and by employing the method with the least number of parameters, it will be possible to parameterize $\mathbf{B}(z)$ and perform the optimization on its associated parameters.

3.4 Prototype Filter Design

In this Section, the design steps towards the final optimized prototype filter for a given triplet (K, M, D) are discussed. Depending on whether M and K are coprime, the design process starts with generating parameterized paraunitary matrices $\mathbf{B}(z;\boldsymbol{\theta})$ or $\mathbf{B}_l(z;\boldsymbol{\theta})$ for $l \in \{0, \ldots, \tau-1\}$ via the methods explained in Section 3.3. In particular, the post-filtering based method (3.56) has been used due to the fact that the required number of parameters to design such matrices by this method is less or equal to the other methods. The entries

Table 3.1 Size of parameter vector $\boldsymbol{\theta}$ for $M = 64$, $K = 72$ and $D = 1728$

Method	μ_r for real prototype	μ_c for complex prototype
Dyadic based	$72 \times 8 = 576$	N/A
Order-based (3.44)	$72 \times 8 = 576$	$144 \times 8 = 1152$
CSD-based (3.50)	$56 \times 8 = 448$	$108 \times 8 = 864$
Post-filtering based (3.56)	$44 \times 8 = 352$	$88 \times 8 = 704$

of these matrices are then mapped to the prototype filter coefficients $f_0[n;\boldsymbol{\theta}]$ using (3.37) or (3.42). Finally, based on the vector of parameters $\boldsymbol{\theta}$, these coefficients are optimized according to the design objectives.

3.4.1 Optimization of Prototype Filter

The prototype filter coefficients $f_0[n;\boldsymbol{\theta}]$ are optimized with respect to the vector of parameters $\boldsymbol{\theta}$. One of the benefits of using a PR FB transceiver is that in the filter design process, the PR property relaxes any flatness condition on the passband region of the filter. Since the transmit and receive prototype filters are paraconjugate of each other, the pass band region of $|F_0(\omega;\theta)|^2$ is constant, where $F_0(\omega;\boldsymbol{\theta}) = \sum_{n=0}^{D-1} f_0[n;\boldsymbol{\theta}]e^{-\jmath\omega n}$ is the discrete-time Fourier transform (DTFT) of $f_0[n;\boldsymbol{\theta}]$ [2]. Therefore, a good spectral containment can be achieved via minimization of the stop-band energy of the filter, denoted as the cost function

$$J(\boldsymbol{\theta}) = \frac{1}{2\pi}\int_{\omega_s}^{2\pi-\omega_s} |F_0(\omega;\boldsymbol{\theta})|^2 d\omega, \tag{3.61}$$

where ω_s is the stop-band angular frequency, given by

$$\omega_s = \frac{\pi}{M} \tag{3.62}$$

In order to calculate the cost function $J(\boldsymbol{\theta})$ (3.61) in an efficient way, we employ a FFT-based algorithm as explained in [36]. Since this optimization problem is a large-scale non-linear one, we used the Broyden-Fletcher-Goldfarb-Shanno (BFGS) algorithm [125], which is a quasi-Newton method, for minimizing the cost function.

Alternatively, we can consider the minimax criterion, which aims to minimize the maximum stop-band ripple instead of the stop-band energy. In minimax design the cost function is defined as

$$J(\boldsymbol{\theta}) = \max_{\omega\in[\omega_s,2\pi-\omega_s]} |F_0(\omega;\boldsymbol{\theta})|. \tag{3.63}$$

The magnitude response of the resulting filter is shaped such that the attenuation is almost equiripple on the overall stop-band region. In general, we find that with the minimax criterion, the attenuation is higher near the edge of the stop-band region and the first few sidelobes are lower than with the stop-band energy minimization criterion, whereas it results in increased total stop-band energy.

3.4.2 Comparison of Prototype Filters

It is known that for a given number of subbands M, better spectral features are obtained if the upsampling factor K and the length of the prototype filter D are increased [36]. However, higher K will sacrifice the bandwidth efficiency of the system and higher D will increase latency of the system and its computational complexity. These trade-offs must be balanced carefully in order to maintain low latency, low computational complexity, and high bandwidth efficiency while benefiting from good spectral features. In this section, we design a real and complex prototype filter for the transceiver system with $M = 64$ subbands, oversampling factor $K = 72$, and filter length $D = 1728$. It has been observed that due to the completeness of the methods (3.44), (3.50), and (3.56), the resulting prototype filters are almost identical in terms of spectral containment. However as noted in Section 3.3, the number of parameters in the post-filtering based method (3.56) is less than the other methods, and consequently, we prefer this method due to its efficient parameterization.

To develop a comprehensive outlook on various FB design and MCM transceiver systems, the real and complex prototype filters designed by means of the objective function in (3.61) are compared with the prototype filters of some other design methods including: NPR-windowing using the generalized windowing-based method [17], NPR-OQAM[6] derived by the frequency sampling technique [18] and OFDM. Table 3.2 lists the filter length D, the stop-band attenuation $J(\boldsymbol{\theta})$ in (3.61) (when $\omega_s = \pi/M$) and the first sidelobe attenuation of these filters. Moreover, Figure 3 shows part of the frequency responses (i.e. first few sidelobes) of these filters. Three key observations must be pointed out: the transition from passband to stop-band, i.e. the rolloff, of the proposed scheme is much steeper than all other FB approaches and OFDM; the stop-band energy of the proposed scheme is the second smallest among its counterparts after the NPR-Windowing method; the attenuations of the first two sidelobes of the proposed scheme are, respectively, about 33 and 40 dB, whereas the attenuations of the first two sidelobes of the OFDM system are 13 and 17 dB, respectively. These observations confirm that the proposed OPRFB offer considerably better spectral containment than OFDM.

As mentioned in Section 3.1, to restore causality in the PR MCM receiver, there is an intrinsic delay in the system that is equal to the prototype filter length D, or equivalently,

[6]Most of the literature regarding the OFDM/OQAM system is focused on NPR systems, whereas the PR version is also developed [34].

$D/K = 24$ symbol durations at the input rate. The issues faced by our proposed system in the case of burst transmissions, e.g. with regard to the use of a preamble in each burst for channel estimation, are similar to those faced by other FB-based MCM systems [43]. In particular, when accurate estimation is needed, the data should not interfere with the preamble signal and the length of the burst must therefore be extended to allow for initial and final transitions of the preamble due to the filter impulse response. Also, in the case of a time-varying channel, a basic requirement is that the filter length should be smaller than the channel coherence time.

3.4.3 Prototype Filter for $M = 128$ and $K = 132$

The design of FBMC systems mainly concentrates on the prototype filter design since all the subband filters are generated from this filter. Moreover, practical applications commonly necessitate transceiver structures with high number of subchannels, that is, a value of M in the order of hundreds or thousands is required, e.g. in Digital Video Broadcasting Terrestrial 2 (DVB-T2) application, the number of subcarriers can go up to $M = 2^{15}$ [126]. Such a demand imposes a significant computational burden on the conventional design processes as the number of parameters to be optimized may increase drastically or even become overwhelming. As shown for instance in [25, 36, 37], the number of subbands does not exceed 80, 128, and 64 respectively.

Moreover, when the ratio K/M approaches 1, the number of parameters increases which complicates the optimization process as well. Meanwhile, this case is important in practice since it replaces a more spectral efficient system. The methods presented in the literature only obtained limited success in improving the spectral efficiency, or equivalently, reducing the oversampling ratio K/M. These efforts start with an oversampling ratio of 2 in [47]

Table 3.2 Spectral containment of different prototype filters for $M = 64$ subbands

Method	D	J(dB)	First Sidelobe (dB)
Proposed Real	1728	-35.31	-33
Proposed Complex	1728	-35.29	-33
NPR-Windowing [17]	1024	-36.56	-72
NPR-OQAM [18]	255	-26.80	-45
OFDM	64	-24.27	-13

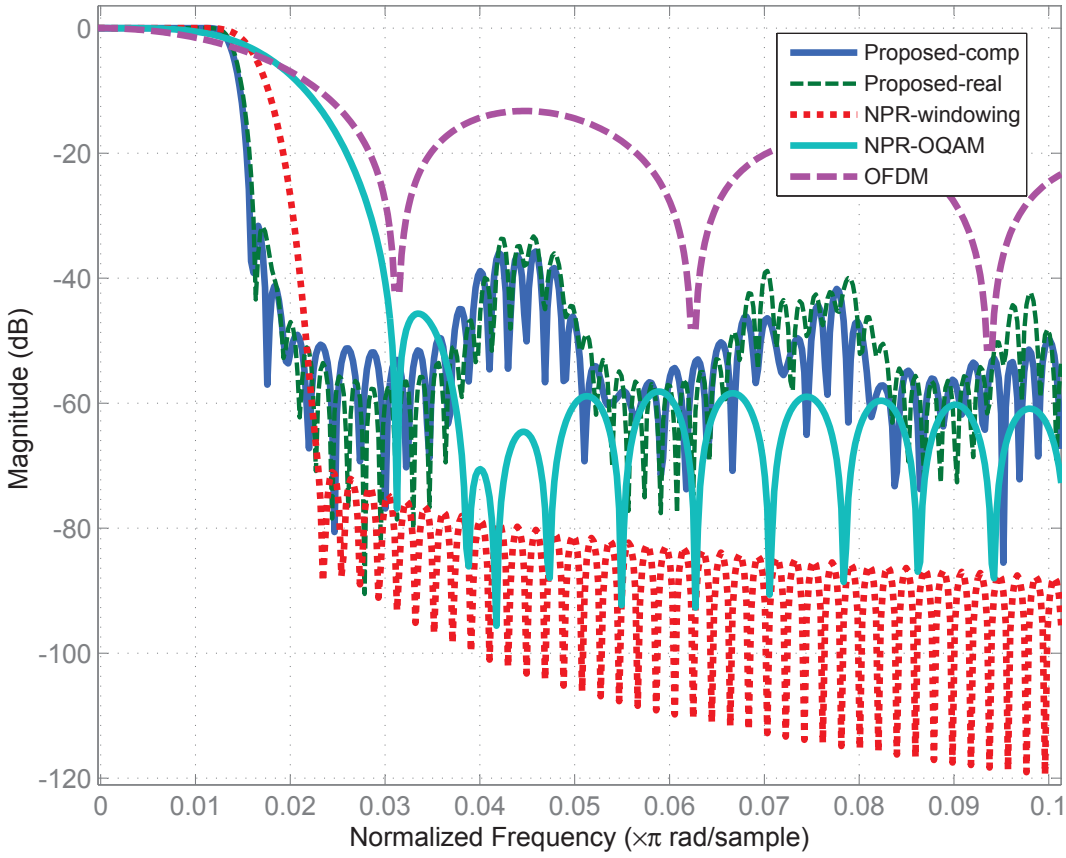

Fig. 3.3 Comparison of the first few sidelobes of magnitude responses for prototype filter of different design approaches with $M = 64$ subbands

and continue with values of 3/2 [55] and 5/4 [25, 35]. It is only recently that authors in [36, 37, 56] succeeded in presenting a 9/8, 9/8 and 17/16 oversampling ratio FBMC design, respectively. Benefiting from effective factorization and efficient parameterization, we are able to design real prototype filters with oversampling ratio of 33/32. Based on stop-band energy minimization and minimax criterion, the magnitude responses of these prototype filters for $M = 128$ and $K = 132$ (oversampling ratio 33/32) are depicted in Figure 3.4. The lengths of these filters are $D = 12672$ ($D/P = 3$) and the size of their parameter vector in the case of a real prototype filter is 560×4 (when using the post-filtering based method with $r_c = 1$). Table 3.3 also lists the stop-band attenuation $J(\boldsymbol{\theta})$ in (3.61) and the first sidelobe attenuation of these filters. As it is shown in the figure and the table, by employing the minimax criterion we can increase the first sidelobe's attenuation

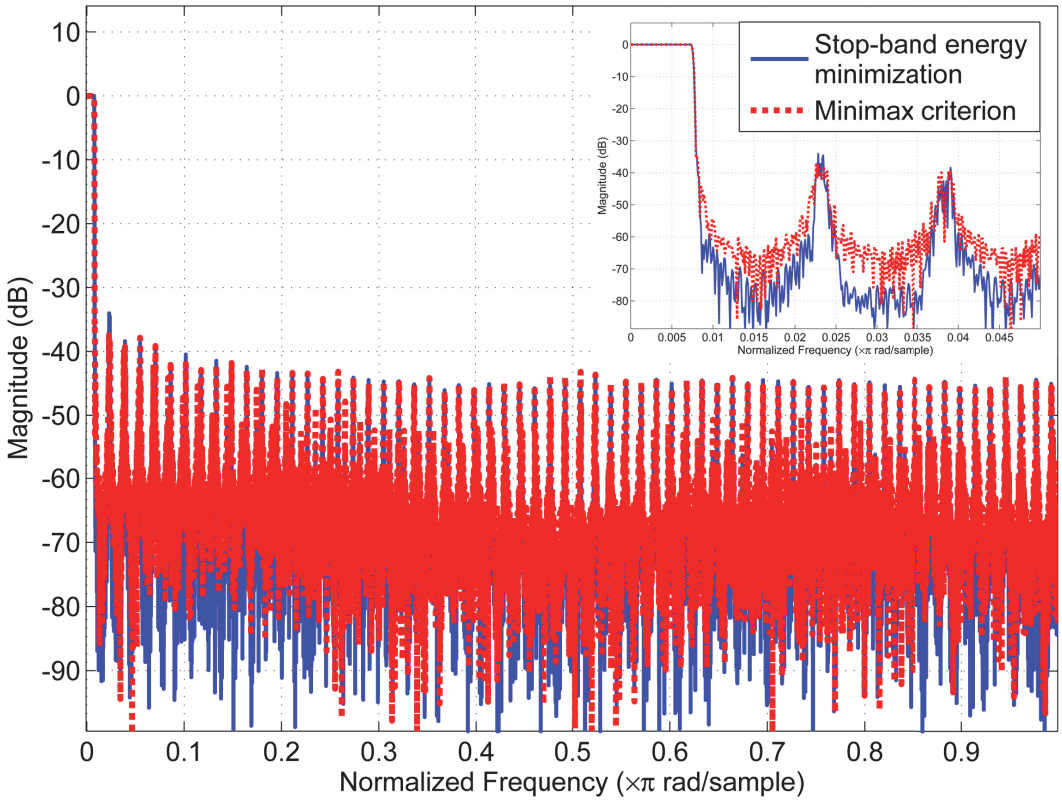

Fig. 3.4 Magnitude responses of prototype filters for $M = 128$ and $K = 132$

by 4 dB, but this results in increased total stop-band energy. Due to the similar spectral characteristics of the resulting filters, we just focus on the stop-band energy minimization method in the sequel.

Table 3.3 Spectral containment of prototype filters for $M = 128$, $K = 132$ and $D = 12672$

Method	J(dB)	First Sidelobe (dB)
Stop-band energy	-41.59	-34
Minimax criterion	-40.55	-38

3.5 Numerical Results

In this section, the performance of an OPRFB transceiver using the proposed FB design approach is investigated through numerical simulations. In particular, the BER of this system when used over a frequency selective channel in the presence of AWGN is compared with other well known MCM schemes. The effects of channel impairments such as CFO and NBI on the BER performance are also examined.

3.5.1 Methodology

Referring to (3.2), we consider two different scenarios for the Q-tap channel $C(z)$ with channel coefficients $c[l]$: (1) an ideal (distortion-less) channel for experimenting AWGN, where $Q = 1$ and $h[0] = 1$ and (2) a frequency selective channel consisting of $Q = 5$ independent Rayleigh-fading taps with an exponentially decaying power delay profile, where $E[|h[l]|^2] = Ce^{-l/4}$ for $l \in \{0, \cdots, 4\}$, and C is a constant such that $\sum_{l=0}^{Q-1} E[|h[l]|^2] = 1$. The received signal includes an additive white Gaussian noise $\eta[m]$ with zero mean and variance $E[|\eta[m]|^2] = N_0$. Moreover, to model a scenario with NBI, a white noise sequence is passed through a narrow band-pass filter with a bandwidth of $2/M$ to generate the narrow band random interference sequence $\beta[m]$. We let $I = E[|\beta[m]|^2]$ denote the interference power. The resulting NBI $\beta[m]$ is then added to the channel output and white Gaussian noise $\eta[m]$ as in (3.2). This simple interference model is realistic for narrow band FM (eg. cordless telephones) and low rate digital modulations [9, 127, 128].

To evaluate the comparative performance of the proposed scheme, BERs versus bit-energy-to-noise ratio (E_b/N_0) of the following MCM systems are compared: proposed OPRFB with real prototype filter, proposed OPRFB with complex prototype filter, the NPR-windowing method [17], the NPR-OQAM method [18] designed by criterion C1 in that reference and a CP-OFDM system. Note that although the NPR schemes are not designed for optimum performance over AWGN channels, it is insightful to compare their behaviour in the non-frequency-selective environment as well as in the frequency selective one. For all of these systems, QPSK modulation is used as an input for each subband where the filter bank is normalized to have a DC gain of 1. Furthermore, to derive the BER in each scenario, a number of 10^4 Monte Carlo trials are performed, where the channel is fixed in each run but independent from one run to another. In order to fairly compare these schemes, the redundancy caused by oversampling should be equal to the redundancy

caused by the cyclic prefix in OFDM. That is, with $M = 64$ and $K = 72$, the length of cyclic prefix is set to $L_{cp} = K - M = 8$ in OFDM.

Due to the large number of subbands and the excellent spectral characteristics of the prototype filters of the systems under consideration, if the channel is mildly frequency selective, each subband channel can be modelled as a simple (flat) complex gain which can be equalized by a single tap, similar to [14]. As a result, we implement a one-tap equalizer per subband assuming perfect CSI, which can be obtained by specialized channel estimation techniques that will be investigated more in Chapter 4.

The equalizer coefficient for the i-th subband is derived as follows

$$E_i = H(z_i)^{-1}, \tag{3.64}$$

where $z_i = e^{-\jmath 2\pi i/M}$ for $i \in \{0, \cdots, M-1\}$. Unless otherwise indicated, we assume perfect frequency synchronization between the transmit and receive FBs.

3.5.2 Results and Discussion

The computational complexity of FB structures can be evaluated by counting the number of real multiplications needed to compute an output sequence of length-M. This information is reported in Table 3.4 for the various MCM systems under consideration, assuming a polyphase implementation [16, 43], complex-valued data $x_i[n]$, and M a power of 2. As a result, the DFT can be replaced by an FFT, which can be realized more efficiently. As expected, OFDM shows a complexity advantage over the FB approaches as it just employs the IFFT/FFT blocks. The proposed design, in addition to the IFFT/FFT blocks and consistent with other FB methods, employs a polyphase block at the transmitter and receiver where the complexity depends on the prototype filter length. Also, in the case of NPR-OQAM, the IFFT/FFT blocks operate at twice the rate of other systems, and the trivial multiplications by ± 1 and $\pm\jmath$ in the pre-processing blocks are not considered in evaluating the complexity.

The BERs versus E_b/N_0 for the various MCM systems in the ideal AWGN channel environment are plotted in Figure 3.5. It can be seen that BER of the FB-based approaches closely match the suggested theoretical value of BER for QPSK and they all exhibit superior performance than OFDM by a margin of 0.5dB. This difference in BER performance can be precisely explained by the use of a CP with 9/8 redundancy ratio. As we have been able

to verify, the BER of OFDM without CP is in full agreement with other methods. In this example, the simulated BER for the real and complex versions of the proposed scheme are almost indistinguishable.

With the NPR-windowing method [17], proper demodulation of the received signal over the frequency selective channel requires the use of computationally expensive post combiners to combat the phase rotation caused by non-linear phase channel. As a result, its BER with only one-tap per subband equalizer is much higher than that of the other MCM systems with the same equalization method. Therefore, in all of the frequency selective scenarios, the results of the NPR-windowing method are not presented. Figure 3.6 shows the BER versus E_b/N_0 of the MCM systems over the frequency selective channel. The proposed schemes exhibit the best performance, followed by NPR-OQAM method at low signal-to-noise ratio (SNR) and OFDM at high SNR. As mentioned before, the performance of the proposed methods and NPR-OQAM can be further improved by utilizing a more complex equalization method. Note that the spectral containment and BER in AWGN and frequency selective channel of the proposed scheme with real and complex prototype filters are almost identical. Therefore, for this particular set-up, there is no clear advantage in using complex prototype filter, although it doubles the number of required parameters in the design process. In the sequel, we just focus our investigation on the case of real prototype filters.

It is well known that the performance of OFDM can be easily impaired by NBI. Due to the better spectral containment of the proposed OPRFB system, as compared to the OFDM, we expect a better performance in the presence of NBI. Figure 3.7 shows the BER versus bit-energy-to-NBI ratio (E_b/I) of the mentioned MCM systems, where the Gaussian noise is set to have a SNR of 7dB. As expected, OFDM exhibits the worst performance due to the low attenuation in the sidelobes, whereas the proposed method provides the best

Table 3.4 Computational complexity in terms of number of real multiplications for systems with M subbands and filter length D

Method	Number of real multiplications
Proposed	$2((M(\log_2 M - 3) + 4) + 2D)$
NPR-Windowing	$2((M(\log_2 M - 3) + 4) + 2D)$
NPR-OQAM	$4(2M + (M(\log_2 M - 3) + 4) + 2D)$
OFDM	$2(M(\log_2 M - 3) + 4)$

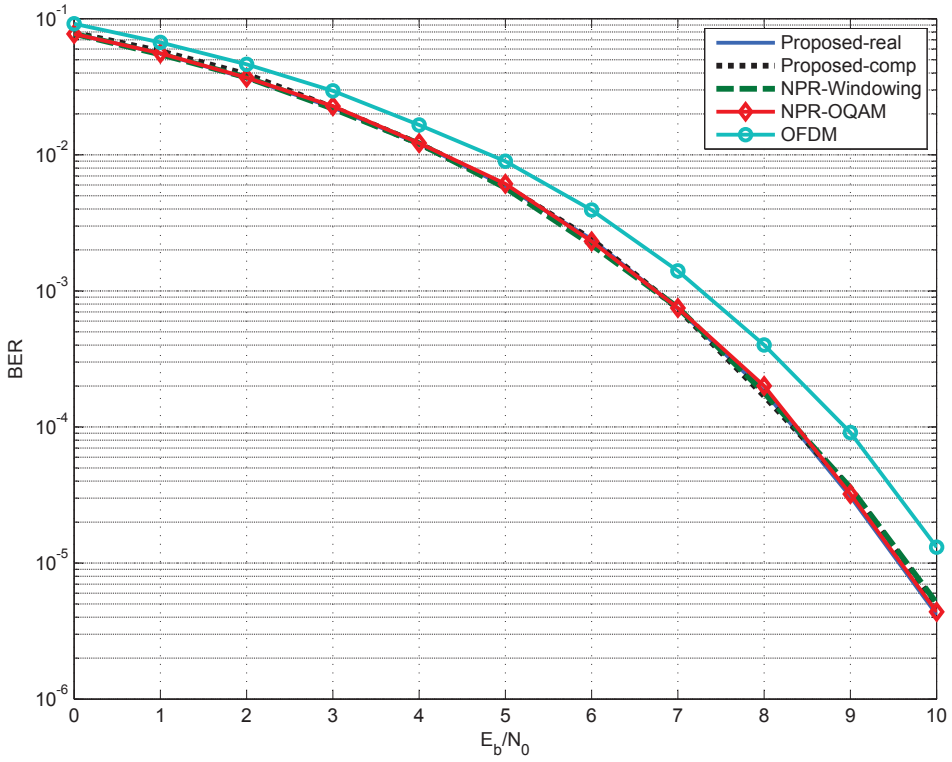

Fig. 3.5 BER versus E_b/N_0 for different MCM systems with $M = 64$ sub-bands over AWGN channel

performance and the NPR-OQAM remains very close to it. At low SIR, the performance of the NPR-windowing is worse than the other two FB-based approaches since it employs cosine modulation and real-coefficient prototype filters. The saturation of BER at very high SIR results from the fixed SNR level. Similarly, Figure 3.8 shows the BER versus E_b/I in the frequency selective channel, where all the MCM systems exhibit a similar behaviour as in the AWGN case and the proposed system offers the best performance over the complete SIR range.

It has been shown that sensitivity to frequency synchronization is one of the disadvantages of OFDM [12]. Small frequency offset in the OFDM receiver results in an attenuation of signal amplitude, loss of orthogonality between subcarriers and consequently intercarrier interference (ICI) from the neighbour subcarriers. The poor spectral containments of the rectangular window of OFDM is the main reason for its performance degradation in the presence of CFO. Similarly, many other MCM schemes may be vulnerable against CFO,

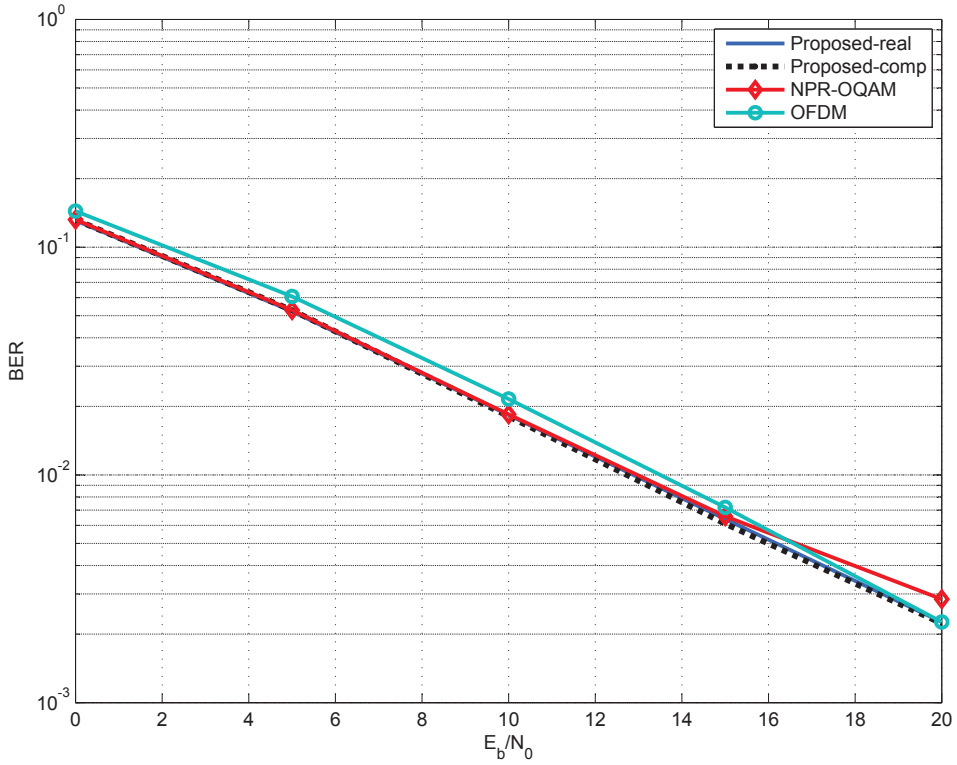

Fig. 3.6 BER versus E_b/N_0 for different MCM systems with $M = 64$ subbands over 5-tap Rayleigh fading channel

since the subbands are tightly spaced in the transmission band [38, 63, 64]. By designing sharp filters with much lower sidelobes, we can lessen the effect of CFO. To investigate this effect, we consider a scenario in which the receive FB is not exactly synchronized in frequency with the transmit FB. That is, we introduce a constant frequency offset on all the received tones [63]. This offset, denoted as Δ_f, is measured as percent frequency deviation, relative to the width of a subband, i.e. intercarrier spacing.

Figure 3.9 and Figure 3.10 show the BERs of all previously compared schemes versus SNR over the ideal AWGN channel with $\Delta_f = 2\%$ and $\Delta_f = 5\%$, respectively. Results show that the proposed OPRFB outperforms OFDM by a margin of more than 0.5dB. We note that for the particular choice of parameters in Figure 3.10, NPR-OQAM is more sensitive to CFO than the other methods under comparison. However, NPR-OQAM can be implemented with different prototype filters whose choice may have an impact on the performance of the FB system in the presence of CFO [64]. Likewise, Figure 3.11 and

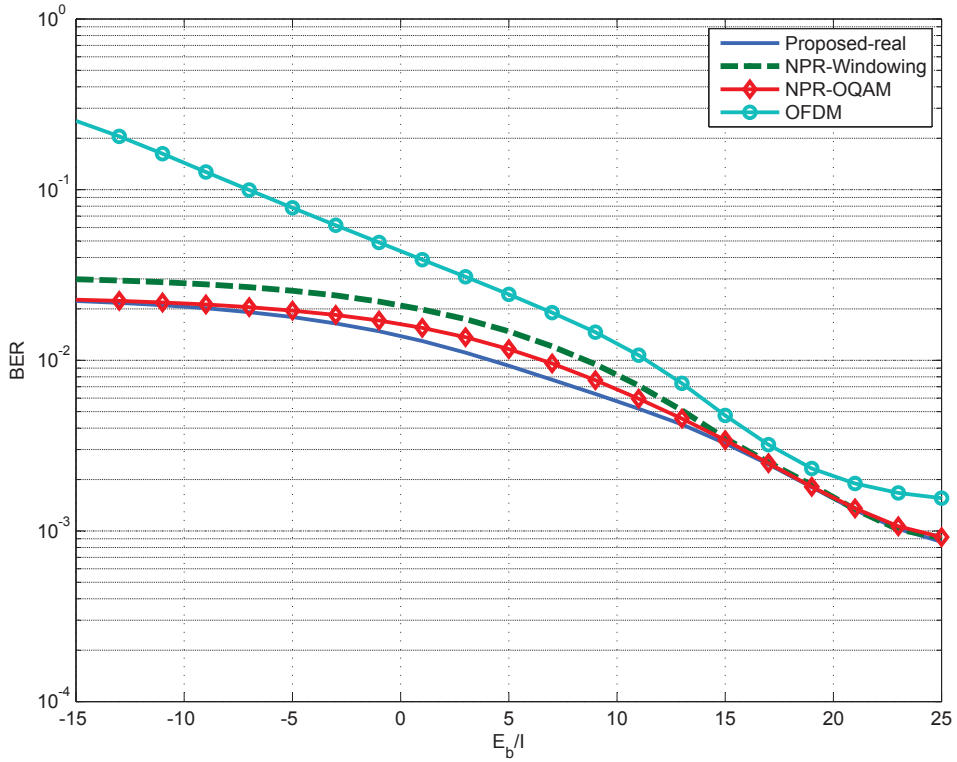

Fig. 3.7 BER versus E_b/I (NBI) for different MCM systems with $M = 64$ subbands over AWGN channel with SNR=7dB

Figure 3.12 show the BERs versus SNR over the frequency selective channel, where the proposed scheme again offers the best performance.

As mentioned in Section 2.1, OFDM and other MCM systems exhibit a high PAPR during their transmission phase. When the signals in many of the various subbands add constructively in phase, large signal peaks in the transmitted signal power occur. In particular, both OFDM and OPRFB have a PAPR in the range of 12 dB and do not provide any advantage over each other in that sense. However, to reduce the PAPR in complex MCM systems, different methods have been reported in the literature, as summarized in [93] and can be applied to OPRFB systems as well.

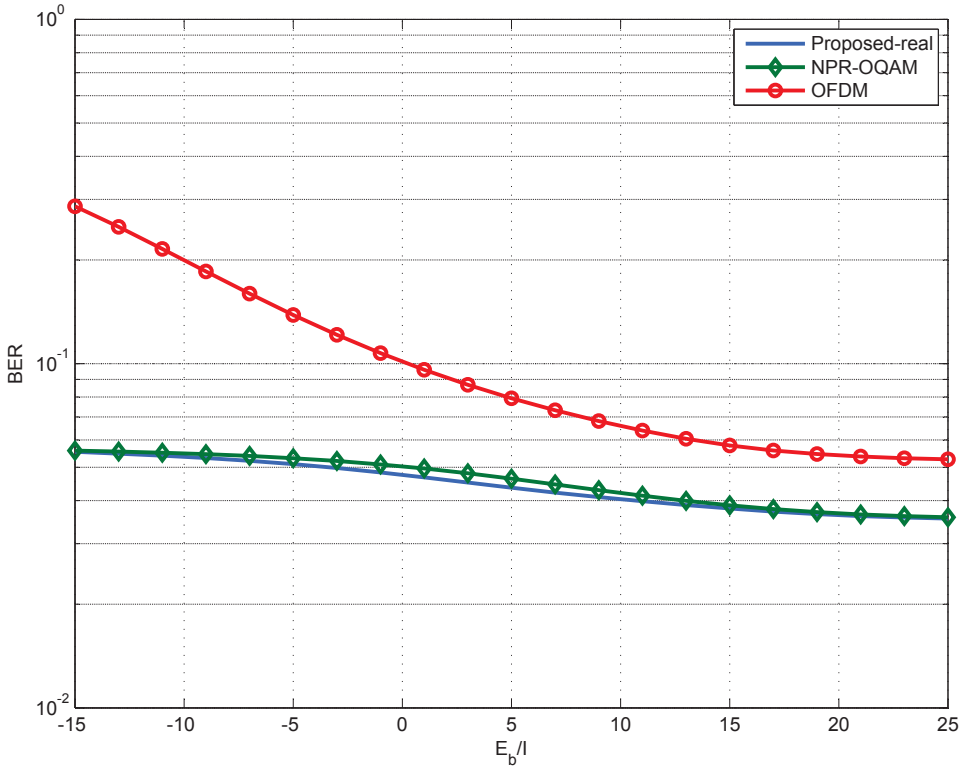

Fig. 3.8 BER versus E_b/I (NBI) for different MCM systems with $M = 64$ subbands over 5-tap Rayleigh fading channel with SNR=7dB

3.6 Conclusion

In this chapter, a design method for OPRFB transceivers was presented. To ensure the PR property of the system, the polyphase matrices of the transmit and the receive FBs were chosen as paraunitary matrices. These matrices were then parameterized, based on factorization methods making use of Givens rotations. Moreover, different methods to reduce the number of parameters were employed and consequently facilitated the optimization process. By minimizing the stop-band energy of the prototype filters with respect to the parameters, prototype filters were designed with good spectral containment such as steeper transition from pass-band to stop-band, lower stop-band energy, and lower sidelobe levels, when compared with OFDM and some recently proposed FBMC systems. Numerical experiments show the the proposed scheme offers the lowest BER over AWGN and frequency selective channels. Furthermore, in the presence of NBI or CFO, the proposed FB is more robust against such channel impairments compared to the other MCM systems. These

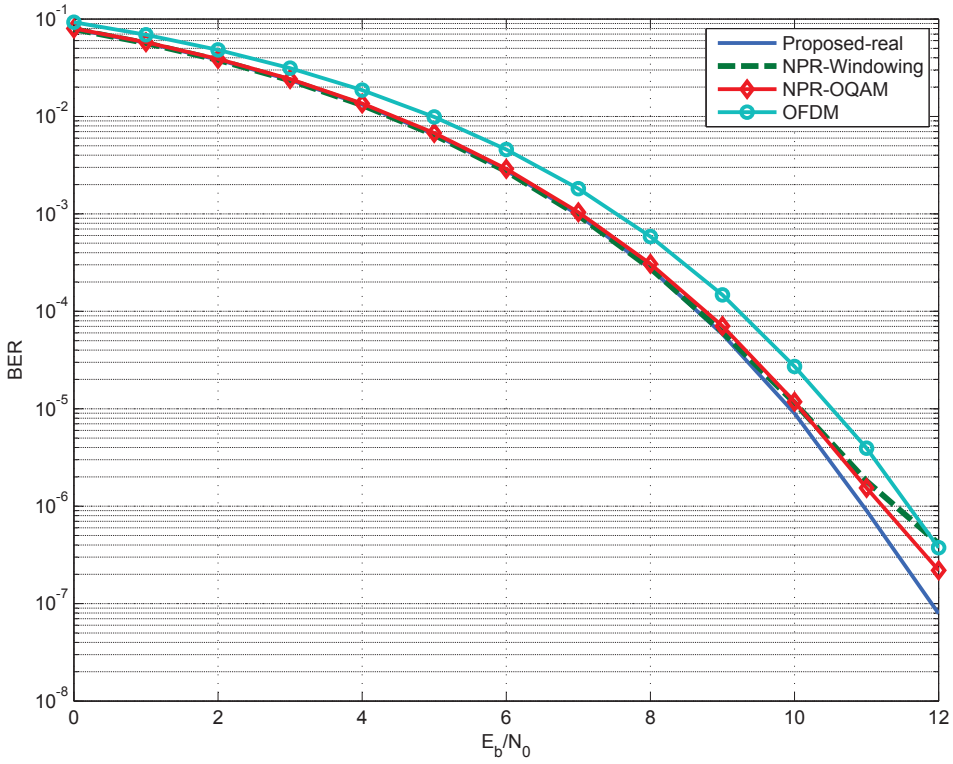

Fig. 3.9 BER versus E_b/N_0 for different MCM systems with $M = 64$ sub-bands over AWGN channel with carrier frequency offset $\Delta_f = 2\%$

attractive features come at the price of an increase in the computational complexity and processing delay of the system.

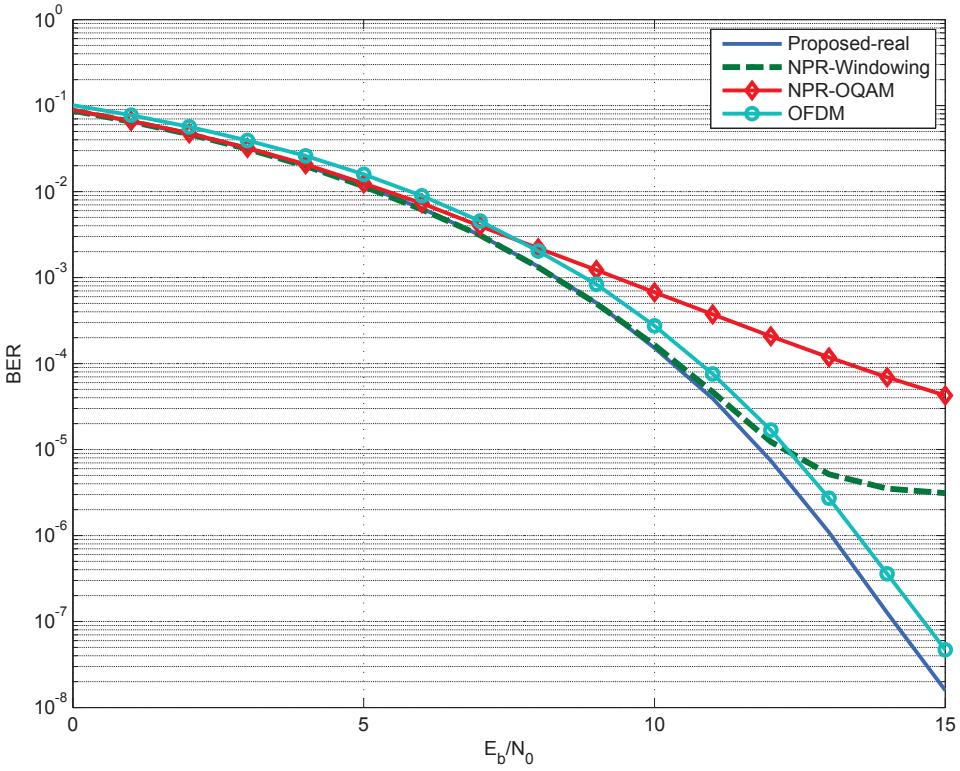

Fig. 3.10 BER versus E_b/N_0 for different MCM systems with $M = 64$ subbands over AWGN channel with carrier frequency offset $\Delta_f = 5\%$

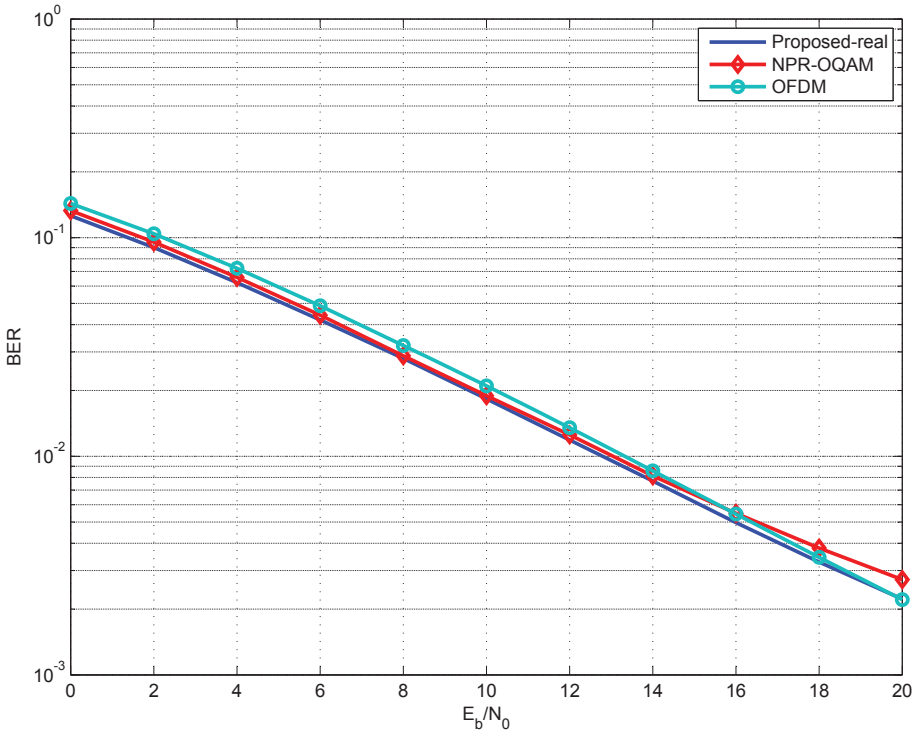

Fig. 3.11 BER versus E_b/N_0 for different MCM systems with $M = 64$ subbands over 5-tap Rayleigh fading channel with carrier frequency offset $\Delta_f = 2\%$

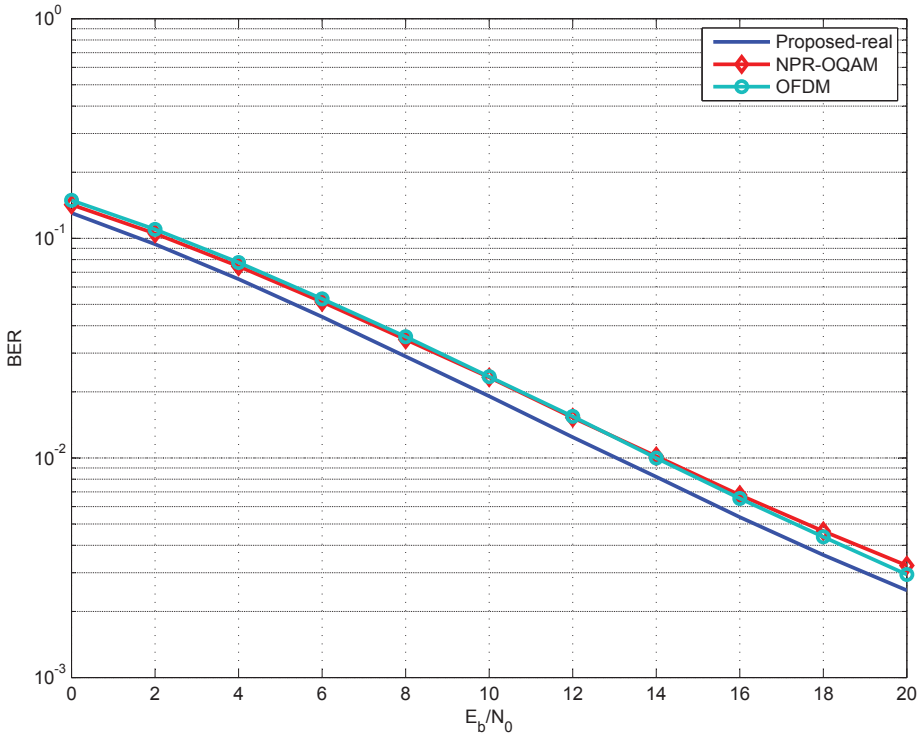

Fig. 3.12 BER versus E_b/N_0 for different MCM systems with $M = 64$ subbands over 5-tap Rayleigh fading channel with carrier frequency offset $\Delta_f = 5\%$

Chapter 4

Joint Channel and Frequency Offset Estimation for OPRFB Systems

In this chapter[1], we consider the problem of joint CFO and CIR estimation for OPRFB systems. Section 4.1 presents the OPRFB system model and discusses the effects of CFO on the signal recovery process at the receiver side. The joint ML estimator of the CFO and CIR is developed in Section 4.2, along with relevant practical simplifications, while the CRB on the joint estimator variance is derived in Section 4.3. The performance of the proposed joint estimator is evaluated in Section 4.4 and some conclusions are offered in Section 4.5.

4.1 Problem Formulation

4.1.1 OPRFB System Model

We consider a DFT-modulated OPRFB transceiver system, as depicted in Figure 4.1. Parameters M and K represent the number of subbands and the upsampling/downsampling factor, respectively, where $K > M$ (oversampling) is assumed as described in Chapter 2. In DFT-modulated FBMC systems, the transmit and receive subband filters can be derived from common prototypes with finite impulse responses (FIR) of length D and respective system functions $F_0(z) = \sum_{n=0}^{D-1} f_0[n]z^{-n}$ and $G_0(z) = \sum_{n=0}^{D-1} g_0[n]z^{n}$, where $f_0[n]$ and $g_0[n]$

[1]Parts of Chapter 4 have been presented at the 2012 IEEE International Symposium Wireless Communication Systems [38] and 2013 International Conference on Wireless and Mobile Communications [79].

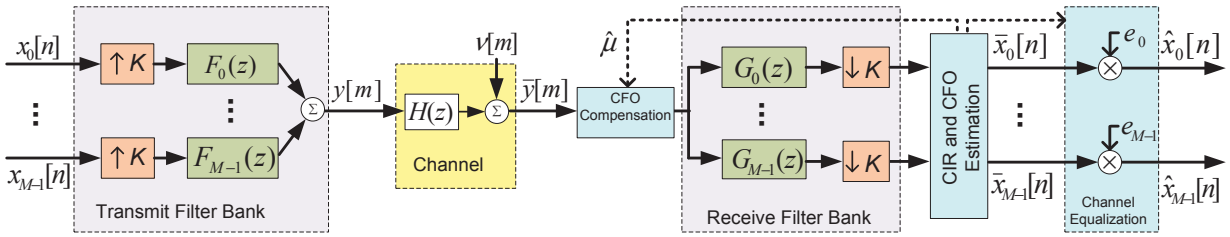

Fig. 4.1 DFT-modulated OPRFB transceiver with CFO and CIR estimation

are the corresponding impulse response coefficients. For convenience in analysis, $G_i(z)$ is assumed non-causal although in practice, causality can be restored simply by introducing an appropriate delay in the receiver. Defining $w = e^{-\jmath 2\pi/M}$, the DFT-modulated transmit and receive filters for the ith subband are respectively obtained as

$$F_i(z) = F_0(zw^i), \quad G_i(z) = G_0(zw^i). \tag{4.1}$$

In this work, the filter length D is restricted to be a multiple of M and K, i.e., $D = d_P P$, where P denotes the least common multiple of M and K and d_P is a positive integer. To enforce the perfect reconstruction (PR) property, the paraconjugates of the transmit filters are employed as receive filters, i.e., $g_i[n] = f_i^*[n]$. Under this setting, PR can be expressed as

$$\sum_{q=-\infty}^{\infty} f_j[q - pK] f_i^*[q - nK] = \delta_{ij}\delta_{np}, \tag{4.2}$$

where δ_{ij} denotes the Kronecker delta function.

Let $x_i[n]$ denote the complex-valued data symbol transmitted on the ith subband at discrete-time nT_s, where $i \in \{0, \ldots, M-1\}$, $n \in \mathbb{Z}$, $T_s = F_s^{-1}$ and F_s is the input sampling rate. On the transmitter side, as shown in Figure 4.1, the input sequences $x_i[n]$ are upsampled by K, passed through their corresponding subband filter $F_i(z)$, and finally summed. Hence, the transmitter output signal at discrete-time mT_s/K is given by

$$y[m] = \sum_{i=0}^{M-1} \sum_{q=-\infty}^{\infty} x_i[q] f_i[m - qK], \tag{4.3}$$

where the range of the summation over q is delimited by the finite support of the subband FIR filter, $f_i[m]$.

In a practical system implementation, the signal $y[m]$ is up-converted to a suitable frequency band via carrier frequency modulation and then transmitted over a noisy channel, while at the receiver, the reverse demodulation operations are applied. Here, we consider a baseband equivalent model of these operations in terms of the signal samples $y[m]$.

We assume that during a time interval equal to the processing delay of the transceiver system (i.e., $2DT_s/K$), the transmission channel can be modelled as a linear time-invariant system with FIR $h[l]$ of length Q and corresponding system function $H(z) = \sum_{l=0}^{Q-1} h[l]z^{-l}$. In this model, the filter length Q is chosen according to the multipath delay spread τ_{ds} of the channel, i.e., $QT_s = K\tau_{ds}$. The channel output is corrupted by an AWGN sequence $\nu[m]$, with zero-mean and variance $E[|\nu[m]|^2] = \sigma_\nu^2$, assumed to be statistically independent from the input data. The input-output relationship of the noisy channel can therefore be expressed as

$$\bar{y}[m] = \sum_{l=0}^{Q-1} h[l]y[m-l] + \nu[m], \tag{4.4}$$

where $\bar{y}[m]$ denotes the received baseband discrete-time signal. On the receiver side, $\bar{y}[m]$ is passed through a bank of M analysis filters and downsampled by K. Accordingly, for each subband, the reconstructed signal $\bar{x}_i[n]$ can be written as

$$\bar{x}_i[n] = \sum_{q=-\infty}^{\infty} \bar{y}[q]f_i^*[q-nK]. \tag{4.5}$$

Note that in the case of an ideal channel with no noise (i.e. $H(z) = 1$ and $\nu[m] = 0$), the PR condition (4.2) ensures that $\bar{x}_i[n] = x_i[n]$, for $i \in \{0, \ldots, M-1\}$ and $n \in \mathbb{Z}$.

4.1.2 Effects of Carrier Frequency Offset

In practice, there often exists a mismatch between the carrier frequency in the receiver and the transmitter, denoted as CFO. In this case, the received signal $\bar{y}[m]$ can be modelled as [71, 129]

$$\bar{y}[m] = e^{\jmath 2\pi \frac{\mu}{M} m} \sum_{l=0}^{Q-1} h[l]y[m-l] + \nu[m], \tag{4.6}$$

where μ is a normalized CFO with respect to the subband spacing F_sK/M.

Upon substitution of (4.6) and then (4.3) into (4.5), the reconstructed signal for the ith

subband, $\bar{x}_i[n]$, can be written in terms of the input signals $x_j[n]$, for $j \in \{0, ..., M-1\}$, as

$$\bar{x}_i[n] = \sum_{l=0}^{Q-1} \lambda_{i,n}(l,\mu)h[l] + \nu_i[n], \tag{4.7}$$

where $\lambda_{i,n}(l,\mu)$ and $\nu_i[n]$ are defined as

$$\lambda_{i,n}(l,\mu) = \sum_{j=0}^{M-1} \sum_{p=-\infty}^{\infty} x_j[p]\gamma_{i,n}^{j,p}(l,\mu), \tag{4.8}$$

$$\gamma_{i,n}^{j,p}(l,\mu) = \sum_{q=-\infty}^{\infty} e^{\jmath 2\pi \frac{\mu}{M} q} f_j[q-l-pK]f_i^*[q-nK], \tag{4.9}$$

$$\nu_i[n] = \sum_{q=-\infty}^{\infty} \nu[q]f_i^*[q-nK]. \tag{4.10}$$

The complex factor $\gamma_{i,n}^{j,p}(l,\mu)$ in (4.9) characterizes the interference level of the pth input sample from the jth subband on the nth output sample of the ith subband, in the presence of CFO with magnitude μ through the lth path of the channel. We note that for $|n-p| > (D+Q)/K$, due to the finite support of $f_i[n]$, $\gamma_{i,n}^{j,p}(l,\mu) = 0$; accordingly, the range of the summation over p in (4.8) is finite. The term $\nu_i[n]$ (4.10) represents the additive noise passed through the ith subband of the receive filter bank. This term has zero-mean and, due to the PR property imposed on $f_i[n]$ in (4.2), its covariance is given by

$$E\left\{\nu_i[p]\nu_j^*[q]\right\} = \delta_{ij}\delta_{pq}\sigma_\nu^2. \tag{4.11}$$

Considering the reconstructed signal $\bar{x}_i[n]$ in (4.7), it appears that even if the channel could be perfectly equalized (equivalent to $h[0] = 1$ and $h[l] = 0$ for $l \neq 0$) the presence of the CFO term $e^{\jmath 2\pi \frac{\mu}{M} q}$ in the interference factor, $\gamma_{i,n}^{j,p}(l,\mu)$ (4.9) would render the transceiver system non-PR. That is, $\gamma_{i,n}^{j,p}(l,\mu)$ would be non-zero for $j \neq i$ or $p \neq n$, and this in turn would result in a loss of performance in the data transmission process. It is worth to mention that in previous works [75, 76], it is assumed that the CFO factor $e^{j2\pi \frac{\mu}{M} q} \simeq 1$. If this was the case, this factor could be taken out of the summation over q in (4.9) and, consequently, the interference terms $\gamma_{i,n}^{j,p}(l,\mu)x_j[p]$ would be negligeagle when $j \neq i$ or $p \neq n$, which does not hold for the OPRFB systems.

4.1.3 Problem Formulation

As seen from Figure 4.1, if a suitable estimate of μ is available, say $\hat{\mu}$, it can be used to compensate the CFO at the receiver front-end and thereby avoid its deleterious effects. Similarly, if estimates of the CIR coefficients $h[l]$ are available, denoted as $\hat{h}[l]$ for $l \in \{0, \ldots, Q-1\}$, they can be used on the receiver side to design a set of subband equalizers to counteract the distortion incurred by the input signals during their transmission. In this work, we focus on single-tap per subcarrier equalizer, as represented by the coefficients e_i in Figure 4.1, where $i \in \{0, \cdots M-1\}$, but generalizations to other, more advanced types of equalizers are possible. This simple equalization scheme inverts the channel at the center frequency of the corresponding subcarrier and it works well in mildly selective channels as long as the number of subcarriers is sufficiently large [14].

Our interest in this work, therefore, lies in the development of an efficient, data-aided ML based approach for the joint estimation of the CFO parameter μ and CIR coefficients $\{h[l]\}_{l=0}^{Q-1}$. We favor the use of data-aided over blind estimation, since the latter generally requires a long data record to achieve a desired level of accuracy, which in turns entails high computational complexity and limits applications to static or slowly time-varying channels. We consider the framework of point estimation theory, where the parameters under estimation are modelled as unknown, yet deterministic quantities, i.e., no prior distribution is assumed. Given the transmission of a known sequence of pilots, and the subsequent observation of the reconstructed subband signals over a given time interval, our aim is to develop and investigate the properties of the joint ML estimator of μ and $\{h[l]\}$.

4.2 Joint Estimation

In this section, we first derive a joint estimator of the CFO and CIR based on the ML principle, which employs known transmitted pilot symbols. We then propose a number of practical simplifications in the calculation of the associated log-likelihood function (LLF) that result in a lower implementation complexity for this estimator.

4.2.1 Data-aided ML estimator

We define a data frame as the set of M subband inputs $x_i[n]$, for $i \in \{0, 1, \ldots, M-1\}$, entering the transmit filter bank at time n. We assume that within a burst of N consecutive

frames, say from time $n = 0$ to $N - 1$, a total of T frames, referred to as pilot-frames and with time indices in $\mathcal{T} = \{t_n | 0 \leq t_0 < t_1 < \cdots < t_{T-1} \leq N - 1\}$, are selected for the transmission of pilots. At any given time t_n, a subset of S subbands, referred to as pilot-subbands and with frequency indices in $\mathcal{S} = \{s_i | 0 \leq s_0 < s_1 \cdots, < s_{S-1} \leq M - 1\}$, are dedicated to the transmission of pilot symbols $\mathsf{p}_{s_i}[t_n]$. In effect, we consider a rectangular lattice of $N_P = TS$ pilot symbols distributed over the time-frequency plane. Note that N_P should be greater than Q to guarantee that there exists enough data to estimate the $Q + 1$ unknown CFO and CIR parameters, i.e., μ and $\mathbf{h}$. Given the limited amount of training data that can be sent to estimate these parameters, it is prudent to select $\mathcal{S}$ and $\mathcal{T}$ such that the resulting estimates achieve a good performance (if not optimal) among other possible choices of $\mathcal{S}$ and $\mathcal{T}$ with the same N_P.

In that regard, we consider two main schemes for the distribution of the pilot symbols over the frequency axis, i.e. choices of the index set $\mathcal{S}$. In the first one, labeled as Scheme A for convenience, the pilot-subbands occupy adjacent positions along the frequency axis, i.e. $s_i - s_{i-1} = 1$. In the second one labeled as Scheme B, the pilot-subbands are equispaced to evenly cover the frequency axis, i.e. $s_i - s_{i-1} = \lfloor M/S \rfloor$, where $\lfloor . \rfloor$ denotes the floor function. Obviously, these two schemes are equivalent when $S = M$. Similarly, in terms of the distribution of pilot symbols over time, the index set $\mathcal{T}$ can be chosen in different ways. Here, we consider a scheme in which the T pilot-frames are divided into G groups evenly distributed throughout a burst, with each group consisting of T/G consecutive frames, where we assume T/G is an integer for simplicity. Examples of the distributions of pilot symbols over the frequency and time axes are depicted in Figure 4.2.

Let $z_{s_i}[t_n]$ denote the reconstructed signal corresponding to the transmitted pilot $\mathsf{p}_{s_i}[t_n]$. From (4.7), it follows that

$$\begin{aligned} z_{s_i}[t_n] &= \sum_{l=0}^{Q-1} \lambda_{s_i,t_n}(l,\mu) h[l] + \nu_{s_i}[t_n] \\ &= \sum_{l=0}^{Q-1} \bar{\lambda}_{s_i,t_n}(l,\mu) h[l] + w_{s_i}[t_n] + \nu_{s_i}[t_n], \end{aligned} \tag{4.12}$$

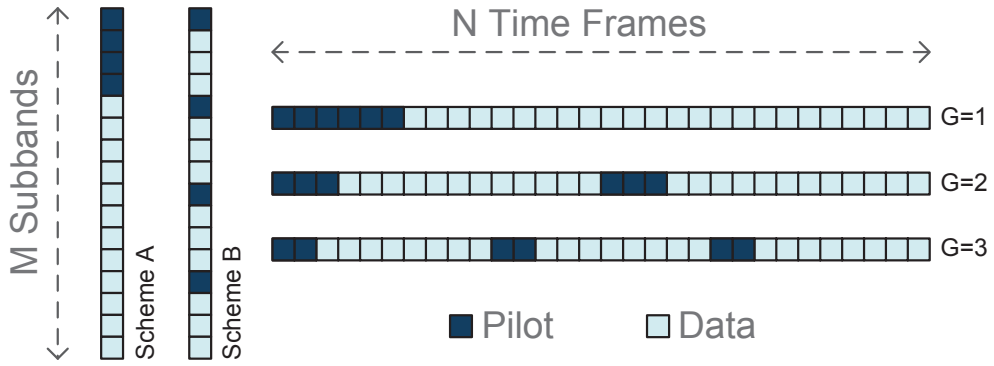

Fig. 4.2 Distribution of pilots over frequency (Scheme A and Scheme B with $S = 4$ pilot-subbands in $M = 16$ subbands) and time ($G = 1, 2$ and 3 groups for $T = 6$ pilot-frames in $N = 30$ frames)

where $\bar{\lambda}_{s_i,t_n}(l,\mu)$ and $w_{s_i}[t_n]$ are defined as

$$\bar{\lambda}^{l}_{s_i,t_n}(\mu) = \sum_{j\in\mathcal{S}}\sum_{p\in\mathcal{T}} \mathsf{p}_j[p]\gamma^{j,p}_{s_i,t_n}(l,\mu), \tag{4.13}$$

$$w_{s_i}[t_n] = \sum_{l=0}^{Q-1}\sum_{j\notin\mathcal{S}}\sum_{p\notin\mathcal{T}} x_j[p]\gamma^{j,p}_{s_i,t_n}(l,\mu)h[l]. \tag{4.14}$$

The term $\bar{\lambda}^{l}_{s_i,t_n}(\mu)$ in (4.13) represents the contribution from all the pilot-carrying time frames and subbands to the output $z_{s_i}[t_n]$, through the lth channel path, whereas $w_{si}[t_n]$ (4.14) is the total contribution from the non-pilot (i.e. data carrying) input symbols to $z_{s_i}[t_n]$ and can be interpreted as a form of *data-interference* on the estimation process. Considering the input symbols $x_j[p]$ as independent and identically distributed random variables with zero-mean and variance σ_x^2, it is shown in the Appendix that these interference terms $w_{s_i}[t_n]$ can be approximated as independent Gaussian random variables with zero-mean and variance

$$\sigma_w^2 = E\left\{|w_{s_i}[t_n]|^2\right\} = \sigma_x^2 \sum_{p\notin\mathcal{T}}\sum_{j\notin\mathcal{S}} |\Gamma^{j,p}_{s_i,t_n}(\mu)|^2, \tag{4.15}$$

where $\Gamma^{j,p}_{s_i,t_n}(\mu) = \sum_{l=0}^{Q-1}\gamma^{j,p}_{s_i,t_n}(l,\mu)h[l]$. Introducing $v_{s_i}[t_n] = w_{s_i}[t_n] + \nu_{s_i}[t_n]$, (4.12) can be

rewritten as

$$z_{s_i}[t_n] = \sum_{l=0}^{Q-1} \bar{\lambda}_{s_i,t_n}(l,\mu)h[l] + v_{s_i}[t_n], \tag{4.16}$$

If we further assume that the data symbols $x_j[p]$ and additive noise $\nu_{s_i}[t_n]$ are independent, it follows that $v_{s_i}[t_n]$ are independent Gaussian random variables with zero-mean and variance $\sigma_v^2 = \sigma_w^2 + \sigma_\nu^2$.

For convenience, we let $\mathbf{h} = [h[0], h[1], \cdots, h[Q-1]]^T$ denote the column vector of unknown channel coefficients and define the row vector

$$\boldsymbol{\lambda}_{s_i,t_n}(\mu) = [\bar{\lambda}_{s_i,t_n}(0,\mu), \bar{\lambda}_{s_i,t_n}(1,\mu), \cdots, \bar{\lambda}_{s_i,t_n}(Q-1,\mu)] \tag{4.17}$$

In terms of these, (4.16) can be expressed as

$$z_{s_i}[t_n] = \boldsymbol{\lambda}_{s_i,t_n}(\mu)\mathbf{h} + v_{s_i}[t_n], \tag{4.18}$$

In order to express the set of equations (4.18) in compact vector form, we first introduce:

$$\mathbf{z}_{s_i} = [z_{s_i}[t_0], z_{s_i}[t_1], \cdots, z_{s_i}[t_{L-1}]]^T \tag{4.19}$$

$$\boldsymbol{\lambda}_{s_i}(\mu) = [\boldsymbol{\lambda}_{s_i,t_0}(\mu)^T, \boldsymbol{\lambda}_{s_i,t_1}(\mu)^T, \cdots, \boldsymbol{\lambda}_{s_i,t_{L-1}}(\mu)^T]^T \tag{4.20}$$

$$\mathbf{v}_{s_i} = [v_{s_i}[t_0], v_{s_i}[t_1], \cdots, v_{s_i}[t_{L-1}]]^T \tag{4.21}$$

From (4.18), we have

$$\mathbf{z}_{s_i} = \boldsymbol{\lambda}_{s_i}(\mu)\mathbf{h} + \boldsymbol{v}_{s_i}. \tag{4.22}$$

We then stack these vectors and matrices over the frequency, and define

$$\mathbf{Z} = [\mathbf{z}_{s_0}^T, \mathbf{z}_{s_1}^T, \cdots, \mathbf{z}_{s_{S-1}}^T]^T, \tag{4.23}$$

$$\boldsymbol{\Lambda}(\mu) = [\boldsymbol{\lambda}_{s_0}(\mu)^T, \boldsymbol{\lambda}_{s_1}(\mu)^T, \cdots, \boldsymbol{\lambda}_{s_{S-1}}(\mu)^T]^T, \tag{4.24}$$

$$\mathbf{V} = [\mathbf{v}_{s_0}^T, \mathbf{v}_{s_1}^T, \cdots, \mathbf{v}_{s_{S-1}}^T]^T. \tag{4.25}$$

so that

$$\mathbf{Z} = \boldsymbol{\Lambda}(\mu)\mathbf{h} + \mathbf{V}, \tag{4.26}$$

where $\mathbf{\Lambda}(\mu)$ is an $N_P \times Q$ matrix, assumed to be of full column rank.

As a consequence of the AWGN model assumption and subsequent approximations on the data-interference $w_{s_i}[t_n]$, it follows that $\mathbf{V}$ is a complex circular Gaussian random vector with zero-mean and diagonal covariance matrix $\mathbf{C_V} = E[\mathbf{V}\mathbf{V}^H] = \sigma_v^2\mathbf{I}$. Accordingly, for given values of the unknown parameters μ and $\mathbf{h}$, the observation vector $\mathbf{Z}$ in (4.26) is also complex circular Gaussian with mean $\mathbf{\Lambda}(\mu)\mathbf{h}$ and covariance $\mathbf{C}_Z = \sigma_v^2\mathbf{I}$. The probability density function (PDF) of $\mathbf{Z}$, say $f(\mathbf{Z};\mu,\mathbf{h})$ can therefore be formulated as

$$\begin{aligned} f(Z;\mu,\mathbf{h}) &= \frac{1}{\pi^{N_P}\det(\mathbf{C}_Z)} \\ &\quad \exp\left[-(\mathbf{Z}-\mathbf{\Lambda}(\mu)\mathbf{h})^H\mathbf{C}_Z^{-1}(\mathbf{Z}-\mathbf{\Lambda}(\mu)\mathbf{h})\right] \end{aligned} \tag{4.27}$$

Taking the natural logarithm of this PDF, the LLF [130] for the parameters μ and $\mathbf{h}$ can be expressed (up to a constant term) in the form

$$\begin{aligned} \mathcal{L}(\mathbf{Z};\mu,\mathbf{h}) &= \log\big(f(\mathbf{Z}|\mu,\mathbf{h})\big) \\ &= -\frac{1}{\sigma_v^2}[\mathbf{Z}-\mathbf{\Lambda}(\mu)\mathbf{h}]^H[\mathbf{Z}-\mathbf{\Lambda}(\mu)\mathbf{h}]. \end{aligned} \tag{4.28}$$

The joint ML estimators of the CFO and CIR is obtained by maximizing the LLF (4.28) with respect to the unknown parameters μ and $\mathbf{h}$. In effect, this maximization amounts to finding the hypothetical values of the CFO and CIR such that the distorted pilots by these parameter values best match (in the LS sense) the reconstructed pilots at the output of the receive filter bank.

Since the LLF (4.28) is quadratic in the CIR parameters, a closed-form solution can be obtained for the optimum $\mathbf{h}$ in terms of μ. Specifically, fixing μ and varying $\mathbf{h}$ in $\mathbb{C}^Q$, the LLF (4.28) achieves its maximum at

$$\mathbf{h}_o(\mu) = \mathbf{\Lambda}(\mu)^\dagger\,\mathbf{Z} \tag{4.29}$$

where $\mathbf{\Lambda}(\mu)^\dagger = (\mathbf{\Lambda}(\mu)^H\mathbf{\Lambda}(\mu))^{-1}\mathbf{\Lambda}(\mu)^H$ is the pseudo-inverse of $\mathbf{\Lambda}(\mu)$. Next, upon substitution of (4.29) in (4.28), the ML estimate of the CFO can be obtained via a 1-dimensional search, i.e.:

$$\hat{\mu} = \arg\max_{\mu\in\mathcal{M}}\{\mathcal{L}(\mathbf{Z};\mu,\mathbf{h}_o(\mu))\}, \tag{4.30}$$

where $\mathcal{M}$ is the search range for μ. In practice, the optimization problem (30) can be solved in two steps. The first step, or coarse search, computes $\mathcal{L}(\mathbf{Z};\mu,\mathbf{h}_o(\mu))$ over a uniform grid of μ values and determines the location of its maximum on the grid, say μ_m. The second step, or fine search, attempts to find the local maximum nearest to μ_m, which can be handled by classic optimization methods due to the observed convexity[2] of the LLF $\mathcal{L}(\mathbf{Z};\mu,\mathbf{h}_o(\mu))$ in the vicinity of the true CFO. Since this LLF is periodic in μ with a period of one subband spacing, the search range $\mathcal{M}$ must be less than half the subband spacing to avoid ambiguity in the estimation. Finally, the ML estimate of the CIR is obtained by substituting the $\hat{\mu}$ in (4.29), that is:

$$\hat{\mathbf{h}} = \mathbf{h}_o(\hat{\mu}) = \mathbf{\Lambda}(\hat{\mu})^{\dagger}\,\mathbf{Z} \tag{4.31}$$

Except for Q, the maximum delay spread[3], no *a priori* information about the channel is required to implement the above ML estimator of the CFO and CIR. We also note that since the CFO μ is estimated first based on (4.30) and then exploited to obtain the CIR $\mathbf{h}$ via (4.31), this approach enables decoupling the estimation of the CFO from the CIR. Finally, for frequency-flat fading channels with $Q = 1$, the proposed method reduces to the ML CFO estimator previously reported by the authors in [79].

4.2.2 Simplifications of the LLF

Here, we propose two simplifications for $\bar{\lambda}_{s_i,t_n}(l,\mu)$ in (4.13), which considerably speed up the calculation of the LLF (4.30).

First consider the terms $\gamma^{j,p}_{s_i,t_n}(l,\mu)$ in (4.9), whose definition given in (4.9) includes a summation over the length D (often large) of the prototype filter $f_0[q]$. Recalling that for DFT-modulated filter banks, we have $f_i[q] = f_0[q]w^{-iq}$, we can write

$$\gamma^{j,p}_{s_i,t_n}(l,\mu) = w^{jl+K(pj-s_it_n)}\varphi^{t_n,p}_{s_i-j}(l,\mu), \tag{4.32}$$

where

$$\varphi^{n,p}_{\alpha}(l,\mu) = \sum_{q=-\infty}^{\infty} e^{j2\pi\frac{\mu}{M}q} f_0[q-l-pK]f_0^*[q-nK]w^{q\alpha}. \tag{4.33}$$

[2]In fact, the LLF is concave in the vicinity of the true CFO, but $-\mathcal{L}(\mathbf{Z};\mu,\mathbf{h}_o(\mu))$ is convex. This characteristic was observed over all of our experiments and for various setup values.

[3]For higher reliability, we can consider larger values of Q in the ML estimation at the expense of higher complexity.

By this simplification, instead of calculating $\gamma_{s_i,n}^{j,p}(l,\mu)$ for all the SM possible pairs (s_i, j), it is sufficient to compute $\varphi_{\alpha}^{n,p}(l,\mu)$ for at most[4] $2M-1$ possible different values of $s_i - j = \alpha \in \{-M+1, \cdots, M-1\}$ and find the corresponding $\gamma_{s_i,t_n}^{j,p}(l,\mu)$ by multiplication with a discrete phase factor as in (4.32). Therefore, we can roughly reduce the number of operations needed to compute the terms $\gamma_{s_i,t_n}^{j,p}(l,\mu)$ by a factor of at least $S/2$.

Next, consider the $\bar{\lambda}_{s_i,t_n}(l,\mu)$ in (4.13). Due to the excellent spectral containment of the prototype filters, we can assume that the main source of the CFO-induced interference on each target subband is due to its first few neighbouring subbands, and that interference from more distant subbands is negligible [79]. Therefore, as the second proposed simplification, to derive the total interference from subbands $j \in \mathcal{S}$ on the subband with index s_i in (4.13), it is sufficient to only factor in the contribution from a few neighbouring pilot-carrying subbands on each side of the s_ith one. As a result, (4.13) is approximated as

$$\bar{\lambda}_{s_i,t_n}^{l}(\mu) \approx \sum_{p\in\mathcal{T}} \sum_{j=i-\beta}^{i+\beta} \mathsf{p}_j[p]\gamma_{s_i,t_n}^{s_j,p}(l,\mu). \tag{4.34}$$

where in practice, the value of β can be set to 2 for Scheme A or less for Scheme B. This allows a reduction in the number of required operations to compute $\bar{\lambda}_{s_i,t_n}(l,\mu)$ by a factor $S/(2\beta+1)$.

4.3 Joint Cramer Rao Bound

In this section, we derive the CRB on the covariance matrix of unbiased estimators of the CFO and CIR, assuming the transmitted signals are known (i.e., pilots). We let $\boldsymbol{\theta}$ denote the complete vector of unknown (real) parameters

$$\boldsymbol{\theta} = [\mu, \mathbf{h}_R^T, \mathbf{h}_I^T]^T, \tag{4.35}$$

where $\mathbf{h}_R = \mathsf{Re}[\mathbf{h}] = [h_R[0], h_R[1], \cdots, h_R[Q-1]]^T$ and $\mathbf{h}_I = \mathsf{Im}[\mathbf{h}] = [h_I[0], h_I[1], \cdots, h_I[Q-1]]^T$ represent the real and imaginary parts of $\mathbf{h} = \mathbf{h}_R + \jmath\mathbf{h}_I$. Vector $\boldsymbol{\theta}$ consists therefore of $2Q+1$ real entries, which will be indexed by a or $b \in \{0, 1, \ldots, 2Q\}$. Let $\mathcal{I}(\boldsymbol{\theta})$ denote the $(2Q+1)\times(2Q+1)$ Fisher information matrix (FIM) for the estimation problem under

[4]Depending on which specific Scheme A or B is used for the distribution of the pilots over the frequency axis.

consideration. Since $\partial \mathbf{C}_{\mathbf{V}}/\partial\theta_a = \mathbf{0}$ for $0 \leq a \leq 2Q$, the (a,b)th entry of $\mathcal{I}(\boldsymbol{\theta})$ is given by [130]

$$\begin{aligned}[\mathcal{I}(\boldsymbol{\theta})]_{a,b} &= E\left\{\frac{\partial^2 \mathcal{L}(\mathbf{Z};\boldsymbol{\theta})}{\partial\theta_a \partial\theta_b}\right\} \\ &= 2\mathsf{Re}\left[\frac{\partial(\boldsymbol{\Lambda}(\mu)\mathbf{h})^H}{\partial\theta_a}\mathbf{C}_Z^{-1}\frac{\partial(\boldsymbol{\Lambda}(\mu)\mathbf{h})}{\partial\theta_b}\right] \\ &= \frac{2}{\sigma_v^2}\mathsf{Re}\left[\sum_{i=0}^{S-1}\sum_{n=0}^{T-1}\frac{\partial(\boldsymbol{\lambda}_{s_i,t_n}(\mu)\mathbf{h})^*}{\partial\theta_a}\frac{\partial(\boldsymbol{\lambda}_{s_i,t_n}(\mu)\mathbf{h})}{\partial\theta_b}\right]\end{aligned} \tag{4.36}$$

To evaluate the FIM, we consider the partial derivative of $\boldsymbol{\lambda}_{s_i,t_n}(\mu)\mathbf{h}$ with respect to θ_a for three different ranges of the index a, namely: $a = 0$, $1 \leq a \leq Q$ and $Q+1 \leq a \leq 2Q$.

When $a = 0$, we have

$$\begin{aligned}\frac{\partial(\boldsymbol{\lambda}_{s_i,t_n}(\mu)\mathbf{h})}{\partial\theta_0} &= \frac{\partial(\boldsymbol{\lambda}_{s_i,t_n}(\mu)\mathbf{h})}{\partial\mu} \\ &= \frac{\partial\boldsymbol{\lambda}_{s_i,t_n}(\mu)}{\partial\mu}\mathbf{h}\end{aligned} \tag{4.37}$$

For $1 \leq a \leq Q$, we can write

$$\begin{aligned}\frac{\partial(\boldsymbol{\lambda}_{s_i,t_n}(\mu)\mathbf{h})}{\partial\theta_a} &= \frac{\partial(\boldsymbol{\lambda}_{s_i,t_n}(\mu)\mathbf{h})}{\partial h_R[l]} = \boldsymbol{\lambda}_{s_i,t_n}(\mu)\frac{\partial\mathbf{h}}{\partial h_R[l]} \\ &= \bar{\lambda}_{s_i,t_n}(l,\mu)\end{aligned} \tag{4.38}$$

where $l = a - 1$. Similarly, for $Q+1 \leq a \leq 2Q$

$$\begin{aligned}\frac{\partial(\boldsymbol{\lambda}_{s_i,t_n}(\mu)\mathbf{h})}{\partial\theta_a} &= \frac{\partial(\boldsymbol{\lambda}_{s_i,t_n}(\mu)\mathbf{h})}{\partial h_I[l]} = \boldsymbol{\lambda}_{s_i,t_n}(\mu)\frac{\partial\mathbf{h}}{\partial h_I[l]} \\ &= \jmath\bar{\lambda}_{s_i,t_n}(l,\mu)\end{aligned} \tag{4.39}$$

where $l = a - (Q+1)$. Therefore, it is straightforward to deduce that

$$\frac{\partial(\boldsymbol{\lambda}_{s_i,t_n}(\mu)\mathbf{h})}{\partial h_I[l]} = \jmath\frac{\partial(\boldsymbol{\lambda}_{s_i,t_n}(\mu)\mathbf{h})}{\partial h_R[l]}. \tag{4.40}$$

As a result, $\mathcal{I}(\boldsymbol{\theta})$ can be partitioned as[5]

$$\mathcal{I}(\boldsymbol{\theta}) = \begin{bmatrix} \mathcal{I}_{0,0} & \mathsf{Re}[\Upsilon] & -\mathsf{Im}[\Upsilon] \\ \mathsf{Re}[\Upsilon]^T & \mathsf{Re}[\Psi] & -\mathsf{Im}[\Psi] \\ -\mathsf{Im}[\Upsilon]^T & \mathsf{Im}[\Psi] & \mathsf{Re}[\Psi] \end{bmatrix} \tag{4.41}$$

where, based on (4.36)-(39),

$$\mathcal{I}_{0,0} = \frac{2}{\sigma_v^2}\mathsf{Re}\left[\sum_{i=0}^{S-1}\sum_{n=0}^{L-1}\left|\frac{\partial(\boldsymbol{\lambda}_{s_i,t_n}(\mu))}{\partial\mu}\mathbf{h}\right|^2\right], \tag{4.42}$$

Υ is a $1 \times Q$ vector with its entries defined as

$$[\Upsilon]_{0,b} = \frac{2}{\sigma_v^2}\sum_{i=0}^{S-1}\sum_{n=0}^{L-1}\frac{\partial(\boldsymbol{\lambda}_{s_i,t_n}(\mu))}{\partial\mu}^* \mathbf{h}^* \bar{\lambda}_{s_i,t_n}(b,\mu) \tag{4.43}$$

and Ψ is a $Q \times Q$ matrix defined as

$$[\Psi]_{a,b} = \frac{2}{\sigma_v^2}\sum_{i=0}^{S-1}\sum_{n=0}^{L-1}(\bar{\lambda}_{s_i,t_n}(a,\mu))^* \bar{\lambda}_{s_i,t_n}(b,\mu). \tag{4.44}$$

The CRB on the covariance matrix of an unbiased estimator of $\boldsymbol{\theta}$, say $\hat{\boldsymbol{\theta}}$, is expressed as $\mathsf{Cov}(\hat{\boldsymbol{\theta}}) \geq \mathcal{I}(\boldsymbol{\theta})^{-1}$. In particular,, we can obtain the CRB on the variance of an unbiased CFO estimator $\hat{\mu}$ as

$$\mathsf{Var}(\hat{\mu}) \geq [\mathcal{I}^{-1}(\boldsymbol{\theta})]_{0,0} = \mathrm{CRB}_\mu \tag{4.45}$$

Note that in general, the entries of the vector Υ in (4.43) are not identically zero nor can they be neglected, and there is a coupling between the achievable estimation errors of μ and $\mathbf{h}$. As a result, the CRB on μ in the absence of channel knowledge will be larger than the one obtained with known CIR, which would be simply $\mathcal{I}_{00}^{-1}$. Similarly, the lower bound

[5]To simplify notations, the dependence of the FIM entries on the parameter vector $\boldsymbol{\theta}$ is omitted.

on the variance of the CIR's lth tap is

$$\begin{aligned}\mathsf{Var}(\hat{h}[l]) &= \mathsf{Var}(\hat{h}_R[l]) + \mathsf{Var}(\hat{h}_I[l]) \\ &\geq [\mathcal{I}^{-1}(\boldsymbol{\theta})]_{l+1,l+1} + [\mathcal{I}^{-1}(\boldsymbol{\theta})]_{Q+l+1,Q+l+1} \\ &= \mathrm{CRB}_{h[l]} \end{aligned} \tag{4.46}$$

Assuming independent estimates of the channel taps, we can obtain a lower bound on the average CIR estimation variance over the different taps by taking the average of (4.46), which can be expressed as

$$\mathrm{CRB}_{\mathbf{h}} = \frac{1}{Q}\left(\mathsf{tr}[\mathcal{I}^{-1}(\boldsymbol{\theta})] - [\mathcal{I}^{-1}(\boldsymbol{\theta})]_{0,0}\right) \tag{4.47}$$

This approach is convenient as it provides a single number against which to benchmark the performance of a particular channel estimation algorithm. Similar to what has been noted in [129,131], it can be seen that the CRB is a function of the particular channel realization. Note that in the above derivation of the CRB, we did not use the approximation given in (4.34) and factored in the contribution from all the input subbands as (4.13), although such simplifications as in Section III.B could also be applied.

4.4 Experimental Results

In this section, we investigate the performance of the proposed joint ML estimator of the CFO and CIR (4.30) and (4.31) through numerical simulations. The performance of the proposed estimator is compared with the derived CRB and some existing methods from the literature.

4.4.1 Methodology and Setup

We consider an OPRFB transceiver system (cf. Figure 4.1) with burst of size $N = 60$ symbols, $M = 64$ subbands, $K = 72$ upsampling/downsampling factor, input sampling rate $F_s = 41.67$kHz and prototype filter of length $D = 1728$ designed as described in Chapter 3. The input data sequence $x_i[n]$ consists of independent and equiprobable 4-QAM symbols with normalized power to unity, i.e. $|x_i[n]| = 1$. Without loss in generality, since the pilot symbols are known to the receiver, we set $\mathsf{p}_{s_i}[t_n] = 1$ for all pair (s_i, t_n).

The data at the output of the transmit filter bank is passed through a frequency selective wireless channel with randomly generated coefficients $h[l]$, based on the International Telecommunication Union (ITU) Vehicular A channel guidelines [132]. The channel consists of 8 taps, where the fifth and seventh taps are set to zero and the other taps with delays 0, 0.33, 0.66, 1, 1.66, 2.33 microseconds obey a Rayleigh distribution with relative average powers of 0, -1, -9, -10, -15, -20 dB, respectively. Here, we consider two different channel models, i.e.: time-invariant and time-varying. In the first case, the channel remains constant in time for the duration of a transmission burst while in the second case, the channel fading coefficients are correlated in time according to Jakes's model [133]. At the channel output, AWGN with power level of σ_ν^2 is added to the baseband received signal to obtain the desired SNR figure, defined as SNR=σ_s^2/σ_ν^2 with $\sigma_s^2 = E\{s[m]^2\}$ where $s[m] = \sum_{l=0}^{Q-1} h[l]y[m-1]$.

In our experiments, the proposed joint ML estimator of the CFO and CIR is implemented and compared to other possible approaches. In particular, based on the developed model for joint estimation in Section 4.2.1, two separate ML estimators for the CFO and CIR alone (i.e., assuming that the other set of parameters is known *a priori*), and respectively denoted as MLE-CFO and MLE-CIR, are considered. Results are also provided for the ML-based CFO estimation method developed by the authors in [79], which assumes a flat fading AWGN channel with known gain and is referred to here as simplified ML estimator (SMLE). In addition to these various estimators, we show results for the CRBs on the minimum achievable estimator variance of the CFO and CIR, as derived in Section 4.3. Since the proposed joint estimator of the CFO and CIR has to estimate more unknown parameters, its performance is expected to be inferior to the separate estimation methods, i.e., MLE-CIR, MLE-CFO and SMLE, which make use of *a priori* knowledge and can therefore be considered as lower bounds on estimation error for comparison purposes.

Experiments are carried out for different values of the system parameters, including: SNR, Doppler frequency, number of pilot-frames and pilot-subbands; we also denote by μ_o the true value of the CFO. For each choice of parameter set, we run 10^3 independent Monte Carlo trials[6] and compute the relevant performance measures under evaluation, i.e., the root mean squared error (RMSE) of the CFO and CIR estimates and the BER of the OPRFB transceiver system with CFO compensation and CIR equalization derived from the

[6]We observed that 10^3 trials are enough to get smooth curves.

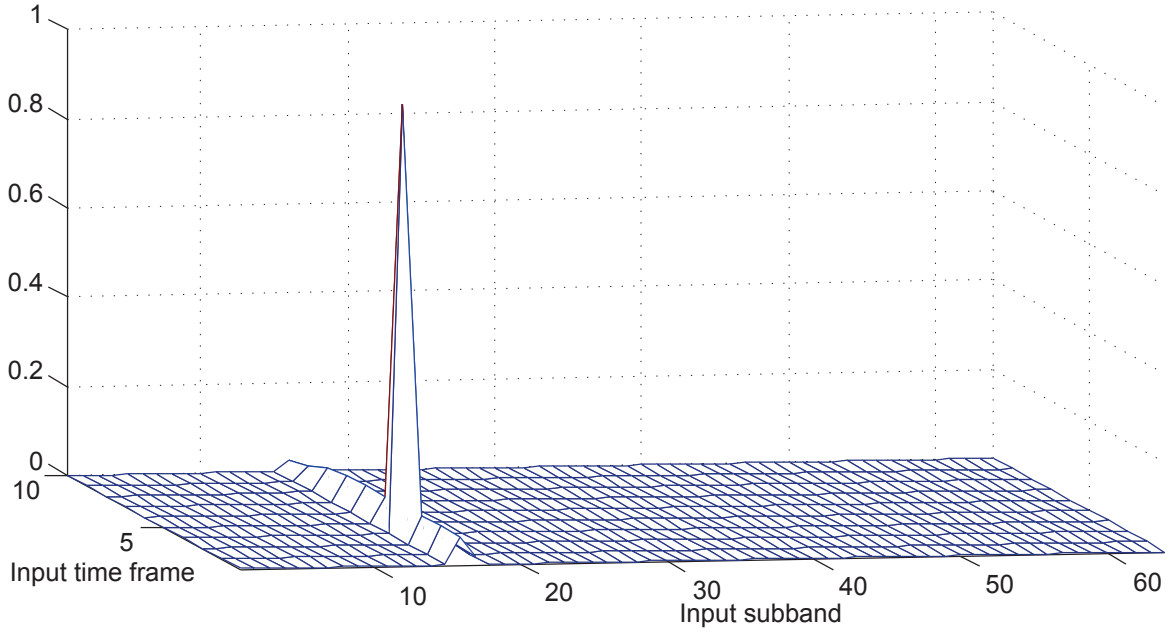

Fig. 4.3 Interference level $|\Gamma_{i,j}^{n,p}(\mu)|$ from pth input sample of jth subband on the nth output sample of ith subband ($p \in \{0, 1, \ldots, 10\}$, $j \in \{0, 1, \ldots, 63\}$, $n = 4$, $i = 16$, $\mu_o = 5\%$)

corresponding estimator[7]. In particular, the CFO is compensated at the receiver front-end and the single-tap per subcarrier equalizer is used at the output of receiver to counteract the channel effects. The coefficients of this equalizer, e_i for $i \in \{0, \cdots M-1\}$, are obtained from the estimated CIR coefficients $\hat{h}[l]$ as

$$e_i = \frac{1}{\hat{H}(z)}\Big|_{z=w^i} \tag{4.48}$$

where $\hat{H}(z) = \sum_{l=0}^{Q-1} \hat{h}[l] z^{-l}$.

4.4.2 Results and Discussions

We first investigate the performance of the proposed method under the assumption of a time-invariant channel, and then later consider the case of a time-varying channel.

We begin with preliminary results aimed at justifying certain assumptions and choices made in our work. In Figure 4.3, we sketch the cross-channel interference $|\Gamma_{i,j}^{n,p}(\mu)|$ for

[7]For the separate estimation methods, we simply assume exact knowledge of the missing parameters.

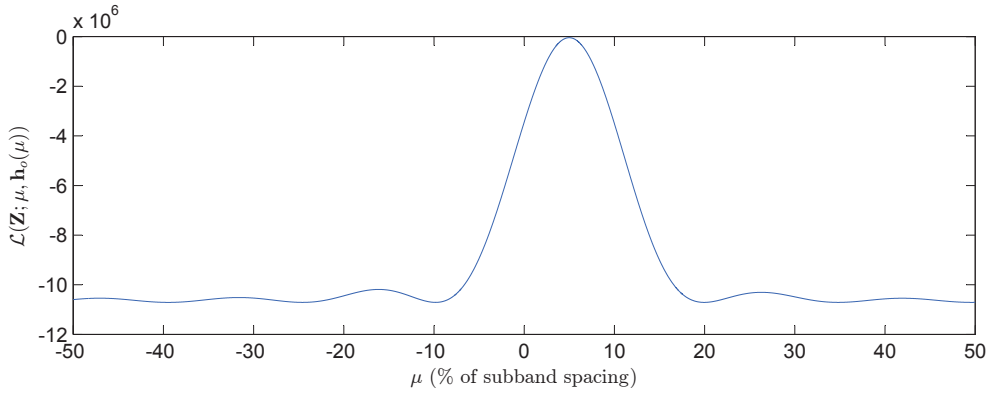

Fig. 4.4 Sample LLF versus CFO μ ($\mu_o = 5\%$, SNR= 40dB, $S = 64$, $T = 6$ and $G = 1$)

different values of p and j when n and i are fixed. It is evident that only a few subbands surrounding the target subband (here $i = 16$) are contributing as interference sources; it is therefore justified to set $\beta = 2$ in (4.34). Also, to support the choice of optimization method, a particular realization of the LLF (4.28) is plotted as a function of μ in Figure 4.4, where the true CFO $\mu_o = 5\%$ of subband spacing. In general, we find that the LLF is convex in a wide region surrounding the true CFO.

Next, we investigate the performance of the proposed estimator as a function of the SNR, where the following parameter values are used: $\mu_o = 5\%$, $S = 64$, $T = 6$ and $G = 1$. Figure 4.5 shows the RMSE performance of the CFO estimation for the proposed joint ML, MLE-CFO and SMLE methods, along with the CRB values as a function of SNR. To examine the effect of data-interference on the estimator accuracy, we also include results for the joint ML estimator when $w_{si}[t_n]$ (4.14) is set to zero (under *Joint without data*). As discussed in Section 4.3, the CRB is a function of the particular channel realization. Therefore, in Figure 4.5, the average, minimum and maximum CRB over the different channel realizations are reported. Similarly, Figure 4.6 shows the RMSE performance of the CIR estimation for the proposed joint ML (with and without data) and the MLE-CIR methods, along with the CRB. However, unlike Figure 4.5 for CFO estimation, the dependency of the CRB on the channel realization is negligible in this case and, accordingly, we just report the average CRB.

It can be seen from Figure 4.5 and 4.6 that at lower SNR, the proposed joint ML estimator provides an accuracy close to the (average) CRB for both the CFO and CIR

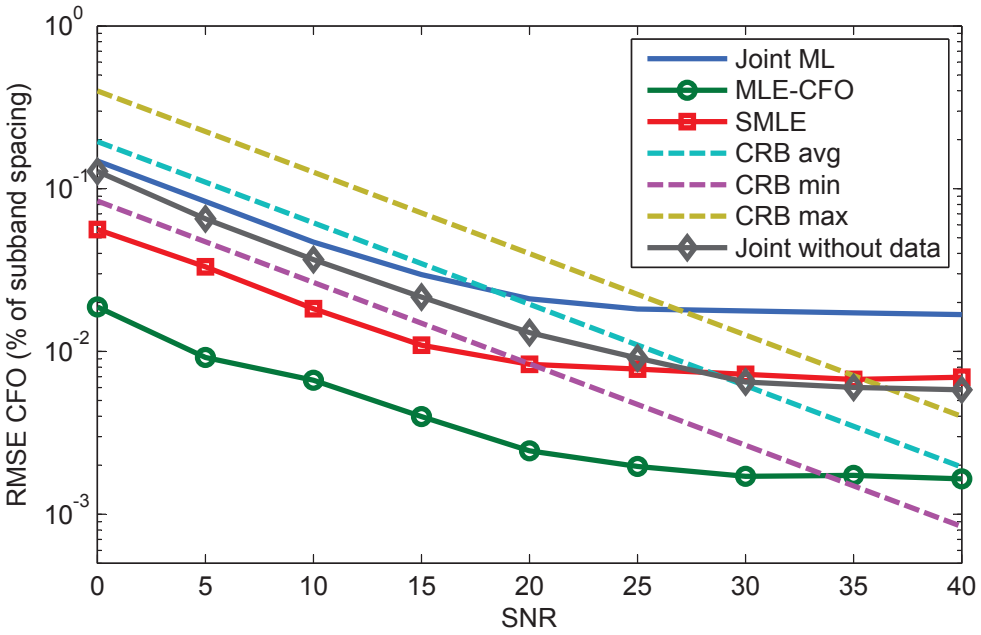

Fig. 4.5 RMSE of CFO estimation versus SNR ($\mu_o = 5\%$, $S = 64$, $T = 6$ and $G = 1$)

parameters. Moreover, as expected, the MLE-CFO and MLE-CIR methods achieve the best performance since they benefit from exact knowldege of the CFO and CIR, respectively. Also, the MLE-CFO derived here outperforms the SMLE method. At higher SNR, the estimation accuracy for all the methods reaches a lower floor due to several reasons. First, the simplifications made in Section 4.2.2 limit the accuracy of the estimator, whereas the CRB computation is exact. By increasing β in (4.34), we observed that the RMSE floor decreases at the cost of higher computational complexity. Another reason is due to the data noise term $w_{si}[t_n]$ in (14) which effectively limits the maximum achievable SNR to about 17dB, consistent with the theoretical value computed from data-interference's power in (4.15). Finally, the accuracy of the estimator is limited by granularity of the search in the optimization process.

The BER performance of the OPRFB system employing single-tap per subcarrier equalizer and CFO compensation using the proposed joint ML, MLE-CFO and MLE-CIR is shown in Figure 4.7, where the BER under ideal CFO and CIR knowledge is also provided as a benchmark. It can be seen that at high SNR, all of the proposed methods can reach the lower bound provided by ideal compensation, whereas the inaccuracy in CFO stimation

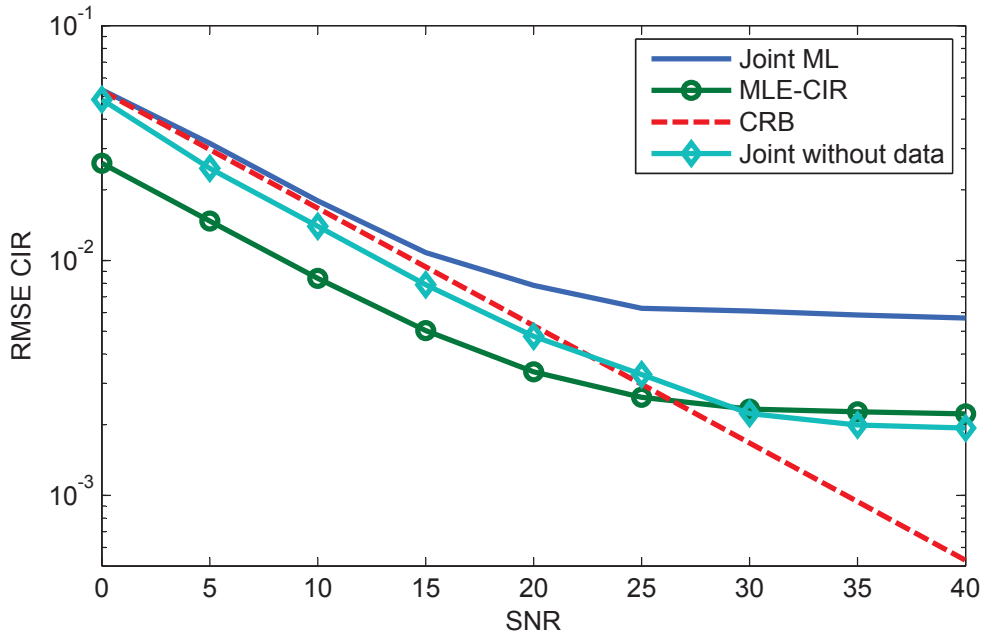

Fig. 4.6 RMSE of CIR estimation versus SNR ($\mu_o = 5\%$, $S = 64$, $T = 6$ and $G = 1$)

at low SNR results in increased BER for the joint ML and MLE-CFO methods.

To clarify the trade-off between estimation accuracy, on the one hand, and spectral efficiency and complexity, on the other hand, the RMSE performance of CFO and CIR estimation as a function of the total number of pilot-frames T is presented in Figs. 4.8 and 4.9, respectively. These results show that the proposed method estimates the CFO with similar accuracy as the average CRB, whereas the CIR estimation performance remains slightly above the CRB. It can also be noted that the reduction in RMSE by increasing T is lower for larger values of T, which is typical of a the $1/T$ behavior in parameter estimation. Similar results (not reported here) are observed by increasing the number of pilot-subbands S with fixed T.

Next, we compare the RMSE performance of the proposed estimator with different distributions of pilots in frequency when the total number of pilots N_P is fixed. In particular, Figs. 4.10 and 4.11 show the RMSE performance of the CFO and CIR estimation as a function of SNR, respectively. It can be observed that in terms of CFO estimation accuracy, scheme A exhibits a superior performance compared to scheme B, due to the reduced effect of the data interference. However, as the pilots in scheme A are not scattered over the

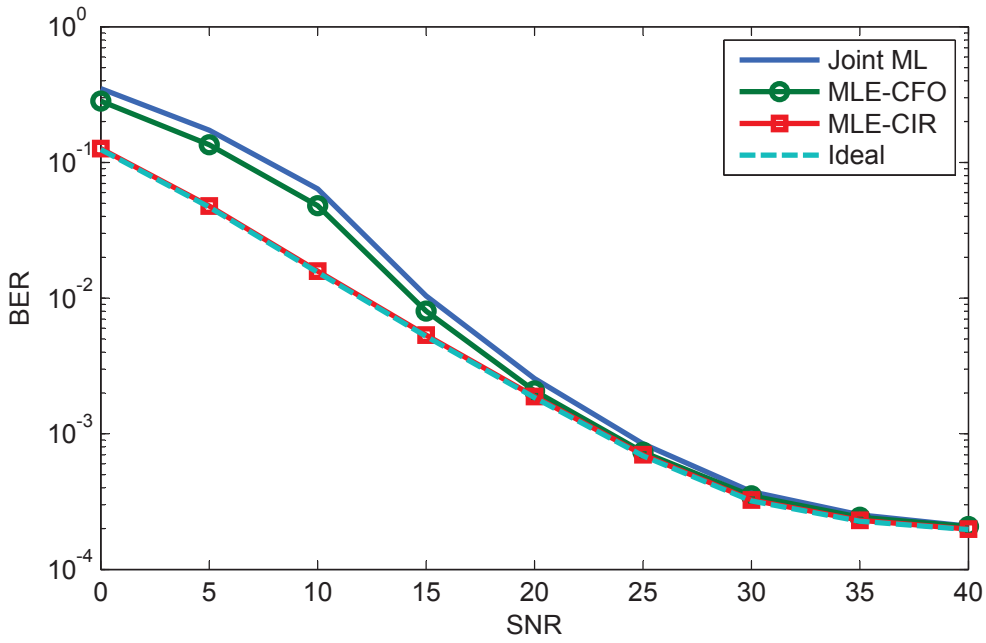

Fig. 4.7 BER versus SNR ($\mu_o = 5\%$, $S = 64$, $T = 6$ and $G = 1$)

whole frequency band, this scheme is not capable of properly estimating the entire channel. Apart from the results associated to CIR estimation with scheme A, it can be seen that smaller values of S (and larger T) result in a higher estimation accuracy.

Alternatively, the RMSE performance of the proposed joint CFO and CIR estimator with different distributions of pilots in time is shown in Figs. 4.12 and 4.13, respectively. In particular, pilots are divided to $G = 1, 2$ and 3 groups and the estimator provides G different estimates of CIR corresponding to each group of pilots, whereas the CFO is assumed to be fixed over time. In this scenario with time-invariant channel model, the preamble implementation of the pilots (i.e., $G = 1$) displays a more accurate estimation of CFO and CIR compared to the case where $G = 2$ or $G = 3$. This superior performance is due to the fact that the data-interference is less when G is smaller.

In the wireless communication, when at least one side of the transmission (transmitter or receiver) is mobile, a Doppler shift spreads the signal in frequency and results in time-variation of the CIR. In Figs. 4.14 and 4.15, the RMSE performance of the proposed joint CFO and CIR estimation method for various distributions of pilots in time is plotted as a function of the maximum Doppler frequency f_D. The maximum Doppler frequency can be derived as $f_D = \frac{v f_c}{c_0}$, where v is the mobile speed in m/s, f_c is the carrier frequency

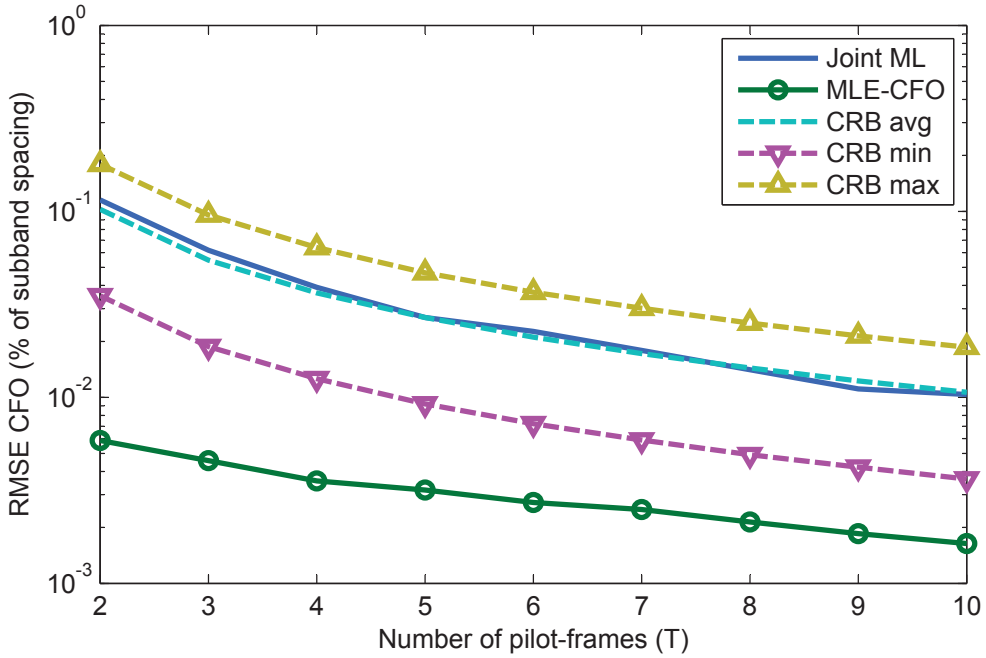

Fig. 4.8 RMSE of CFO estimation versus number of pilot-frames ($\mu_o = 5\%$, $S = 64$, $G = 1$ and SNR= 20dB)

and $c_0 = 3 \times 10^8$m/s is the speed of light. Here, we assume $f_c = 800$MHz (similar to LTE and GSM). The values of f_D in Figs. 4.14 and 4.15, are equivalent to 4 different mobile speeds, that is 5, 60, 120 and 250 km/h corresponding to the speed of pedestrian, car in the urban area, car in the highway and high-speed train, respectively. The comparisons between these patterns show that for low mobility, CFO can be better estimated by the preamble implementation of the pilots. However, with increased mobility, the difference between the CFO estimation accuracy with $G = 1, 2$ and 3 is negligible, whereas the scattered pilot schemes, i.e., $G = 2$ or 3, estimate the CIR slightly better than the preamble implementation of the pilots.

4.5 Conclusion

In this chapter, we proposed a data-aided joint ML estimator of CFO and CIR for OPRFB transceivers, where its complexity was considerably reduced through simplifying the underlying LLF. The CRB on the joint estimator variance was also derived and used as a benchmark. Moreover, different distributions of pilots over time-frequency plane were con-

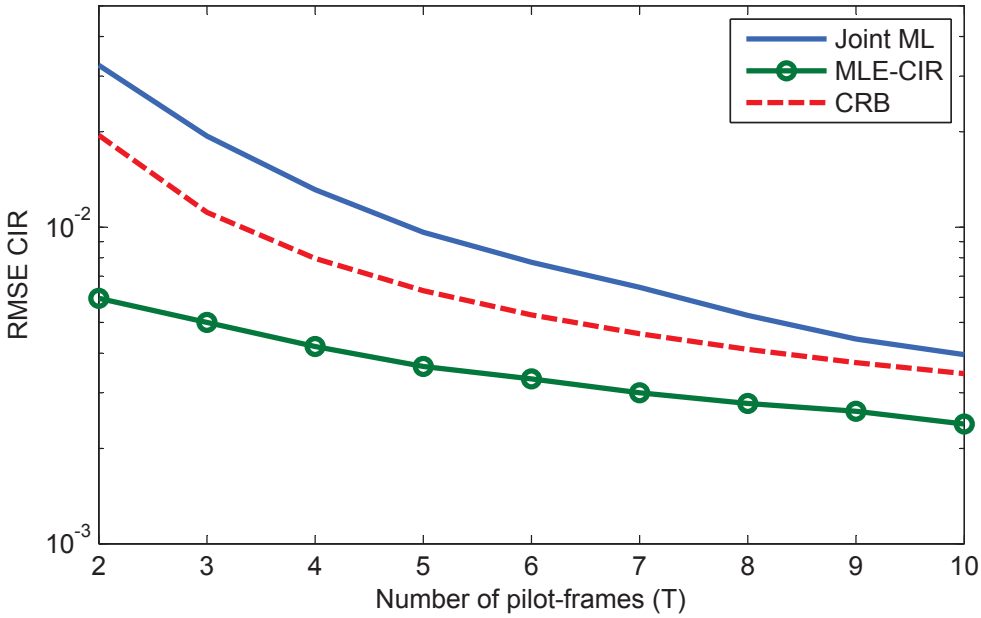

Fig. 4.9 RMSE of CIR estimation versus number of pilot-frames ($\mu_o = 5\%$, $S = 64$, $G = 1$ and SNR= 20dB)

sidered and tested for various scenarios over time-invariant and time-varying frequency selective channels. Simulation results demonstrated that the proposed estimator exhibits a performance close to the CRB and can robustly estimate CFO and CIR over different experimental setups.

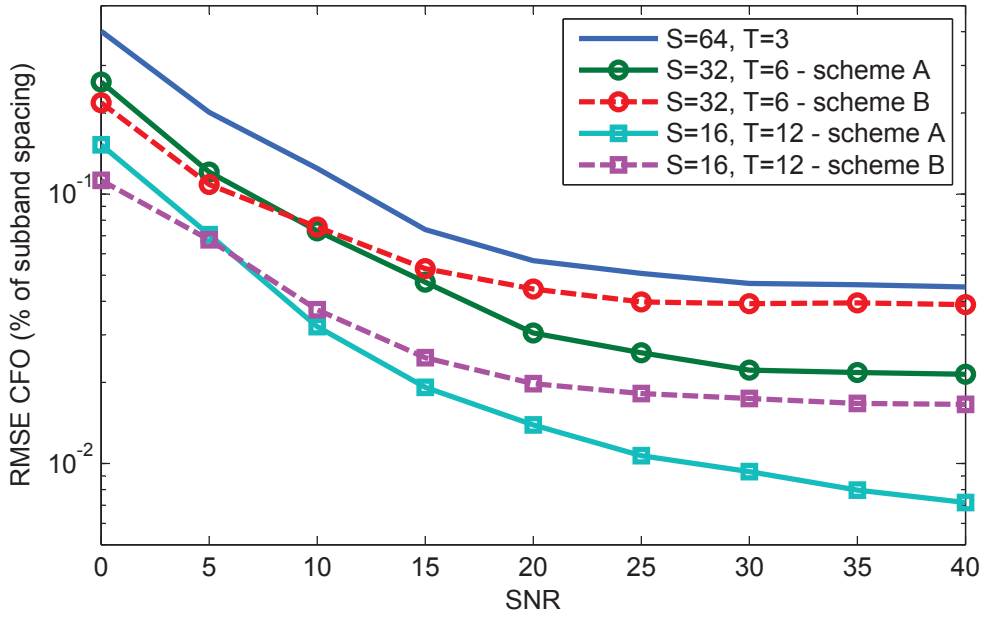

Fig. 4.10 RMSE of CFO estimation versus SNR for various pilot distributions in frequency ($\mu_o = 5\%$, $N_P = 192$, $G = 1$)

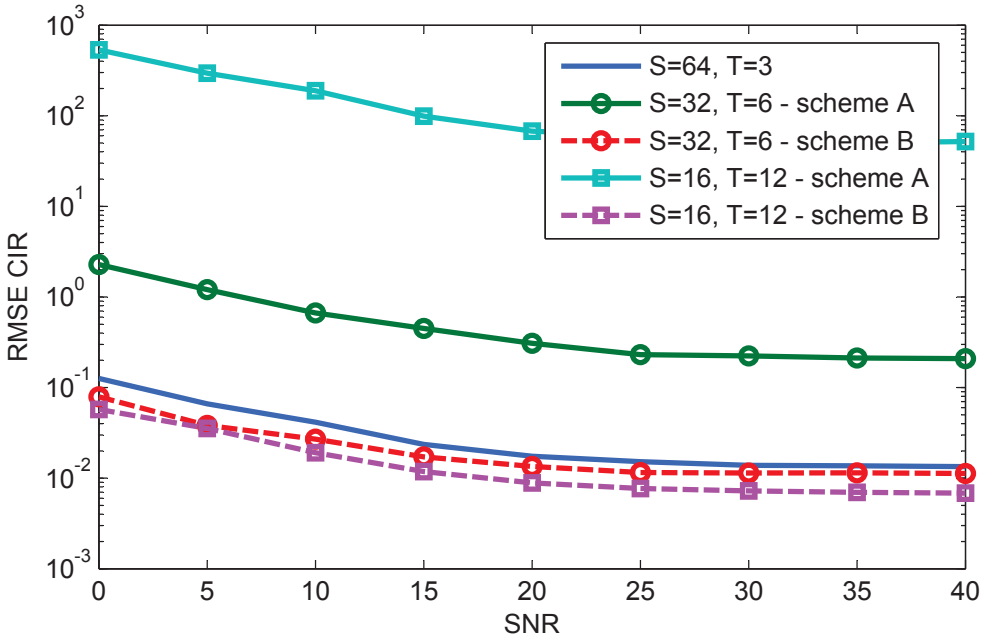

Fig. 4.11 RMSE of CIR estimation versus SNR for various pilot distributions in frequency ($\mu_o = 5\%$, $N_P = 192$, $G = 1$)

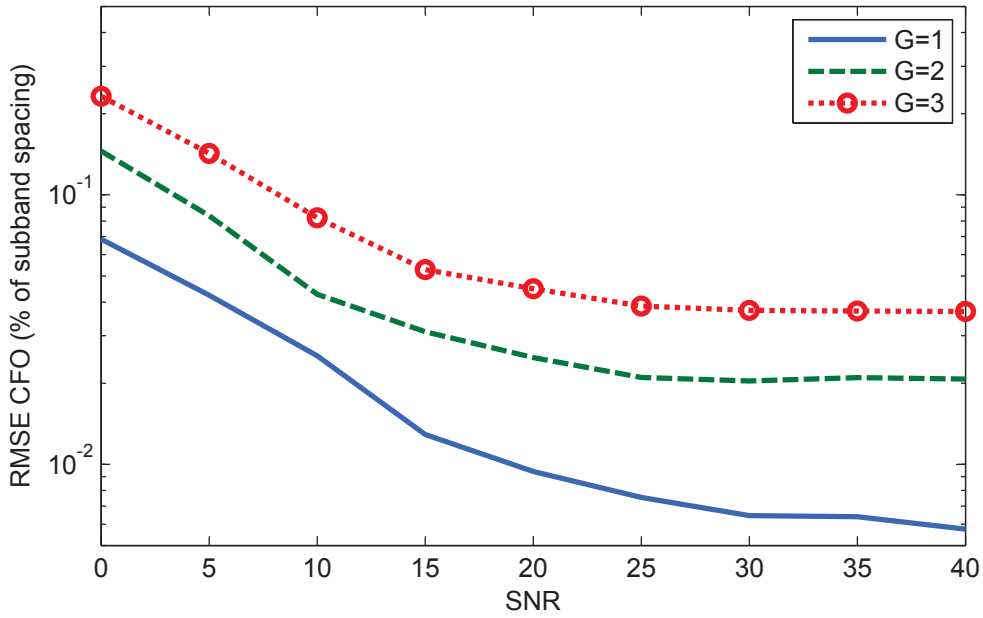

Fig. 4.12 RMSE of CFO estimation versus SNR for various pilot distributions in time ($\mu_o = 5\%$, $S = 64$, $T = 12$)

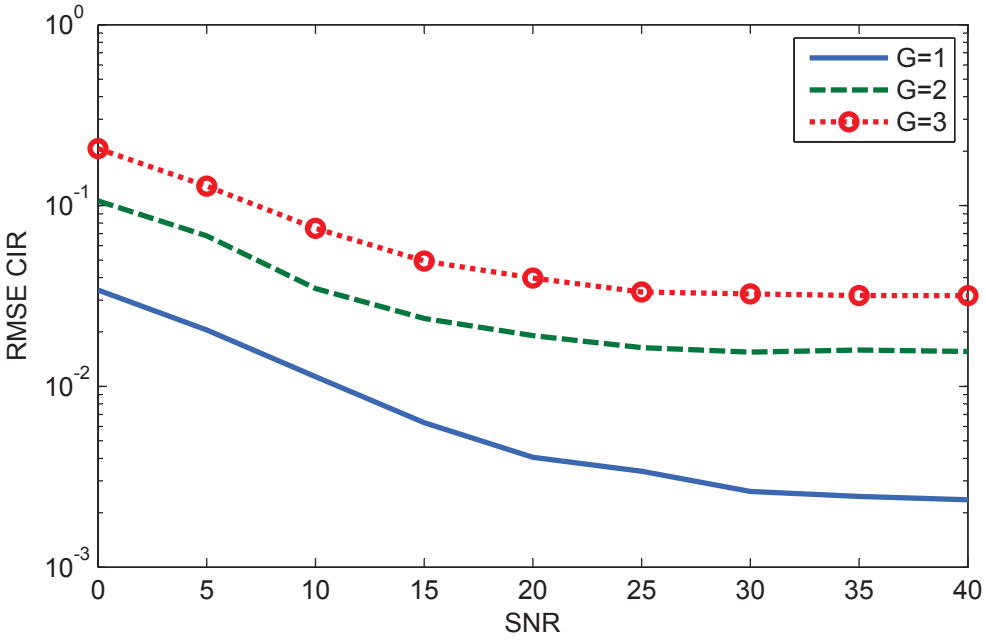

Fig. 4.13 RMSE of CIR estimation versus SNR for various pilot distributions in time ($\mu_o = 5\%$, $S = 64$, $T = 12$)

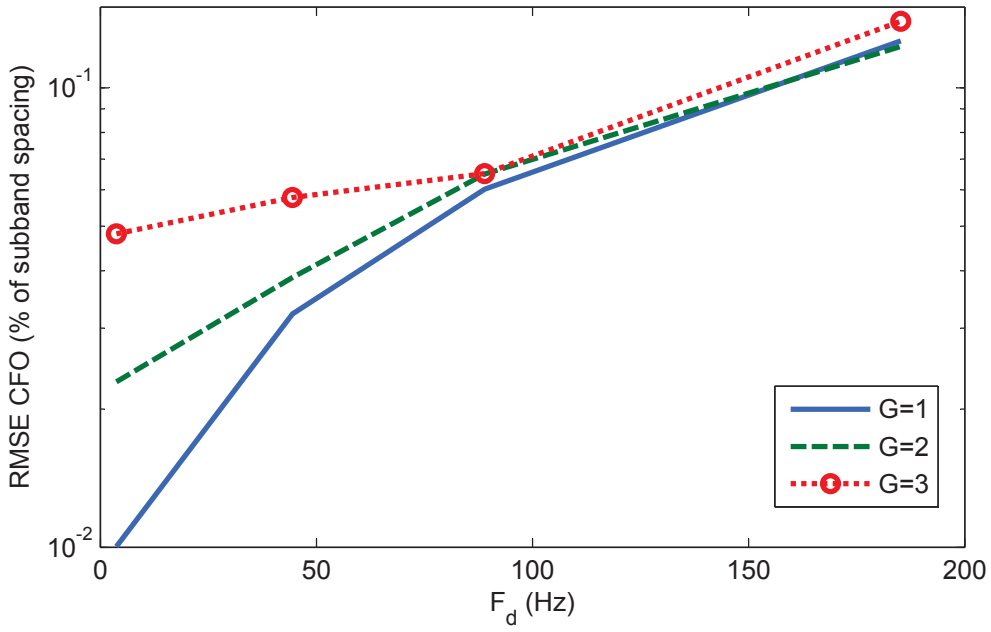

Fig. 4.14 RMSE of CFO estimation versus Doppler Frequency ($\mu_o = 5\%$, $T = 12$ and SNR= 20dB)

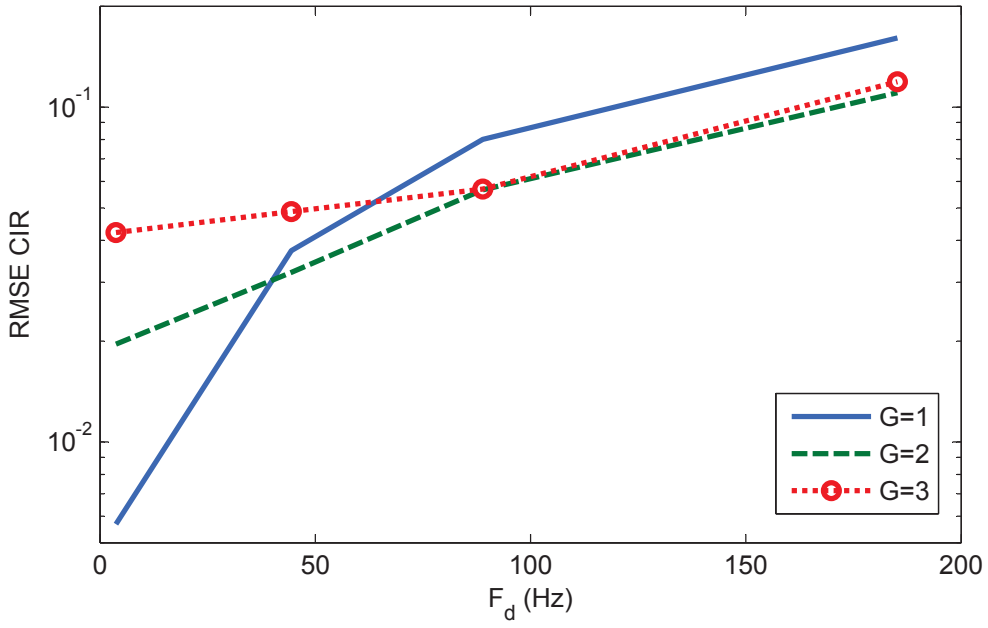

Fig. 4.15 RMSE of CIR estimation versus Doppler Frequency ($\mu_o = 5\%$, $T = 12$ and SNR= 20dB)

Chapter 5

Joint Synchronization and Equalization in the Uplink of MU-OPRFB

In this chapter, we develop a data-aided joint maximum likelihood (ML) estimator of the CFO and CIR that is specifically designed for MU-OPRFB systems operating over frequency selective fading channels. The estimated CFO and CIR parameters are used to design effective compensation mechanisms for each individual user, i.e. frequency synchronization and single-tap per subband equalizer. Section 5.1 presents the MU-OPRFB system model along with various subband allocation schemes and discusses the effects of CFO on the signal recovery process at the receiver side for each user. The joint ML estimator of the CFO and CIR is developed in Section 5.2, whereas an iterative approach is also proposed to improve the estimation accuracy. The performance of the proposed synchronization and equalization methods is investigated in Section 5.3 via computer simulations for various subband allocation schemes with different pilot distributions over time-invariant and (mobile) time-varying channels and some conclusions are offered in Section 5.4.

5.1 Multi-user OPRFB System Model

We consider the uplink transmission in a MU-OPRFB system, as depicted in Fig. 5.1, where U denotes the number of users. A total of M subbands, indexed from 0 to $M-1$, are

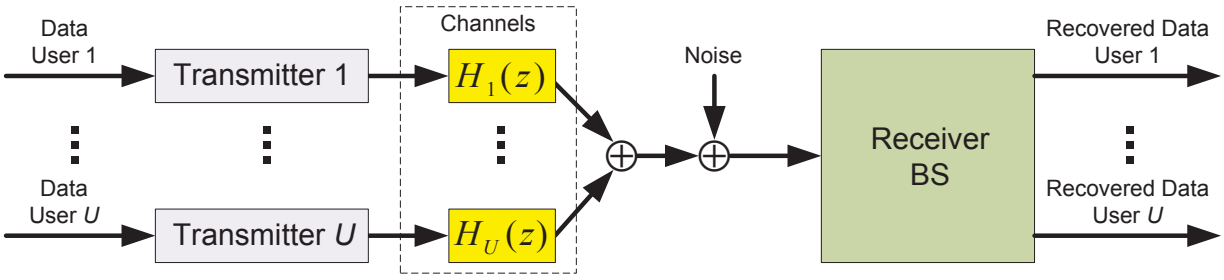

Fig. 5.1 Uplink transmission in MU-OPRFB system

available for multicarrier transmission, where they are shared among the U users. The set of subbands allocated to user $u \in \{1, \ldots, U\}$ is represented as $\mathcal{S}_u = \{\iota_1^u, \ldots, \iota_{|\mathcal{S}_u|}^u\}$, where $0 \leq \iota_1^u < \ldots < \iota_{|\mathcal{S}_u|}^u \leq M-1$ and $|\mathcal{S}_u|$ denotes the cardinal number of set $\mathcal{S}_u$. Note that no subband is shared between different users, i.e., $\mathcal{S}_u \cap \mathcal{S}_v = \emptyset$, for $u \neq v$. Three common subband allocation schemes, namely blocked, blocked with guard and interleaved, are considered in this work, as depicted in Fig. 5.2. The blocked scheme allocates a contiguous group of subbands to each user, whereas in blocked with guard scheme, one subband is left unused between the blocks of subbands assigned to different users. Alternatively, to exploit the frequency diversity of multipath channels, the interleaved scheme is considered where each user's allocated subbands are uniformly spaced over the channel bandwidth. Although the available subbands are evenly divided between users in our presentation, these schemes can easily be expanded to uneven allocations to meet specific quality of service (QoS) or data rate requirements for different users in a given application.

It is shown in [81] that the proper choice of CFO estimation method in the multi-user context depends on the adopted subband allocation scheme. Moreover, channel estimation can only be performed within the allocated subbands of each individual user separately, as each user is only assigned a subset of the whole frequency band. Recently, the block allocation has drawn more attention from the industry and standard bodies, as in e.g. LTE release 8 [80] where users can select the best available blocks based on SNR indicators, although the details of such allocation falls outside the scope of this work. Hence, it is of special interest to develop synchronization and equalization methods that perform well with common allocation schemes and, in particular, with the blocked scheme.

The MU-OPRFB transceiver for the uth user is depicted in block diagram form in Fig. 5.3, where K represents the upsampling/ downsampling factor and $K > M$ is assumed

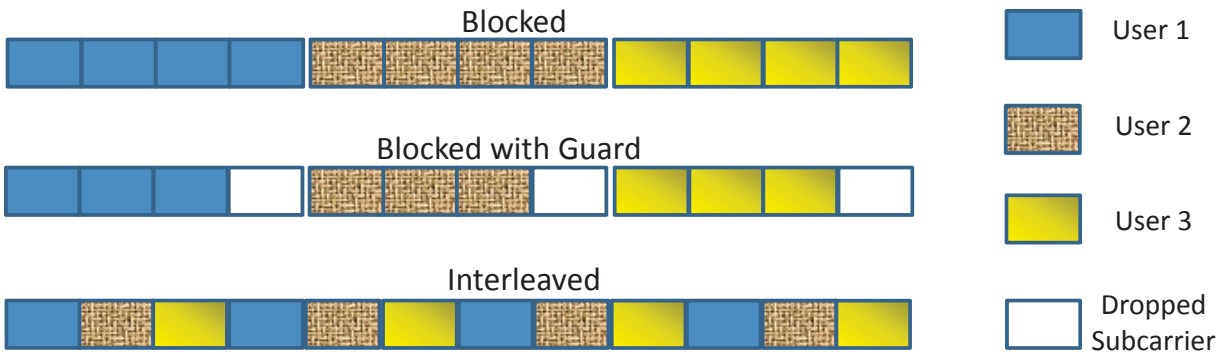

Fig. 5.2 Allocation schemes with $U = 3$ users over $M = 12$ subbands

(oversampled). For $i \in \{1, \cdots, |\mathcal{S}_u|\}$, $x_i^u[n]$ denotes the complex-valued data sequence transmitted by this user on the ith subband of the set $\mathcal{S}_u$ at discrete-time nT_s, where $n \in \mathbb{Z}$, $T_s = F_s^{-1}$ and F_s is the input sampling rate. In MU-OPRFB systems, the transmit and receive subband filters are derived from common prototypes with FIR of length D and respective system functions $F_0(z) = \sum_{n=0}^{D-1} f_0[n]z^{-n}$ and $G_0(z) = \sum_{n=0}^{D-1} g_0[n]z^n$. For convenience in analysis, $G_i^u(z)$ is assumed non-causal although in practice, causality can be restored simply by introducing an appropriate delay in the receiver. Defining $w = e^{-\jmath 2\pi/M}$, the DFT modulated transmit and receive filters for the ith subband of the uth user are respectively obtained as $F_i^u(z) = F_0(zw^{\iota_i^u})$, $G_i^u(z) = G_0(zw^{\iota_i^u})$. As proposed in Chapter 3, to enforce the perfect reconstruction (PR) property, the paraconjugates of the transmit filters are employed as receive filters, i.e., $g_i^u[n] = f_i^u[n]^*$. In this work, the filter length D is restricted to be a multiple of M and K, i.e., $D = d_P P$, where P denotes the least common multiple of M and K and d_P is an integer. The transmitter output signal of the uth user at discrete-time mT_s/K, is given by

$$y_u[m] = \sum_{i \in \mathcal{S}_u} \sum_{q} x_i^u[q] f_i^u[m - qK] \tag{5.1}$$

where the range of the summation over q is delimited by the finite support of the subband FIR filters, $f_i^u[m]$.

We assume that during a time interval equal to the processing delay of the transceiver system (i.e., $2DT_s/K$), the transmission channel of the uth user can be modeled as a linear time-invariant system with FIR $h_u[l]$ of length Q and corresponding system function,

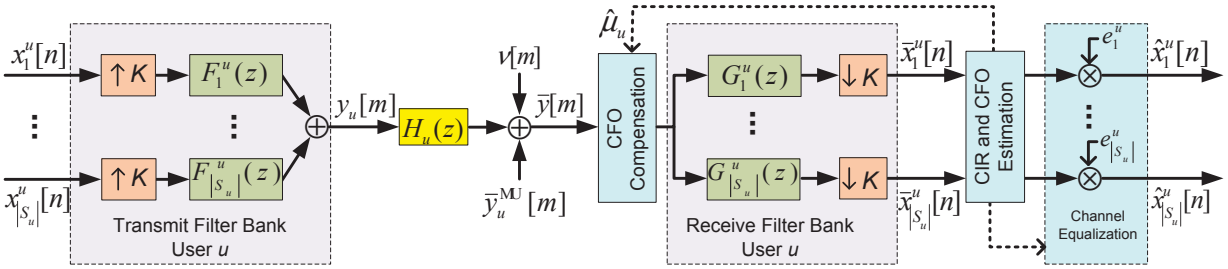

Fig. 5.3 Transceiver chain of the uth user in a MU-OPRFB system with CFO and channel estimation

$H_u(z) = \sum_{l=0}^{Q-1} h_u[l]z^{-l}$. Note that Q is chosen according to the maximum expected delay spread for the assumed conditions of radio propagation. Similar to OFDMA, the channel coherence time is much larger than the symbol duration in MU-OPRFB systems. Consequently, we can assume that channel remains static over several MU-OPRFB symbols. In the presence of CFO, the received signal from the uth user, can be modeled as

$$\bar{y}_u[m] = e^{j2\pi\frac{\mu_u}{M}m} \sum_{l=0}^{Q-1} h_u[l]y_u[m-l] \tag{5.2}$$

where μ_u is the normalized CFO with respect to the subband spacing F_sK/M.

The received signal at the BS is corrupted by an AWGN sequence $\nu[m]$, with zero-mean and variance $E\{|\nu[m]|^2\} = \sigma_\nu^2$, where $E\{.\}$ denotes statistical expectation; the noise is assumed to be statistically independent from the input data. The received baseband discrete-time signal $\bar{y}[m]$ can therefore be expressed as

$$\bar{y}[m] \;\; = \;\; \sum_{u=1}^{U} \bar{y}_u[m] + \nu[m] \tag{5.3}$$

Alternatively, from the perspective of the uth user, (5.3) can be written as

$$\bar{y}[m] = \bar{y}_u[m] + \bar{y}_u^{\mathrm{MU}}[m] + \nu[m] \tag{5.4}$$

where $y_u^{\mathrm{MU}}[m]$ represents the transmitted signals from all users other than the u-th one:

$$\bar{y}_u^{\mathrm{MU}}[m] = \sum_{\substack{v=1 \\ v\neq u}}^{U} \bar{y}_v[m] \tag{5.5}$$

On the receiver side, signal $\bar{y}[m]$ is passed through a bank of analysis filters and downsampled by K. Accordingly, the reconstructed signal for the ith subband of the uth user can be written as

$$\begin{aligned} \bar{x}_i^u[n] &= \sum_q \bar{y}[q] f_i^u[q-nK]^* \\ &= \sum_{l=0}^{Q-1} \sum_p \sum_{j\in\mathcal{S}_u} x_j^u[p] \gamma_{i,n}^{j,p}(l,\mu_u,u) h_u[l] + \psi_i^u[n] + \nu_i^u[n] \end{aligned} \tag{5.6}$$

where $\gamma_{i,n}^{j,p}(l,\mu_u,u)$, $\psi_i^u[n]$ and $\nu_i^u[n]$ are defined as

$$\gamma_{i,n}^{j,p}(l,\mu_u,u) = \sum_q e^{\jmath 2\pi \frac{\mu_u}{M} q} f_j^u[q-l-pK] f_i^u[q-nK]^* \tag{5.7}$$

$$\psi_i^u[n] = \sum_q \bar{y}_u^{\mathrm{MU}}[q] f_i^u[q-nK]^* \tag{5.8}$$

$$\nu_i^u[n] = \sum_q \nu[q] f_i^u[q-nK]^*. \tag{5.9}$$

The complex factor $\gamma_{i,n}^{j,p}(l,\mu_u,u)$ characterizes the interference level of the pth input sample from the jth subband of user u on the nth output sample of the ith subband of the same user, in the presence of CFO with magnitude μ_u through the lth path of the channel between this user and the BS. The terms $\psi_i^u[n]$ and $\nu_i^u[n]$ represent the total contribution from the other users' input symbols (i.e., MAI) and the additive noise to $\bar{x}_i^u[n]$, respectively.

Based on our earlier assumptions on the additive noise $\nu[q]$ in (5.3) and the PR properties of the subband filters, it follows that the noise term $\nu_i^u[n]$ in (5.9) is normally distributed with zero-mean and covariance $E\left\{\nu_i^u[p]\nu_j^u[q]^*\right\} = \delta_{ij}\delta_{pq}\sigma_\nu^2$, where δ_{ij} denotes the Kronecker

delta function. A similar conclusion can be reached for the multi-user interference term $\psi_i^u[n]$ in (5.8), if we model the input signals from the interfering users, i.e. $x_i^v[q]$ for all $v \neq u$ and $i \in \mathcal{S}_v$, as independent zero-mean white data sequences with variance σ_x^2. In this case, it follows from (5.1), (5.2), (5.5) and (5.8) that the multi-user interference term $\psi_i^u[n]$ is the sum of a large number of independent random contributions and based on the central limit theorem [134], this term can be approximated[1] as a normally distributed random variable with zero-mean. In this work, we further assume that in the subband domain, $\psi_i^u[n]$ can be modeled as a white noise sequence, i.e. with covariance $E\left\{\psi_i^u[p]\psi_j^u[q]^*\right\} \simeq \delta_{ij}\delta_{pq}\sigma_\psi^2$ where σ_ψ^2 is the corresponding variance. While it is not possible to provide a simple proof of this result based on the above equations, we have been able to verify its validity through numerical simulations. In practice, σ_ψ^2 can be obtained based on measurements of interference power.

As seen from Fig. 5.3, if a suitable estimate of μ_u is available, say $\hat{\mu}_u$, it can be used to compensate the CFO at the receiver front-end on the allocated subbands of the uth user and thereby avoid its deleterious effects. Similarly, equalizer coefficients, e.g., e_i^u for a single-tap per subcarrier equalizer, can be derived based on estimates of the channel coefficients, say $\hat{h}_u[l]$ for $0 \leq l < Q$, in order to reverse the distortion incurred by the input $x_i^u[n]$ their transmission. Our interest in this work, therefore, lies in the development of an efficient, data-aided ML-based approach for the estimation of the CFO parameter μ_u and the equalizer coefficients e_i^u for the uth user. Considering the requirements of multi-user applications, this estimation approach should be able to determine the parameter of interest of the uth user independently of the transmission state of the other users.

5.2 Joint Estimation

In this section, we derive a joint estimator of CFO and equalizer coefficients for the uth user. We define a data frame as the set of $\mathcal{S}_u$ subband inputs $x_i^u[n]$, for $u \in \{1, \ldots, U\}$ and $i \in \mathcal{S}_u$, entering the transmit filter bank at time n. We assume that within a burst of N consecutive frames, say from $n = 0$ to $N-1$, a total of T_u frames, denoted as pilot-frames, with time indices t_n in $\mathcal{T}_u = \{t_1, \ldots, t_{T_u}\}$ are selected for the transmission of pilot tones, where $t_1 < t_2 < \ldots < t_{T_u}$ and $t_n \in \{0, \ldots, N-1\}$ for $n \in \{1, \ldots, T_u\}$. At any given pilot-

[1] Minor deviations from this assumption are not critical in our work, in the sense that the resulting ML estimator of CFO and CIR can still be applied to the observed data and produce useful results.

frame t_n, all the $|\mathcal{S}_u|$ allocated subbands to the user u with indices $i \in \mathcal{S}_u$ are dedicated to the transmission of pilot symbols $\mathsf{p}_i^u[t_n]$. In order to track the time-varying channel, various distributions of pilots over time are considered. $\mathcal{T}_u$ is chosen such that the T_u pilot-frames are divided into G groups evenly distributed throughout a burst, with each group consisting of T_u/G (integer) consecutive frames, i.e., $t_n = (\lceil nG/T_u \rceil - 1)N/G + ((n-1) \mod (T_u/G))$, where $\lceil . \rceil$ and $\mod$ denote the ceil function and modulo operation, respectively. However, our approach can be applied to other distributions of pilot symbols.

Let $z_i^u[t_n]$ denote the reconstructed signal corresponding to the transmitted pilot $\mathsf{p}_i^u[t_n]$. From (5.6), it follows that

$$z_i^u[t_n] = \sum_{l=0}^{Q-1} \lambda_{i,t_n}(l, \mu_u, u) h_u[l] + v_i^u[t_n] \tag{5.10}$$

where we defined

$$\lambda_{i,t_n}^u(l, \mu_u) = \sum_{p \in \mathcal{T}_u} \sum_{j \in \mathcal{S}_u} \mathsf{p}_j[p] \gamma_{i,t_n}^{j,p}(l, \mu_u, u) \tag{5.11}$$

$$v_i^u[t_n] = w_i^u[t_n] + \psi_i^u[t_n] + \nu_i^u[t_n] \tag{5.12}$$

$$w_i^u[t_n] = \sum_{l=0}^{Q-1} \sum_{p \notin \mathcal{T}_u} \sum_{j \in \mathcal{S}_u} x_j^u[p] \gamma_{i,t_n}^{j,p}(l, \mu_u, u) h_u[l] \tag{5.13}$$

Here, the term $\lambda_{i,t_n}^u(l, \mu_u)$ represents the contribution from all the pilot-carrying time frames and subbands to the output $z_i^u[t_n]$, through the lth channel path, whereas $w_i^u[t_n]$ (5.13) is the total contribution from the non-pilot (i.e., data carrying) input symbols to $z_i^u[t_n]$ and can be interpreted as a form of data-interference. Also, $w_i^u[t_n]$ can be approximated as an independent Gaussian with zero-mean and covariance $E\{w_i^u[t_n] w_{i'}^u[t_{n'}]^*\} \simeq \delta_{ii'} \delta_{t_n t_{n'}} \sigma_w^2$ and

$$\sigma_w^2 = \sigma_x^2 \sum_{p \notin \mathcal{T}_u} \sum_{j \in \mathcal{S}_u} |\Gamma_{i,t_n}^{j,p}(\mu_u, u)|^2 \tag{5.14}$$

where $\Gamma_{i,t_n}^{j,p}(\mu_u, u) = \sum_{l=0}^{Q-1} \gamma_{i,t_n}^{j,p}(l, \mu_u, u) h_u[l]$. As a result, $v_i^u[t_n]$ is zero-mean with variance of $\sigma_{v^u}^2 = \sigma_w^2 + \sigma_\psi^2 + \sigma_\nu^2$.

For convenience, we let $\mathbf{h}_u = [h_u[0]\ h_u[1] \cdots h_u[Q-1]]^T$ denote the column vector of unknown channel coefficients between the uth user and BS and define the row vector

$$\boldsymbol{\lambda}^u_{i,t_n}(\mu_u) = [\lambda^u_{i,t_n}(0,\mu_u)\ \cdots\ \lambda^u_{i,t_n}(Q-1,\mu_u)] \tag{5.15}$$

As a result, (5.10) can be written as

$$z^u_i[t_n] = \boldsymbol{\lambda}^u_{i,t_n}(\mu_u)\mathbf{h}_u + v^u_i[t_n] \tag{5.16}$$

In order to express the set of equations (5.16) in compact vector form, we first introduce:

$$\mathbf{z}^u_i = [z^u_i[t_0]\ z^u_i[t_1]\ \cdots\ z^u_i[t_{T_u-1}]]^T \tag{5.17}$$

$$\boldsymbol{\lambda}^u_i(\mu_u) = \left[\boldsymbol{\lambda}^u_{i,t_0}(\mu_u)^T\boldsymbol{\lambda}^u_{i,t_1}(\mu_u)^T\cdots\boldsymbol{\lambda}^u_{i,t_{T_u-1}}(\mu_u)^T\right]^T \tag{5.18}$$

$$\boldsymbol{v}^u_i = [v^u_i[t_0]\ v^u_i[t_1]\ \cdots\ v^u_i[t_{T_u-1}]]^T \tag{5.19}$$

Therefore, we can write

$$\mathbf{z}^u_i = \boldsymbol{\lambda}^u_i(\mu_u)\mathbf{h}_u + \mathbf{v}^u_i \tag{5.20}$$

We then stack these vectors and matrices over the frequency, and define

$$\mathbf{Z}^u = [(\mathbf{z}^u_1)^T\ (\mathbf{z}^u_2)^T\cdots(\mathbf{z}^u_{|\mathcal{S}_u|})^T]^T \tag{5.21}$$

$$\boldsymbol{\Lambda}^u(\mu_u) = [\boldsymbol{\lambda}^u_1(\mu_u)^T\ \boldsymbol{\lambda}^u_2(\mu_u)^T\cdots\boldsymbol{\lambda}^u_{|\mathcal{S}_u|}(\mu_u)^T]^T \tag{5.22}$$

$$\mathbf{V}^u = [(\mathbf{v}^u_1)^T\ (\mathbf{v}^u_2)^T\cdots(\mathbf{v}^u_{|\mathcal{S}_u|})^T]^T \tag{5.23}$$

So that

$$\mathbf{Z}^u = \boldsymbol{\Lambda}^u(\mu_u)\mathbf{h}_u + \mathbf{V}^u \tag{5.24}$$

where $\mathbf{\Lambda}^u(\mu_u)$ is a $(T_u M/U) \times Q$ matrix, assumed to be of full column rank.

As a consequence of the AWGN model assumption, it follows that $\mathbf{V}^u$ is a complex circular Gaussian random vector with zero-mean and diagonal covariance matrix $\mathbf{C}_{\mathbf{V}^u} = E[\mathbf{V}^u(\mathbf{V}^u)^*] = \sigma_{v^u}^2\mathbf{I}$. Accordingly, for a given value of the unknown parameters μ_u and $\mathbf{h}_u$, the observation vector $\mathbf{Z}^u$ in (5.24) is also Gaussian with mean $\mathbf{\Lambda}^u(\mu_u)\mathbf{h}_u$ and covariance $\mathbf{C}_{Z^u} = \sigma_{v^u}^2\mathbf{I}$. The PDF of $\mathbf{Z^u}$, say $f(\mathbf{Z^u}; \mu_\mathbf{u}, \mathbf{h_u})$ can therefore be formulated as

$$f(Z^u; \mu_u, \mathbf{h}_u) = \frac{1}{\pi^{N_u}\det(\mathbf{C}_{Z^u})} \times \\ \exp\left[-(\mathbf{Z}^u - \mathbf{\Lambda}^u(\mu_u)\mathbf{h}_u)^H \mathbf{C}_{Z^u}^{-1}(\mathbf{Z}^u - \mathbf{\Lambda}^u(\mu)\mathbf{h}_u)\right] \tag{5.25}$$

Taking the natural logarithm of this PDF, the LLF [130] for the parameters μ_u and $\mathbf{h}_u$ can be expressed (up to a constant term) in the form

$$\mathcal{L}(\mathbf{Z}^u; \mu_u, \mathbf{h}_u) = -\frac{1}{\sigma_{v^u}^2}[\mathbf{Z^u} - \mathbf{\Lambda}^u(\mu_u)\mathbf{h}_u]^H[\mathbf{Z}^u - \mathbf{\Lambda}^u(\mu_u)\mathbf{h}_u] \tag{5.26}$$

The joint ML estimators of CFO and CIR is obtained by maximizing the LLF (5.26) with respect to the unknown parameters μ_u and $\mathbf{h}_u$. Since LLF is quadratic in the CIR parameters, a closed-form solution can be obtained for the optimum $\mathbf{h}_u$ in terms of μ_u at

$$\mathbf{h}_u^o(\mu_u) = \mathbf{\Lambda}^u(\mu_u)^\dagger \mathbf{Z}^u \tag{5.27}$$

where $\mathbf{\Lambda}(\mu_u)^\dagger = (\mathbf{\Lambda}(\mu_u)^H\mathbf{\Lambda}(\mu_u))^{-1}\mathbf{\Lambda}(\mu)^H$ is the pseudo-inverse of $\mathbf{\Lambda}(\mu_u)$. Next, upon substituting (5.27) in (5.26), the ML estimate of the μ_u can be obtained via a 1-dimensional search as

$$\hat{\mu}_u = \arg\max_{\mu \in \mathcal{M}_u} \{\mathcal{L}(\mathbf{Z}^u; \mu_u, \mathbf{h}_u^o(\mu_u))\} \tag{5.28}$$

where $\mathcal{M}_u$ is the search range for μ_u. The first step in the maximization of the (5.28) is the coarse search where $\mathcal{L}(\mathbf{Z}^u; \mu_u, \mathbf{h}_u^o(\mu_u))$ is computed over a uniform grid of μ_u values and determines the location of its maximum on the grid, say μ_u^m. The second step, or fine search, attempts to find the local maximum nearest to μ_u^m, which can be handled by classic optimization methods due to the observed convexity of the $\mathcal{L}(\mathbf{Z}^u; \mu_u, \mathbf{h}_u^o(\mu_u))$ in the vicinity of the true CFO. Then, the ML estimate of the CIR is obtained by substituting the $\hat{\mu}_u$ in

(5.27), that is:

$$\hat{\mathbf{h}}_u = \mathbf{h}_u^o(\hat{\mu}_u) = \mathbf{\Lambda}^u(\hat{\mu}_u)^\dagger \, \mathbf{Z}^u \tag{5.29}$$

Finally, the single-tap per subband equalizer coefficients e_i for $i \in \mathcal{S}_u$, are obtained from the estimated CIR coefficients as

$$e_i = \frac{1}{\hat{H}_u(z)}\Big|_{z=w^i} \tag{5.30}$$

where $\hat{H}_u(z) = \sum_{l=0}^{Q-1} \hat{h}_u[l] z^{-l}$. Note that except for Q, no *a priori* information is required to implement the above estimator. We also note that the proosed approach enables decoupling the estimation of the CFO from the CIR. Finally, since the subband allocation scheme is known to the receiver, CFO and CIR of each user can be independently estimated.

5.2.1 Iterative Joint Estimation

To improve the performance of the estimation, the CFO can be estimated iteratively in two steps. The first steps is to estimate the CFO as in (5.28), where $\hat{\mu}_u^{(1)}$ denotes this value. The Second step starts with using $\hat{\mu}_u^{(1)}$ at the receiver front-end to compensate the CFO for each user as

$$\hat{y}_u^{(1)}[m] = \bar{y}[m] e^{-\jmath 2\pi \frac{\hat{\mu}_u^{(1)}}{M} m} \tag{5.31}$$

where $\hat{y}_u^{(1)}[m]$ denotes the received signal that will be feed into the receiver. The same estimation process will then repeat and $\hat{\mu}_u^{(2)}$ is derived through (5.28). Eventually, the CIR and equalizer coefficients are derived based on the second estimated value of the CFO $\hat{\mu}_u^{(2)}$ via (5.29) and (5.30). The motivation behind this proposal is that the interference terms (in particular, the data-interference term $w_i^u[t_n]$ in (5.12)) are smaller when CFO is almost compensated and the estimation accuracy will therefore increase. Note that in this setup, only one iteration is considered whereas more iterations are also possible.

5.3 Results

In this section, we investigate the performance of the proposed joint ML estimator of the CFO and Equalizer coefficients (5.28) and (5.30) through numerical simulations. We consider an MU-OPRFB system (cf. Fig. 5.1) with $U = 4$ users, burst of size $N = 60$ symbols, $M = 64$ subbands, $K = 72$ upsampling/downsampling factor, input sampling rate $F_s = 41.67$kHz and prototype filter of length $D = 1728$ designed as described in Chapter 3. The input data sequence $x_i[n]$ consists of independent and equiprobable 4-QAM symbols with the normalized power of unity, i.e. $|x_i[n]| = 1$. Without loss of generality, since the pilot symbols are known to the receiver, we set $\mathsf{p}_{i_r^u}[t_n] = 1$ for all pairs (i_r^u, t_n).

The data at the output of each user's transmitter is passed through a frequency selective wireless channel with randomly generated coefficients $h_u[l]$, based on the ITU Vehicular A channel guidelines [132]. The channel consists of 8 taps, where the fifth and seventh taps are set to zero and the other taps with delays 0, 0.33, 0.66, 1, 1.66, 2.33 microseconds obey a Rayleigh distribution with relative average powers of 0, -1, -9, -10, -15, -20 dB, respectively. Here, we consider two different channel models, i.e.: time-invariant and time-varying. In the first case, the channel remains constant in time for the duration of a transmission burst while in the second case, the channel fading coefficients are correlated in time according to Jakes's model [133]. At the channel output, AWGN with a power level of σ_ν^2 is added to the baseband received signal to obtain the desired SNR figure, defined as SNR=σ_s^2/σ_ν^2 with $\sigma_s^2 = E\{s[m]^2\}$ where $s[m] = \sum_{u=1}^{U} y_u[m]$. Experiments are carried for different values of the system parameters, including: SNR and Doppler frequency; we also denote by μ_u^o the true value of the CFO. For each choice of parameter set, we run 10^3 independent Monte Carlo trials and compute the relevant performance measures under evaluation, i.e., the RMSE of the CFO and equalizer coefficients estimates.

The RMSE performance of the proposed CFO and equalizer coefficients' estimator for various subband allocation schemes is presented in Fig. 5.4 as a function of SNR, where the following parameter values are used: $\mu_o = 5\%$, $T_u = 6$ and $G = 1$. It can be seen that the performance of the proposed estimator is very similar for the blocked and blocked with guard allocation schemes. Therefore, considering the fact that some subbands are not utilized in the blocked with guard scheme, it is preferred to employ the block scheme. Also, except the CFO estimation low SNR, the interleaved scheme exhibits the highest estimation error among the allocation schemes. Keeping the same settings, the BER performance of

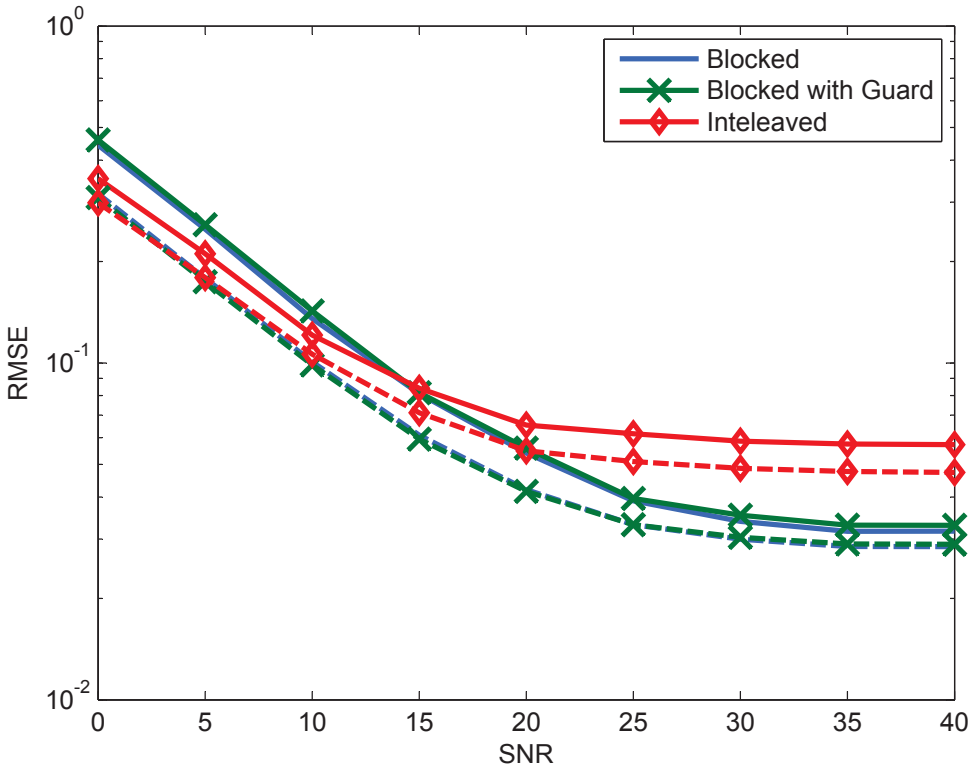

Fig. 5.4 RMSE of CFO (solid lines) and Equalizer (dashed lines) estimation versus SNR ($\mu = 5\%$, $T_u = 6$ and $G = 1$)

the proposed CFO compensation and equalization method using estimated parameters is plotted in Fig. 5.5. Similar to the RMSE performance, the proposed method shows a superior performance for the blocked scheme (with or wothout guard).

The RMSE performance of the proposed CFO and equalizer coefficients' estimator using the iterative method as described in 5.2.1 is depicted in Fig. 5.6, where same parameters as Fig. 5.4 are used. It can be seen that in general, the performance of the joint estimator considerably improves. Moreover, in contrast to the not iterative routine, the proposed method performs equally well for all the considered allocation schemes. Similarly, the BER performance of the proposed CFO compensation and equalization method using iteratively estimated parameters is plotted in Fig. 5.5. As expected, compared to Fig. 5.5, the BER of the system employing iterative estimation method is greatly improved.

Next, we investigate the performance of the joint estimator in time-varying channel for the blocked subband allocation scheme. In Fig. 5.8, the RMSE performance of the

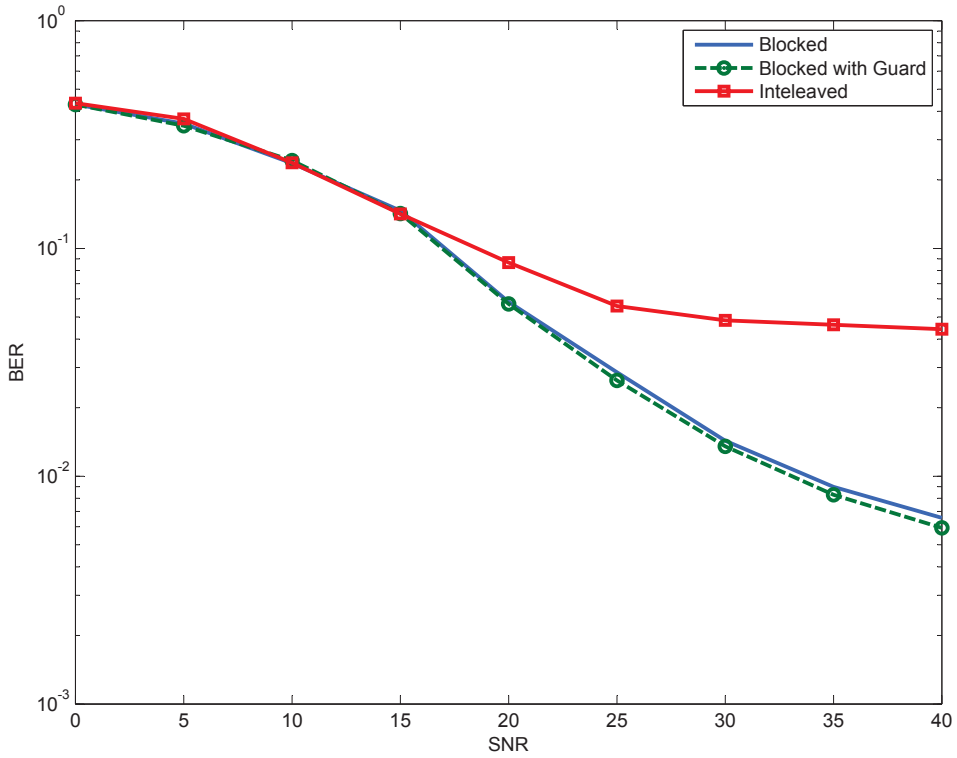

Fig. 5.5 BER versus SNR ($\mu = 5\%$, $T_u = 6$ and $G = 1$)

proposed estimation method for various distributions of pilots in time is plotted as a function of the maximum Doppler frequency F_d, where the following parameter values are used: $\mu_o = 5\%$, $T_u = 12$ and SNR=30dB. In particular, pilots are divided to $G = 1, 2$ and 3 groups and the estimator provides G different estimates of equalizer's coefficients corresponding to each group of pilots, whereas the CFO is assumed to be fixed over time. The maximum Doppler frequency can be derived as $F_d = \frac{vf_c}{c_0}$, where v is the mobile speed in m/s, f_c is the carrier frequency and $c_0 = 3 \times 10^8$m/s is the speed of light. Here, we assume $f_c = 800$MHz (similar to LTE and GSM). The values of F_d in Fig. 5.8, are equivalent to 4 different mobile speeds, that is 5, 60, 120 and 250 km/h corresponding to the speed of pedestrian, car in the urban area, car in the highway and high-speed train, respectively. The comparisons between these patterns show that for low mobility, CFO can be better estimated by the preamble implementation, i.e., $G = 1$, of the pilots. However, with increased mobility, the scattered pilot schemes, i.e., $G = 2$ or 3, estimate the CFO and equalizer coefficients slightly better than the preamble implementation of the pilots.

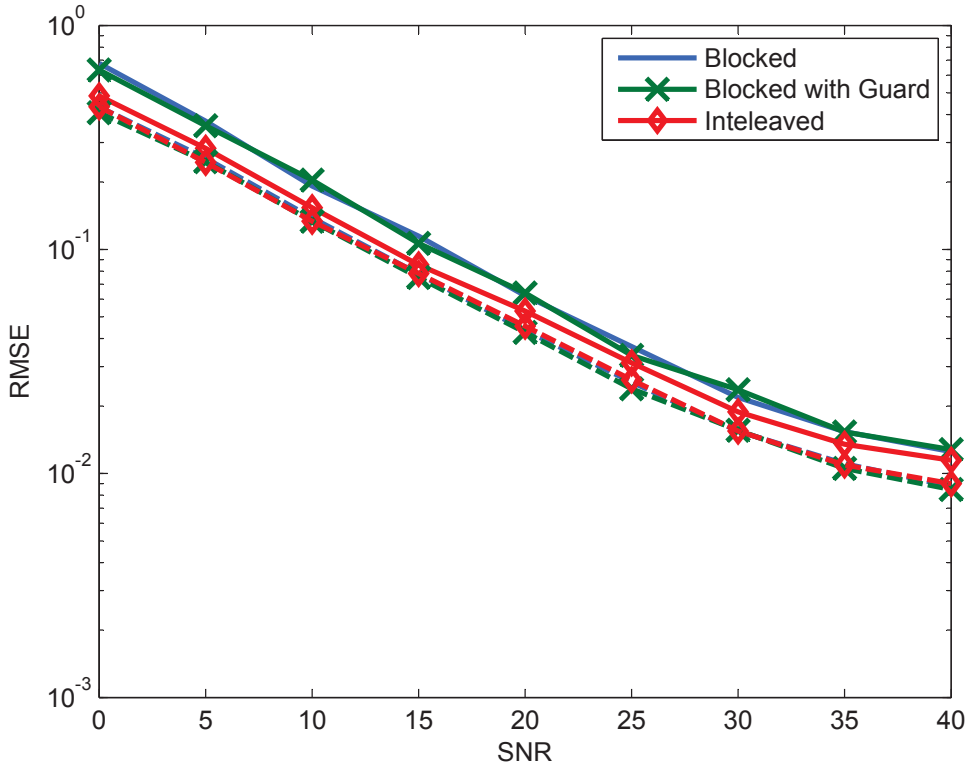

Fig. 5.6 RMSE of CFO (solid lines) and Equalizer (dashed lines) iterative estimation versus SNR ($\mu = 5\%$, $T_u = 6$ and $G = 1$)

The results of the joint iterative estimator in the time-varying environment is shown in Fig. 5.9, where same parameters as Fig. 5.8 are used. Predictably, compared to the non-iterative routine, significant increase in the estimation accuracy can be achieved.

5.4 Conclusion

In this chapter, we considered the problem of joint data-aided CFO and equalizer coefficients estimation in the uplink of MU-OPRFB systems. By exploiting statistical properties of inserted pilots transmitted by such systems over a frequency selective channel, the ML estimator for the unknown parameters was derived. This method was tested over frequency selective channel with different subband allocation schemes. Moreover, different pilot patterns were considered for the proposed estimation method over the time varying channel. Simulation results demonstrated that, over different experimental setups, the proposed

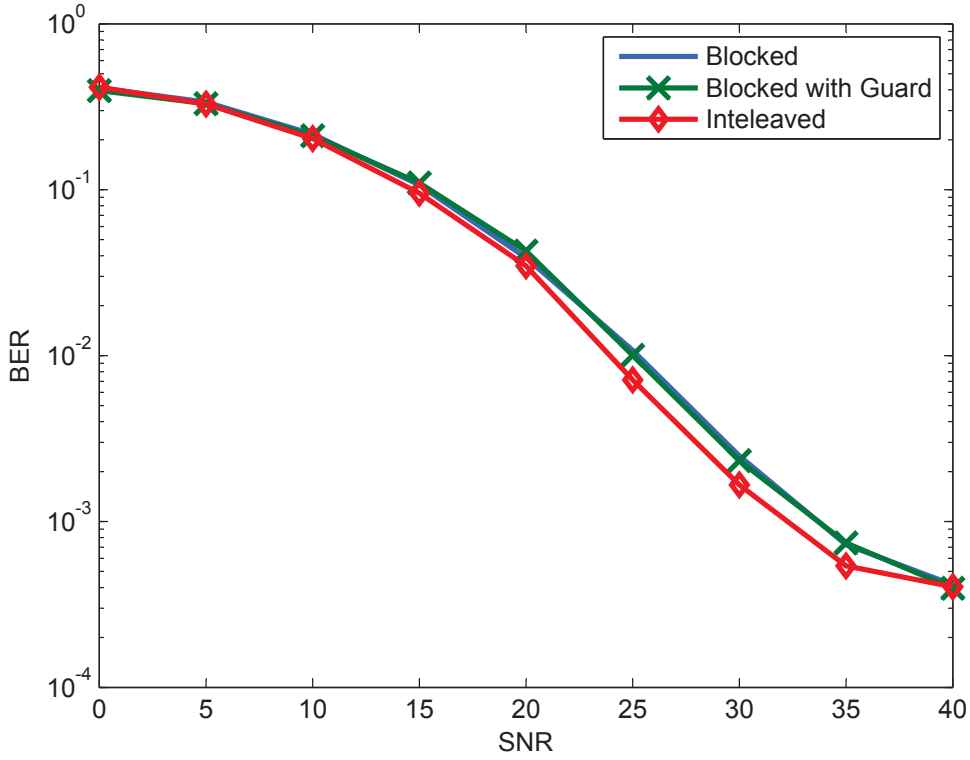

Fig. 5.7 BER versus SNR ($\mu = 5\%$, $T_u = 6$ and $G = 1$) with iterative estimation

estimator provides a reliable performance.

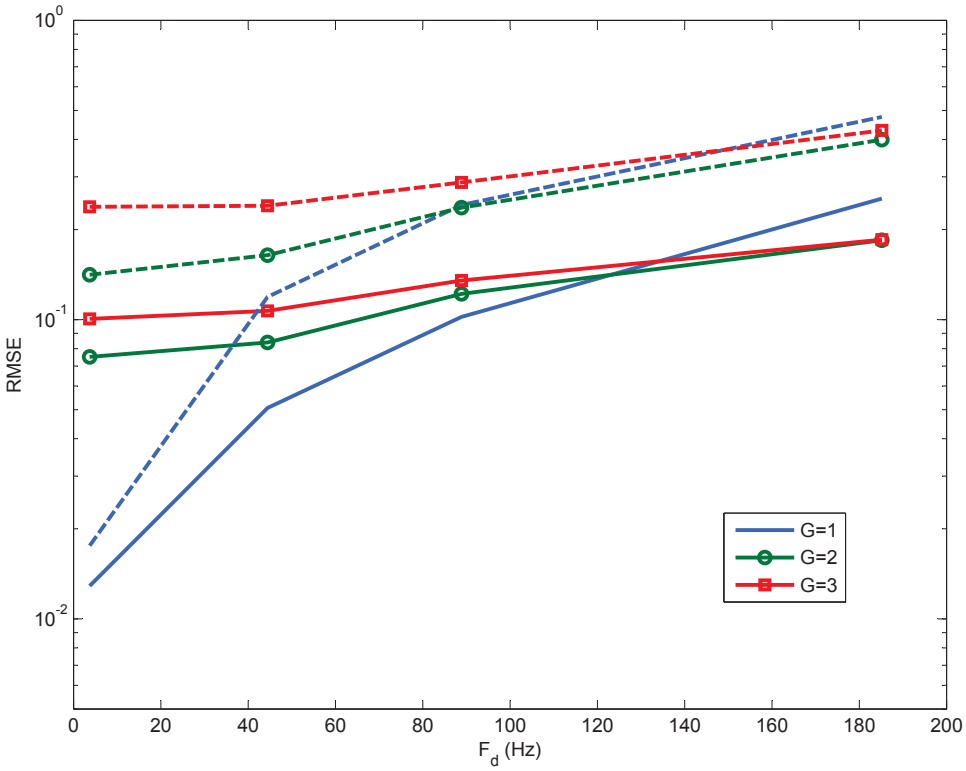

Fig. 5.8 RMSE of CFO (solid lines) and Equalizer (dashed lines) estimation versus Doppler frequency ($\mu = 5\%$, $T_u = 12$ and SNR=30dB)

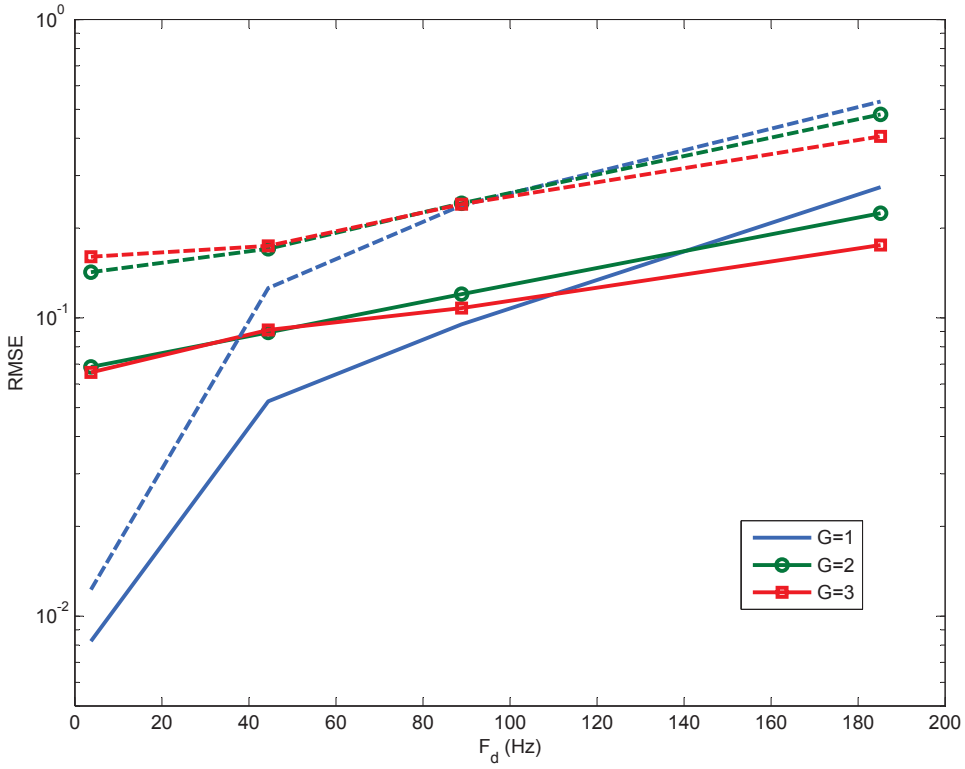

Fig. 5.9 RMSE of CFO (solid lines) and Equalizer (dashed lines) iterative estimation versus Doppler frequency ($\mu = 5\%$, $T_u = 12$ and SNR=30dB)

Chapter 6

Conclusions and Future Works

In this final chapter, we summarize the main contributions of this thesis and discuss some possible avenues for future works.

6.1 Summary and Conclusions

In this thesis, we have studied the design and application of OPRFB transceivers to MCM systems. We first focused on efficient design method for OPRFB transceivers. Then we considered the synchronization and channel equalization problems for single-user and multi-user applications of OPRFB transceivers.

In the first chapter, we began by introducing the MCM technology and its applications in broadband communications from a high level perspective. This was followed by a literature review of different MCM systems, related prototype filter design techniques and corresponding parameter estimation methods, with special emphasis on CFO and CIR estimation for OPRFB transceivers, both for single-user and multi-user applications. The main objectives and research contributions of the thesis were then stated.

In Chapter 2, the main focus was on the presentation of the necessary background information on MCM techniques and FB structures. We first reviewed OFDM system principles along with the function of the CP and the discussed limitations of OFDM. This was followed by a detailed description of basic multirate FB operations, including the transfer function relationship and PR conditions. The two main approaches for modulated FBs, i.e., cosine modulation and DFT modulation, were then presented for both critically sampled and oversampled ones. Finally, some notable FBMC methods including cosine

modulated multitone, OFDM/OQAM, FMT and OPRFB transceivers were presented.

In Chapter 3, a novel and efficient design method for OPRFB transceivers was presented. To ensure the PR property of the system, the polyphase matrices of the transmit and the receive FBs were chosen as paraunitary matrices. Based on factorization methods making use of Givens rotations, these polyphase matrices were then parameterized. To reduce the number of these parameters, three different factorization methods were employed and compared. In turn, the prototype filter coefficients of the analysis and synthesis FBs could be naturally expressed in terms of the entries of these paraunitary polyphase matrices, allowing for a complete yet efficient parameterization of the desired OPRFB. By minimizing the stop-band energy of the prototype filters with respect to the new parameter space, prototype filters were designed with good spectral containment, such as steeper transition from pass-band to stop-band, lower stop-band energy and lower sidelobe levels when compared with OFDM and some recently proposed FBMC systems. The BER performance of the proposed FBs in MCM transceiver applications was evaluated via extensive computer experiments in AWGN and frequency selective channels. The result showed that the proposed scheme offers the lowest BER over these channels. Furthermore, in the presence of NBI or CFO, the proposed FB was shown to be more robust against such channel impairments compared to the other MCM systems.

In Chapter 4, a data-aided joint ML estimator of CFO and CIR that was specifically designed for the purpose of synchronization and equalization of single-user OPRFB systems was developed. Then, by exploiting the structural and spectral properties of these systems, it was possible to considerably reduce the complexity of the proposed estimator through simplifications of the underlying likelihood function. The CRB on the joint estimator variance was also derived as a by-product of the ML analysis and used as a performance benchmark. The performance of the proposed joint ML estimator was investigated by means of numerical simulations under realistic conditions of transmission with CFO and frequency selective fading channels. Moreover, different distributions of pilots over the time-frequency plane were considered and tested for both scenarios of time-invariant and time-varying frequency selective channels. Simulation results demonstrated that the proposed estimator exhibits a performance close to the CRB and can robustly estimate the unknown CFO and CIR over different experimental setups. Using these estimates, it is possible to compensate the effects of CFO and frequency selective fading channels on the transmission performance of OPRFB-based MCM systems.

In Chapter 5, the extension of the joint CFO and CIR estimation and compensation method for application to the uplink of a multi-user OPRFB system operating over frequency selective fading channels was presented. More specifically, we considered an iterative joint estimation of the CFO and channel equalizer coefficients based on the ML principle in the presence of MAI. Different distribution of pilot tones were tested for the proposed estimation method, especially for application over time-varying channels. The performance of the proposed joint ML estimator over realistically modeled frequency selective channels was examined for various mutli-user subband allocation schemes by means of numerical simulations. The simulation results demonstrated that the proposed estimation scheme can provide a reliable performance in the application of MU-OPRFB.

In conclusion, an efficient transmission system for broadband wireless communication, called OPRFB transceiver, was proposed and thoroughly investigated in this thesis. We paid special attention to exploring an efficient design technique for the prototype filter of such transceivers. We employed paraunitary matrices as the basis to construct polyphase matrices of the transmit and receive FBs and then factorize these matrices into elementary building blocks using Givens rotations. Then, we developed a data-aided joint ML-based CFO and CIR estimation method for OPRFB transceivers operating over frequency-selective noisy channel in order to synchronize the CFO and equalize the channel effects. Different pilot distributions were considered to improve the performance in time-varying channels. Finally, an iterative estimation method of CFO and equalizer coefficients in uplink transmission for multi-user application of OPRFB was proposed. Simulation results demonstrated that, over different experimental setups, the proposed estimator provides a reliable performance.

All in all, comprehensive studies as well as simulation experiments demonstrated the effectiveness of the proposed OPRFB transceiver and its potential for application in broadband data transmission as an alternative to OFDM. In particular, benefiting from the spectral containment and the PR property, this transceiver demonstrated a clear advantage in the presence of realistic channel impairments such as NBI or CFO, where it can be effectively synchronized and equalized in both single-user and multi-user scenarios. However, these attractive features come at the cost of an increase in the computational complexity and processing delay of the system.

6.2 Future Works

In this thesis, we have considered the design and application of OPRFB transceivers to MCM systems. There are several potential research topics that can be further developed based on our contribution. These topics provide both challenges and opportunities for researchers and engineers. Some of these points of interest are briefly summarized below:

1. *Time and phase offset synchronization*: Similar to the CFO, time offset and phase offset can lead to performance degradation in OPRFB systems. Consequently, in order for an OPRFB system to function properly, some time and phase offset estimation/correction techniques must be put in place. This process can be implemented in the time domain before the AFB or be incorporated as part of the proposed joint estimation technique in the frequency-domain. These two options need to be compared in terms of the performance-complexity trade-off.

2. *MIMO-OPRFB*: Employing multiple antennas at both the transmitter and receiver in the communication systems, i.e., MIMO, can increase the throughput and the reliability of the system; consequently, it has become very popular in the past decade. Benefiting from the complex orthogonality of OPRFB systems, which does not hold for CMT and OFDM/OQAM as mentioned in Section 2.3, the MIMO implementation of OPRFB is relatively straightforward and similar to MIMO-OFDM. However, the detailed implementation of various MIMO coding schemes combined with OPRFB systems has not been investigated and their performance has not been compared to MIMO-OFDM. In that regard, it is of particular interest to explore the potential advantages of OPRFB systems in the context of a MIMO implementation and possibly develop corresponding coding schemes.

3. *Cognitive radio applications of OPRFB*: The demand for precious wireless spectrum has been on the rise in the past and this trend is expected to continue in the future. Unfortunately, most of the available spectral resources have been already licensed. Unless some of the existing licenses are discontinued, there is little or no room to add any new services. Interestingly, studies have shown that a big part of the already licensed spectrum is left unused for most of the time [94]. CR networks, in which unused portions of spectrum are detected and assigned to secondary (i.e., unlicensed) users to transmit and receive data without interfering with the primary (i.e., licensed)

users, have been proposed to ease this problem. OFDM has been introduced as the first candidate for the physical layer of such CR networks, where DFT output of the OFDM receiver can also be used for spectrum sensing. Considering the shortcomings of OFDM in CR network [135, 136], FBMC systems provide an attractive physical layer alternative for future CR networks [137, 138]. In particular, OFDM/OQAM has been studied and compared with OFDM as a potential physical layer for CR networks. Similarly, OPRFB can be considered as a serious candidate for spectrum sensing and CR networks applications due to its following attributes:

- Flexible multiplexing of silent sensing windows within data symbols in a secondary transmission for spectrum monitoring purposes;
- Flexible way of building decision statistics from basic AFB observations within the sensing window;
- High spectral resolution and therefore better noise and interference rejection;
- Commonality of sensing and communication functions.

Therefore, it is of particular interest to examine OPRFB in CR applications and compare it with OFDM and other FBMC methods.

4. *Application to subband processing systems*: Due to the duality of oversampled DFT modulated FBs used in transceivers and subband processing systems as explained in Section 2.2.4, the proposed prototype filter design method of OPRFB can also be employed in the subband processing configuration. In particular, the PR property of the proposed prototype filter is highly desirable in these applications including subband coding and echo cancellation [98, 109, 110].

Appendix A

Factorization of $\mathbf{P}(z)$

In this appendix, we show in details how to factor $\mathbf{P}(z)$ as given by (3.14). Recall that, $\mathbf{W}$ is the DFT matrix defined as $[\mathbf{W}]_{i,j} = w^{ij}$, $i, j \in \{0, \ldots, M-1\}$ and the block matrices $\mathbf{L}_0$ and $\mathbf{L}_1(z)$, of respective size $D \times M$ and $K \times D$, are defined as follows

$$\mathbf{L}_0 = [I_M, I_M, \ldots, I_M]^T, \tag{A.1}$$

$$\mathbf{L}_1(z) = [I_K, z^{-1} I_K, \ldots, z^{-(d_K-1)} I_K]. \tag{A.2}$$

Also, diagonal matrix $\mathbf{\Gamma}_f$ is given by

$$\mathbf{\Gamma}_f = \mathrm{diag}(f_0[0], \ldots, f_0[D-1]). \tag{A.3}$$

Let us consider $K \times M$ matrix $\hat{\mathbf{P}}(z)$ as

$$\hat{\mathbf{P}}(z) = \mathbf{L}_1(z) \mathbf{\Gamma}_f \mathbf{L}_0 \mathbf{W}^* \tag{A.4}$$

Therefore the (r, i)th entry of $\hat{\mathbf{P}}(z)$ can be written as

$$[\hat{\mathbf{P}}(z)]_{r,i} = \mathbf{L}_{1,r}(z) \mathbf{\Gamma}_f \mathbf{W}_i^*, \tag{A.5}$$

where $1 \times D$ matrix $\mathbf{L}_{1,r}(z)$ is the r-th row of $\mathbf{L}_1(z)$ and $D \times 1$ matrix $\mathbf{W}_i$ is the product of $\mathbf{L}_0$ and i-th column of $\mathbf{W}^*$.

$$\mathbf{L}_{1,r}(z) = [\ldots, 0, 1, 0, \ldots, 0, z^{-1}, 0, \ldots, 0, z^{-(dK-1)}, 0, \ldots] \tag{A.6}$$

Note that non-zero elements of $\mathbf{L}_{1,r}(z)$ are situated at $(nK+r)$-th columns , where $n \in \{0,\dots,d_K-1\}$. Consequently, we can further simplify the product of $\mathbf{L}_{1,r}(z)\mathbf{\Gamma}_f$ and write

$$\begin{aligned}\mathbf{L}_{1,r}(z)\mathbf{\Gamma}_f &= [\dots,0,f_0[r],0,\dots,0,f_0[K+r]z^{-1},0 \\ &\quad ,\dots,0,f_0[(dK-1)K+r]z^{-(dK-1)},0,\dots]\end{aligned} \tag{A.7}$$

Moreover, considering the fact that $w^{M+c}=w^c$, $D\times 1$ matrix $\mathbf{W}_i$ can be simplified as

$$\mathbf{W}_i = \begin{bmatrix} I_M \\ I_M \\ \vdots \\ I_M \end{bmatrix} \begin{bmatrix} w^{-0i} \\ w^{-1i} \\ w^{-2i} \\ \vdots \\ w^{-(M-1)i} \end{bmatrix} = \left[\begin{array}{c} w^{-0i} \\ \vdots \\ w^{-(M-1)i} \\ \hline w^{-0i} \\ \vdots \\ w^{-(M-1)i} \\ \hline \vdots \\ \hline w^{-0i} \\ \vdots \\ w^{-(M-1)i} \end{array}\right] = \left[\begin{array}{c} w^{-0i} \\ \vdots \\ w^{-(M-1)i} \\ \hline w^{-Mi} \\ \vdots \\ w^{-(2M-1)i} \\ \hline \vdots \\ \hline w^{-(D-M)i} \\ \vdots \\ w^{-(D-1)i} \end{array}\right] \tag{A.8}$$

Finally, by substituting (A.7) and (A.8) in (A.5) we can write

$$[\hat{\mathbf{P}}(z)]_{r,i} = \sum_{n=0}^{d_K-1} f_0[nK+r]w^{-i(nK+r)}z^{-n}, \tag{A.9}$$

which is in full accordance with (3.7). Thus, it can be stated that $\hat{\mathbf{P}}(z)=\mathbf{P}(z)$ and equation (3.14) is verified.

$$\mathbf{P}(z) = \mathbf{L}_1(z)\mathbf{\Gamma}_f\mathbf{L}_0\mathbf{W}^*. \tag{A.10}$$

Appendix B

Statistical Properties of Data-interference

Considering the input signal as an independent zero-mean random data sequence with variance σ_x^2 and based on the central limit theorem, we can model $w_{s_i}[t_n]$ as a zero-mean Gaussian random signal with

$$E\{w_{s_i}[t_n]w^*_{s_{i'}}[t_{n'}]\} = \sigma_x^2 \sum_{j\notin\mathcal{S}} \sum_{p\notin\mathcal{T}} \Gamma^{j,p}_{s_i,t_n}(\mu)(\Gamma^{j,p}_{s_{i'},t_{n'}}(\mu))^* \tag{B.1}$$

where $\Gamma^{j,p}_{s_i,t_n}(\mu) = \sum_{l=0}^{Q-1} \gamma^{j,p}_{s_i,t_n}(l,\mu)h[l]$. When $s_i \neq s_{i'}$, due to excellent frequency selectivity of the prototype filters and similar to the simplification in (4.34), we can write that either $\Gamma^{j,p}_{s_i,t_n}(\mu) \simeq 0$ or $\Gamma^{j,p}_{s_{i'},t_n}(\mu) \simeq 0$ for $j \notin \mathcal{S}$. As a result, (B.1) can be approximated

$$\begin{aligned} E\{w_{s_i}[t_n]w^*_{s_{i'}}[t_{n'}]\} \;\simeq\; & \delta_{s_i s_{i'}}\sigma_x^2 \sum_{j\notin\mathcal{S}} \sum_{p\notin\mathcal{T}} \Gamma^{j,p}_{s_i,t_n}(\mu) \\ & \times(\Gamma^{j,p}_{s_i,t_{n'}}(\mu))^* \end{aligned} \tag{B.2}$$

Similarly, when $t_n \neq t_{n'}$, either $|p - t_n| \geq 2$ or $|p - t_{n'}| \geq 2$ for $p \notin \mathcal{T}$ in any implemented scheme of pilot distributions in time. As a result, for small values of μ and based on the PR property of the system, we can deduce that either $\Gamma^{j,p}_{s_i,t_n}(\mu) \simeq 0$ or $\Gamma^{j,p}_{s_i,t_{n'}}(\mu) \simeq 0$ for $p \notin \mathcal{T}$. Therefore, we can write

$$E\{w_{s_i}[t_n]w^*_{s_{i'}}[t_{n'}]\} \simeq \delta_{s_i s_{i'}}\delta_{t_n t_{n'}}\sigma_w^2, \tag{B.3}$$

where σ_w^2 is the variance of $w_{si}[t_n]$

$$\sigma_w^2 = E\left\{|w_{s_i}[t_n]|^2\right\} = \sigma_x^2 \sum_{p \notin \mathcal{T}} \sum_{j \notin \mathcal{S}} |\Gamma_{s_i,t_n}^{j,p}(\mu)|^2. \tag{B.4}$$

References

[1] J. A. C. Bingham, "Multicarrier modulation for data transmission: an idea whose time has come," *IEEE Commun. Mag.*, vol. 28, no. 5, pp. 5–14, May 1990.

[2] P. P. Vaidyanathan, *Multirate Systems and Filter Banks*. Upper Saddle River, NJ, USA: Prentice-Hall, 1993.

[3] H. S. Malvar, *Signal Processing with Lapped Transforms*. Norwood, MA, USA: Artech House, Inc., 1992.

[4] N. J. Fliege, *Multirate Digital Signal Processing: Multirate Systems, Filter Banks, Wavelets*. New York, NY, USA: John Wiley & Sons, Inc., 1994.

[5] R. Van Nee and R. Prasad, *OFDM for Wireless Multimedia Communications*. Norwood, MA, USA: Artech House, Inc., 2000.

[6] IEEE, "Part 11: Wireless LAN medium access control (MAC) and physical layer (PHY) specifications high-speed physical layer in the 5 GHz band," 2003. [Online]. Available: http://standards.ieee.org/getieee802/download/802.11a-1999.pdf

[7] C. Eklund, R. Marks, K. Stanwood, and S. Wang, "IEEE standard 802.16: a technical overview of the WirelessMAN/sup TM/ air interface for broadband wireless access," *IEEE Communications Mag.*, vol. 40, no. 6, pp. 98–107, June 2002.

[8] E. Dahlman, S. Parkvall, J. Skold, and P. Beming, *3G Evolution: HSPA and LTE for Mobile Broadband*. Burlington, MA, USA: Academic Press, 2008.

[9] A. J. Coulson, "Bit error rate performance of OFDM in narrowband interference with excision filtering," *IEEE Trans. Wireless Commun.*, vol. 5, pp. 2484–2492, Sept. 2006.

[10] S. H. Han and J. H. Lee, "An overview of peak-to-average power ratio reduction techniques for multicarrier transmission," *IEEE Wireless Commun. Mag.*, vol. 12, pp. 56–65, Feb. 2005.

[11] P. Moose, "A technique for orthogonal frequency division multiplexing frequency offset correction," *IEEE Trans. Commun.*, vol. 42, pp. 2908–2914, Oct. 1994.

[12] T. Pollet, M. Van Bladel, and M. Moeneclaey, "BER sensitivity of OFDM systems to carrier frequency offset and Wiener phase noise," *IEEE Trans. Commun.*, vol. 43, pp. 191–193, Feb. 1995.

[13] B. Farhang-Boroujeny, "OFDM versus filter bank multicarrier," *IEEE Signal Process. Mag.*, vol. 28, pp. 92–112, May 2011.

[14] F. Duplessis-Beaulieu and B. Champagne, "One-tap equalizer for perfect reconstruction DFT filter bank transceivers," in *Proc. Int. Symp. Signals, Syst. Electron.*, Montreal, Canada, Aug. 2007, pp. 391–394.

[15] M. Bellanger, "Specification and design of a prototype filter for filter bank based multicarrier transmission," in *Proc. IEEE Int. Conf. Acoustics, Speech, and Signal Process.*, Salt Lake City, UT , USA, May 2001, pp. 2417–2420.

[16] L. Lin and B. Farhang-Boroujeny, "Cosine-modulated multitone for very-high-speed digital subscriber lines," *EURASIP J. Appl. Signal Process.*, vol. 2006, ID 19329, 16 pages, Jan. 2006.

[17] P. Martin-Martin, R. Bregovic, A. Martin-Marcos, F. Cruz-Roldan, and T. Saramaki, "A generalized window approach for designing transmultiplexers," *IEEE Trans. Circuits and Systems*, vol. 55, no. 9, pp. 2696–2706, Oct. 2008.

[18] A. Viholainen, T. Ihalainen, T. Stitz, M. Renfors, and M. Bellanger, "Prototype filter design for filter bank based multicarrier transmission," in *Proc. European Signal Process. Conf.*, Glasgow, Scotland, Aug. 2009, pp. 1359–1363.

[19] B. Farhang-Boroujeny and C. H. Yuen, "Cosine modulated and offset QAM filter bank multicarrier techniques: a continuous-time prospect," *EURASIP J. Adv. Signal Process.*, vol. 2010, Article ID 165654, 16 pages, Jan. 2010.

[20] F. Mintzer, "On half-band, third-band, and Nth-band FIR filters and their design," *IEEE Trans. Acous., Speech, Signal Process.*, vol. 30, pp. 734–738, Oct. 1982.

[21] N. Benvenuto, S. Tomasin, and L. Tomba, "Equalization methods in OFDM and FMT systems for broadband wireless communications," *IEEE Trans. Commun.*, vol. 50, pp. 1413–1418, Sept. 2002.

[22] X.-G. Xia, "New precoding for intersymbol interference cancellation using nonmaximally decimated multirate filterbanks with ideal FIR equalizers," *IEEE Trans. Signal Process.*, vol. 45, pp. 2431–2441, Oct. 1997.

[23] A. Scaglione, S. Member, G. B. Giannakis, and S. Barbarossa, "Redundant filterbank precoders and equalizers part i: Unification and optimal designs," *IEEE Trans. Signal Processing*, vol. 47, pp. 2007–2022, July 1999.

[24] Y.-P. Lin and S.-M. Phoong, "Minimum redundancy for ISI free FIR filterbank transceivers," *IEEE Trans. Signal Process.*, vol. 50, pp. 842–853, Apr. 2002.

[25] S.-M. Phoong, Y. Chang, and C.-Y. Chen, "DFT-modulated filterbank transceivers for multipath fading channels," *IEEE Trans. Signal Process.*, vol. 53, pp. 182–192, Jan. 2005.

[26] C. B. Ribeiro, M. L. R. de Campos, and P. S. R. Diniz, "Time-varying FIR transmultiplexers with minimum redundancy," *IEEE Trans. Signal Process.*, vol. 57, pp. 1113–1127, Mar. 2009.

[27] T. Q. Nguyen, "Near-perfect-reconstruction pseudo-qmf banks," *IEEE Trans. Signal Process.*, vol. 42, pp. 65–76, Jan. 1994.

[28] H. Bolcskei and F. Hlawatsch, "Oversampled cosine modulated filter banks with perfect reconstruction," *IEEE Trans. Circuits Syst. II, Analog Digit. Signal Process.*, vol. 45, no. 8, pp. 1057–1071, Aug. 1998.

[29] B. Farhang-Boroujeny, "Multicarrier modulation with blind detection capability using cosine modulated filter banks," *IEEE Trans. Commun.*, vol. 51, pp. 2057–2070, Dec. 2003.

[30] P. Martin-Martin, F. Cruz-Roldan, and S. Saramaki, "A new window for the design of cosine-modulated multirate systems," in *Proc. Int. Symp. Circuits and Systems*, vol. 3, Vancouver, Canada, May 2004, pp. 529–532.

[31] P. Martin-Martin, F. Cruz-Roldan, and T. Saramaki, "Optimized transmultiplexers for multirate systems," in *Proc. Int. Symp. Circuits and Systems*, Kobe, Japan, May 2005, pp. 1106–1109.

[32] G. Cherubini, E. Eleftheriou, S. Oker, and J. Cioffi, "Filter bank modulation techniques for very high speed digital subscriber lines," *IEEE Commun. Mag.*, vol. 38, pp. 98–104, May 2000.

[33] G. Cherubini, E. Eleftheriou, and S. Olcer, "Filtered multitone modulation for very high-speed digital subscriber lines," *IEEE J. Sel. Areas Commun.*, vol. 20, pp. 1016–1028, June 2002.

[34] P. Siohan, C. Siclet, and N. Lacaille, "Analysis and design of OFDM/OQAM systems based on filterbank theory," *IEEE Trans. Signal Process.*, vol. 50, pp. 1170–1183, May 2002.

[35] C. Siclet, P. Siohan, and D. Pinchon, "Perfect reconstruction conditions and design of oversampled DFT-modulated transmultiplexers," *EURASIP J. Appl. Signal Process.*, vol. 2006, Article ID 15756, 14 pages, Jan. 2006.

[36] F. Duplessis-Beaulieu and B. Champagne, "Design of prototype filters for perfect reconstruction DFT filter bank transceivers," *Signal Process.*, vol. 89, pp. 87–98, Jan. 2009.

[37] S. Rahimi and B. Champagne, "Perfect reconstruction DFT modulated oversampled filter bank transceivers," in *Proc. European Signal Process. Conf.*, Barcelona, Spain, Aug. 2011, pp. 1588–1592.

[38] ——, "On the robustness of oversampled filter bank multi carrier systems against frequency offset," in *Proc. Int. Symp. Wireless Commun. Syst.*, Paris, France, Aug. 2012, pp. 944–948.

[39] A. D. Rizos, J. Proakis, and T. Nguyen, "Comparison of DFT and cosine modulated filter banks in multicarrier modulation," in *Proc. IEEE Global Telecommun. Conf.*, vol. 2, San Francisco, USA, Nov. 1994, pp. 687–691.

[40] S. D. Sandberg and M. A. Tzannes, "Overlapped discrete multitone modulation for high speed copper wire communications," *IEEE J. Sel. Areas Commun.*, vol. 13, pp. 1571–1585, Sept. 1995.

[41] A. M. Tonello and F. Pecile, "Analytical results about the robustness of FMT modulation with several prototype pulses in time-frequency selective fading channels," *IEEE Trans. Wireless Commun.*, vol. 7, pp. 1634–1645, May 2008.

[42] B. Borna and T. Davidson, "Efficient design of FMT systems," *IEEE Trans. Commun.*, vol. 54, pp. 794–797, May 2006.

[43] M. Bellanger *et al.*, "FBMC physical layer: a primer," *PHYDYAS*, May 2010. [Online]. Available: http://www.ict-phydyas.org/teamspace/internal-folder/special-session-at-crowncom-2010

[44] C. Lélé, P. Siohan, and R. Legouable, "The Alamouti scheme with CDMA-OFDM/OQAM," *EURASIP J. Adv. Signal Process.*, vol. Volume 2010, Article ID 703513, 13 pages, Jan. 2010.

[45] M. Renfors, T. Ihalainen, and T. Stitz, "A block-alamouti scheme for filter bank based multicarrier transmission," in *Proc. European Wireless Conf.*, Lucca, Italy, April 2010, pp. 1031–1037.

[46] H. Bolcskei, F. Hlawatsch, and H. Feichtinger, "Frame-theoretic analysis of oversampled filter banks," *IEEE Trans. Signal Process.*, vol. 46, pp. 3256 –3268, Dec. 1998.

[47] Z. Cvetkovic and M. Vetterli, "Oversampled filter banks," *IEEE Trans. Signal Process.*, vol. 46, no. 5, pp. 1245–1255, May 1998.

[48] ——, "Tight Weyl-Heisenberg frames in $l^2(z)$," *IEEE Trans. Signal Process.*, vol. 46, pp. 1256–1259, May 1998.

[49] J. Kovacevic and A. Chebira, "Life beyond bases: The advent of frames (part I)," *IEEE Signal Process. Mag.*, vol. 24, pp. 86–104, July 2007.

[50] ——, "Life beyond bases: The advent of frames (part II)," *IEEE Signal Process. Mag.*, vol. 24, pp. 115–125, Sept. 2007.

[51] ——, *An Introduction to Frames*. Hanover, MA, USA: Now Publishers Inc., 2008.

[52] P. Vaidyanathan, "Theory and design of M-channel maximally decimated quadrature mirror filters with arbitrary M, having the perfect-reconstruction property," *IEEE Trans. Acoust., Speech, Signal Process.*, vol. 35, pp. 476–492, Apr. 1987.

[53] X. Gao, T. Nguyen, and G. Strang, "On factorization of M-channel paraunitary filterbanks," *IEEE Trans. Signal Process.*, vol. 49, pp. 1433–1446, July 2001.

[54] L. Gan and K.-K. Ma, "On simplified order-one factorizations of paraunitary filterbanks," *IEEE Trans. Signal Process.*, vol. 52, pp. 674–686, Mar. 2004.

[55] Z. Cvetkovic, "Modulating waveforms for OFDM," in *Proc. IEEE Int. Conf. Acoustics, Speech, and Signal Process.*, vol. 5, Phoenix, AZ, USA, Mar. 1999, pp. 2463–2466.

[56] D. Pinchon and P. Siohan, "Oversampled paraunitary DFT filter banks: A general construction algorithm and some specific solutions," *IEEE Trans. Signal Process.*, vol. 59, pp. 3058–3070, July 2011.

[57] Y.-J. Chen, S. Oraintara, and K. Amaratunga, "Dyadic-based factorizations for regular paraunitary filterbanks and M-band orthogonal wavelets with structural vanishing moments," *IEEE Trans. Signal Process.*, vol. 53, pp. 193–207, Jan. 2005.

[58] T. Wang, J. G. Proakis, and J. R. Zeidler, "Interference analysis of filtered multitone modulation over time-varying frequency-selective fading channels," *IEEE Trans. Commun.*, vol. 55, pp. 717–727, Apr. 2007.

[59] T. H. Stitz, T. Ihalainen, A. Viholainen, and M. Renfors, "Pilot-based synchronization and equalization in filter bank multicarrier communications," *EURASIP J. Adv. Signal Process*, vol. 2010, pp. 1–18, Jan. 2010.

[60] P. K. Remvik and N. Holte, "Carrier frequency offset robustness for OFDM systems with different pulse shaping filters," in *Proc. IEEE Global Telecommun. Conf.*, vol. 1, Phoenix, USA, Nov. 1997, pp. 11–15.

[61] P. K. Remvik, N. Holte, and A. Vahlin, "Fading and carrier frequency offset robustness for different pulse shaping filters in OFDM," in *Proc. IEEE Veh. Tech. Conf.*, vol. 2, Ottawa, Canada, May 1998, pp. 777–781.

[62] T. Bianchi, F. Argenti, and E. DelRe, "Performance of filterbank and wavelet transceivers in the presence of carrier frequency offset," *IEEE Trans. Commun.*, vol. 53, pp. 1323–1332, July 2005.

[63] T. Fusco, A. Petrella, and M. Tanda, "Sensitivity of multi-user filter-bank multicarrier systems to synchronization errors," in *Proc. Int. Symp. Commun., Control, Signal Process.*, St. Julians, Malta, Mar. 2008, pp. 393–398.

[64] H. Saeedi-Sourck, Y. Wu, J. W. Bergmans, S. Sadri, and B. Farhang-Boroujeny, "Sensitivity analysis of offset QAM multicarrier systems to residual carrier frequency and timing offsets," *Signal Processing*, vol. 91, no. 7, pp. 1604–1612, 2011.

[65] F. Daffara and O. Adami, "A new frequency detector for orthogonal multicarrier transmission techniques," in *Proc. IEEE Veh. Tech. Conf.*, vol. 2, Chicago, IL, USA, July 1995, pp. 804–809.

[66] J. van de Beek, M. Sandell, and P. Borjesson, "ML estimation of time and frequency offset in OFDM systems," *IEEE Trans. Signal Process.*, vol. 45, pp. 1800–1805, July 1997.

[67] X. Ma, H. Kobayashi, and S. Schwartz, "Joint frequency offset and channel estimation for OFDM," in *Proc. IEEE Global Telecommun. Conf.*, vol. 1, San Francisco, USA, Dec. 2003, pp. 15–19.

[68] T. Cui and C. Tellambura, "Robust joint frequency offset and channel estimation for OFDM systems," in *Proc. IEEE Veh. Tech. Conf.*, vol. 1. IEEE, 2004, pp. 603–607.

[69] J.-H. Lee, J. C. Han, and S. C. Kim, "Joint carrier frequency synchronization and channel estimation for OFDM systems via the EM algorithm," *IEEE Trans. Veh. Technol.*, vol. 55, pp. 167–172, Jan. 2006.

[70] M. Nissila and S. Pasupathy, "Joint estimation of carrier frequency offset and statistical parameters of the multipath fading channel," *IEEE Trans. Commun.*, vol. 54, pp. 1038–1048, June 2006.

[71] T. Fusco, A. Petrella, and M. Tanda, "Data-aided symbol timing and CFO synchronization for filter bank multicarrier systems," *IEEE Trans. Wireless Commun.*, vol. 8, pp. 2705–2715, May 2009.

[72] D. Mattera and M. Tanda, "Data-aided synchronization for OFDM/OQAM systems," *Signal Process.*, vol. 92, pp. 2284–2292, Sept. 2012.

[73] E. Kofidis, D. Katselis, A. Rontogiannis, and S. Theodoridis, "Preamble-based channel estimation in OFDM/OQAM systems: A review," *Signal Process.*, vol. 93, pp. 2038 – 2054, July 2013.

[74] A. Tonello and F. Rossi, "Synchronization and channel estimation for filtered multitone modulation," in *Proc. Int. Symp. Wireless Personal Multimedia Commun.*, Abano Terme, Italy, Sept. 2004, pp. 590–594.

[75] M. Carta, V. Lottici, and R. Reggiannini, "Frequency recovery for filter-bank multicarrier transmission on doubly-selective fading channels," in *Proc. IEEE Int. Conf. Commun.*, Glasgow, Scotland, June 2007, pp. 5212–5217.

[76] V. Lottici, R. Reggiannini, and M. Carta, "Pilot-aided carrier frequency estimation for filter-bank multicarrier wireless communications on doubly-selective channels," *IEEE Trans. Signal Process.*, vol. 58, pp. 2783 –2794, May 2010.

[77] V. Lottici, M. Luise, C. Saccomando, and F. Spalla, "Blind carrier frequency tracking for filterbank multicarrier wireless communications," *IEEE Trans. Commun.*, vol. 53, pp. 1762 – 1772, Oct. 2005.

[78] T. Fusco, A. Petrella, and M. Tanda, "Blind CFO estimation for noncritically sampled FMT systems," *IEEE Trans. Signal Process.*, vol. 56, pp. 2603 –2608, June 2008.

[79] S. Rahimi and B. Champagne, "Carrier frequency recovery for oversampled perfect reconstruction filter bank transceivers," in *Proc. Int. Conf. Wireless Mobile Commun.*, Nice, France, July 2013, pp. 1–5.

[80] A. Larmo, M. Lindstrom, M. Meyer, G. Pelletier, J. Torsner, and H. Wiemann, "The LTE link-layer design," *IEEE Commun. Mag.*, vol. 47, pp. 52–59, Apr. 2009.

[81] M. Morelli, C.-C. Kuo, and M.-O. Pun, "Synchronization techniques for orthogonal frequency division multiple access (OFDMA): A tutorial review," *Proceedings of the IEEE*, vol. 95, pp. 1394–1427, July 2007.

[82] H. Saeedi-Sourck, Y. Wu, J. Bergmans, S. Sadri, and B. Farhang-Boroujeny, "Complexity and performance comparison of filter bank multicarrier and OFDM in uplink of multicarrier multiple access networks," *IEEE Trans. Signal Process*, vol. 59, pp. 1907 –1912, Apr. 2011.

[83] G. Stuber, J. Barry, S. McLaughlin, Y. Li, M. Ingram, and T. Pratt, "Broadband MIMO-OFDM wireless communications," *Proceedings of the IEEE*, vol. 92, pp. 271 – 294, Feb. 2004.

[84] J. G. Proakis and D. K. Manolakis, *Digital Signal Processing*, 4th ed. Upper Saddle River, NJ, USA: Pearson Prentice Hall, Mar. 2007.

[85] B. Muquet, Z. Wang, G. Giannakis, M. de Courville, and P. Duhamel, "Cyclic prefixing or zero padding for wireless multicarrier transmissions?" *IEEE Tran. Commun.*, vol. 50, pp. 2136–2148, Dec. 2002.

[86] T. Starr, J. M. Cioffi, and P. J. Silverman, *Understanding Digital Subscriber Line Technology*. Upper Saddle River, NJ, USA: Prentice Hall, 1999.

[87] A. Coulson, "Maximum likelihood synchronization for OFDM using a pilot symbol: algorithms," *IEEE J. Select. Areas Commun.*, vol. 19, pp. 2486–2494, Dec. 2001.

[88] ——, "Maximum likelihood synchronization for OFDM using a pilot symbol: analysis," *IEEE J. Select. Areas Commun.*, vol. 19, pp. 2495–2503, Dec. 2001.

[89] D. Landstrom, S. Wilson, J.-J. van de Beek, P. Odling, and P. Borjesson, "Symbol time offset estimation in coherent OFDM systems," *IEEE Trans. Commun.*, vol. 50, pp. 545–549, Apr. 2002.

[90] J. Li, G. Liu, and G. Giannakis, "Carrier frequency offset estimation for OFDM-based WLANs," *IEEE Signal Process. Lett.*, vol. 8, pp. 80–82, Mar. 2001.

[91] T. Schmidl and D. Cox, "Robust frequency and timing synchronization for OFDM," *IEEE Trans. Commun.*, vol. 45, pp. 1613–1621, Dec. 1997.

[92] S. Kapoor and S. Nedic, "Interference suppression in DMT receivers using windowing," in *Proc. IEEE Int. Conf. Commun.*, vol. 2, New Orleans, LA, USA, June 2000, pp. 778–782 vol.2.

[93] S. H. Han and J. H. Lee, "An overview of peak-to-average power ratio reduction techniques for multicarrier transmission," *IEEE Wireless Commun.*, vol. 12, pp. 56–65, Feb. 2005.

[94] M. McHenry, P. Tenhula, D. McCloskey, D. Roberson, and C. Hood, "Chicago spectrum occupancy measurements & analysis and a long-term studies proposal," in *Proc. Int. workshop on Technol. and policy for accessing spectrum.* ACM, 2006, p. 1.

[95] T. A. Weiss and F. K. Jondral, "Spectrum pooling: an innovative strategy for the enhancement of spectrum efficiency," *IEEE Commun. Mag.*, vol. 42, pp. S8–14, Mar. 2004.

[96] A. Spanias, "Speech coding: a tutorial review," *Proceedings of the IEEE*, vol. 82, pp. 1541–1582, Oct. 1994.

[97] H. Xiong, L. Zhu, N. Ma, and Y. Zheng, "Scalable video compression framework with adaptive orientational multiresolution transform and nonuniform directional filterbank design," *IEEE Trans. Circuits Syst. Video Technol.*, vol. 21, pp. 1085–1099, Aug. 2011.

[98] Q.-G. Liu, B. Champagne, and D. K. Ho, "Simple design of oversampled uniform DFT filter banks with applications to subband acoustic echo cancellation," *Signal Process.*, vol. 80, pp. 831 – 847, May 2000.

[99] M. Tzannes, M. Tzannes, J. Proakis, and P. Heller, "DMT systems, DWMT systems and digital filter banks," in *Proc. IEEE Int. Conf. Commun.*, New Orleans, LA, USA, May 1994, pp. 311–315.

[100] A. Croisier, D. Esteban, and C. Galand, "Perfect channel splitting by use of interpolation, decimation, tree decomposition techniques," in *Proc. Int. Symp. Info., Circuits, and Syst.*, vol. 2, Patras, Greece, Aug. 1976, pp. 443–446.

[101] M. J. T. Smith and I. Barnwell, T.P., "A new filter bank theory for time-frequency representation," *IEEE Trans. Acous., Speech and Signal Process.*, vol. 35, pp. 314–327, Mar. 1987.

[102] M. Vetterli, "Filter banks allowing perfect reconstruction," *Signal Process.*, vol. 10, pp. 219–244, Apr. 1986.

[103] ——, "A theory of multirate filter banks," *IEEE Trans. Acoust., Speech, Signal Process.*, vol. 35, pp. 356 – 372, Mar. 1987.

[104] S. Alamouti, "A simple transmit diversity technique for wireless communications," *IEEE J. Select. Areas Commun.*, vol. 16, pp. 1451 –1458, Oct. 1998.

[105] S. Mirabbasi and K. Martin, "Overlapped complex-modulated transmultiplexer filters with simplified design and superior stopbands," *IEEE Trans. Circuits Syst. II*, vol. 50, pp. 456–469, Aug. 2003.

[106] J. Alhava and M. Renfors, "Exponentially-modulated filter bank-based transmultiplexer," in *Proc. Int. Symp. Circuits and Systems*, vol. 4, Bangkok, Thailand, May 2003, pp. 233–236.

[107] ——, "Exponentially-modulated filter bank transmultiplexer with fine-coarse adaptive filtering," in *Proc. Int. Symp. Commun. Control Signal Process.*, St. Julians, Malta, 2008, pp. 68–72.

[108] S. Kasturia, J. Aslanis, and J. Cioffi, "Vector coding for partial response channels," *IEEE Trans. Inf. Theory*, vol. 36, pp. 741–762, Apr. 1990.

[109] F. Labeau, J.-C. Chiang, M. Kieffer, P. Duhamel, L. Vandendorpe, and B. Macq, "Oversampled filter banks as error correcting codes: theory and impulse noise correction," *IEEE Trans. Signal Process.*, vol. 53, pp. 4619–4630, Dec. 2005.

[110] F. Labeau, "Synthesis filters design for coding gain in oversampled filter banks," *IEEE Signal Process. Lett.*, vol. 12, pp. 697–700, Oct. 2005.

[111] M. Vetterli, "Perfect transmultiplexers," in *Proc. IEEE Int. Conf. Acoustics, Speech, and Signal Process.*, vol. 11, Tokyo, Japan, Apr. 1986, pp. 2567 – 2570.

[112] R. Hleiss, P. Duhamel, and M. Charbit, "Oversampled OFDM systems," in *Proc. Digital Signal Process.*, vol. 1, Santorini, Greece, July 1997, pp. 329–332.

[113] M. Rossi, J.-Y. Zhang, and W. Steenaart, "Iterative least squares design of perfect reconstruction QMF banks," in *Canadian Conf. Elect. Comput. Eng.*, vol. 2, Calgary, Alberta, Canada, May 1996, pp. 762–765.

[114] B. Farhang-Boroujeny and C. Schlegel, "Efficient multicarrier realization of full-rate space-time orthogonal block coded systems," in *Proc. IEEE Int. Conf. Commun.*, vol. 4, Anchorage, Alaska, USA, May 2003, pp. 2267–2271.

[115] T. W. Parks and C. S. Burrus, *Digital Filter Design*. New York, NY, USA: Wiley-Interscience, 1987.

[116] N. Moret and A. M. Tonello, "Design of orthogonal filtered multitone modulation systems and comparison among efficient realizations," *EURASIP J. Adv. Signal Process*, vol. 2010, pp. 10:1–10:11, Jan. 2010.

[117] Y. Yang, G. Kang, J. Liu, and P. Zhang, "Pilot sequence design for inter-cell interference mitigation in MIMO FMT systems," in *Proc. IEEE Wireless Commun. and Networking Conf.*, Kowloon, Hong Kong, Mar. 2007, pp. 1216–1220.

[118] A. Tonello and M. Bellin, "Implementation complexity analysis of the concatenated MIMO DMT-FMT multiuser system," in *Proc. Int. Symp. on Spread Spectrum Techniques and Applicat.*, Bologna, Italy, Aug. 2008, pp. 708–713.

[119] P. Amini and B. Farhang-Boroujeny, "Design and performance evaluation of filtered multitone (FMT) in doubly dispersive channels," in *Proc. IEEE Int. Conf. Commun.*, Kyoto, Japan, June 2011, pp. 1–5.

[120] E. Costa, A. Filippi, S. Ometto, M. Weckerle, and E. Schulz, "Asynchronous uplink transmission in FMT-FDMA systems," in *Proc. Personal Indoor Mobile Radio Commun.*, vol. 2, Beijing, China, Sept. 2003, pp. 1090–1094.

[121] S. Weiss and R. W. Stewart, "Fast implementation of oversampled modulated filter banks," *Electronics Letters*, vol. 36, pp. 1502–1503, Aug. 2000.

[122] G. Hardy, E. Wright, and J. Silverman, *An Introduction to the Theory of Numbers*. New York, USA: Oxford University Press, 2008.

[123] R. Raffenetti and K. C. Ruedenberg, "Parametrization of an orthogonal matrix in terms of generalized Eulerian angles," *J. Quantum Chemistry*, vol. III S, pp. 625–634, 1969.

[124] G. Golub and C. Van Loan, *Matrix Computations*. Johns Hopkins University Press, Baltimore, MD, 1996.

[125] J. Nocedal and S. J. Wright, *Numerical Optimization*. Springer, Berlin, 2000.

[126] L. Vangelista, N. Benvenuto, S. Tomasin, C. Nokes, J. Stott, A. Filippi, M. Vlot, V. Mignone, and A. Morello, "Key technologies for next-generation terrestrial digital television standard DVB-T2," *IEEE Commun. Mag.*, vol. 47, pp. 146–153, Oct. 2009.

[127] A. Tonello and F. Pecile, "Efficient architectures for multiuser FMT systems and application to power line communications," *IEEE Trans. Commun.*, vol. 57, pp. 1275–1279, May 2009.

[128] D. Umehara, H. Nishiyori, and Y. Morihiro, "Performance evaluation of CMFB transmultiplexer for broadband power line communications under narrowband interference," in *Proc. Int. Symp. on Power Line Commun. and Its Applicat.*, Orlando, USA, Mar. 2006, pp. 50–55.

[129] M. Morelli and U. Mengali, "Carrier-frequency estimation for transmissions over selective channels," *IEEE Trans. Commun.*, vol. 48, pp. 1580–1589, Sept. 2000.

[130] S. Kay, *Fundamentals of Statistical Signal Processing, Vol. I: Estimation Theory*. Upper Saddle River, NJ, USA: Prentice Hall, 2001.

[131] P. Stoica and O. Besson, "Training sequence design for frequency offset and frequency-selective channel estimation," *IEEE Trans. Commun.*, vol. 51, pp. 1910–1917, Nov. 2003.

[132] Recommendation ITU-R M. 1225. (1997) Guidelines for evaluation of radio transmission technologies for IMT-2000. [Online]. Available: http://www.itu.int/rec/R-REC-M.1225/en

[133] W. Jakes, *Microwave Mobile Communications*. Piscataway, NJ, USA: Wiley-IEEE Press, 1994.

[134] J. A. Rice, *Mathematical Statistics and Data Analysis*, 2nd ed. Stamford, CT, USA: Cengage Learning, 2007.

[135] T. Ihalainen, A. Viholainen, and M. Renfors, "On spectrally efficient multiplexing in cognitive radio systems," in *Proc. Int. Symp. Wireless Pervasive Computing*, Santorini, Greece, May 2008, pp. 675–679.

[136] H. Zhang, D. Le Ruyet, and M. Terre, "Spectral efficiency analysis in OFDM and OFDM/OQAM based cognitive radio networks," in *Proc. IEEE Veh. Tech. Conf.*, Barcelona, Spain, Apr. 2009, pp. 1–5.

[137] B. Farhang-Boroujeny, "Filter bank spectrum sensing for cognitive radios," *IEEE Trans. Signal Process.*, vol. 56, pp. 1801 –1811, May 2008.

[138] B. Farhang-Boroujeny and R. Kempter, "Multicarrier communication techniques for spectrum sensing and communication in cognitive radios," *IEEE Commun. Mag.*, vol. 46, pp. 80 –85, Apr. 2008.